

AERODYNAMIC AND STATIC ANALYSIS OF A HORIZONTAL AXIS WIND
TURBINE BLADE & TOWER STRUCTURE MODELING CONSIDERING
DESIGN WIND LOAD

A Thesis

by

BULENT GUDUK

Submitted to the Graduate and Professional School of
Texas A&M University
in partial fulfillment of the requirements for the degree of

MASTER OF SCIENCE

Chair of Committee, Jeffrey Falzarano
Committee Members, David Allen
Hamn-Ching Chen

Head of Department, Sharath Girimaji

August 2022

Major Subject: Ocean Engineering

Copyright 2022 Bulent Guduk

ABSTRACT

In this study, computational fluid dynamics (CFD) simulations were performed using the Fluent and Mechanic module of ANSYS application to characterize the aerodynamic and static behavior of a horizontal axis wind turbine with a 43.2 m long blade. The blade geometry was chosen from NREL S-series, and it is 43.2 meters long and starts with a cylindrical shape at the root and then continues to the S818, S825, and S826 airfoils, which are used in NREL phase 2 and phase 3 wind turbines. This blade was modeled to be similar in size to a GE 1.5XLE turbine by Cornell University.

The focus of the first part of the study is to investigate the aerodynamic analysis of the wind turbine blade by using the Ansys Fluent module and to verify these findings using some physics formulas. Then, the pressure load obtained from aerodynamic analysis for velocities that varies between 8-20 m/s will be applied to the blade surface. In this way, the static performance of the wind turbine will be examined by calculating Von Misses stress and deformation on the blade for four different materials commonly used in the industry. Later, the effect of mechanical properties of materials on the static performance of the turbine blade will be highlighted.

Since it is not possible to access the geometries of the sample turbines due to confidentiality, and a certain blade-tower length ratio cannot be mentioned in the studies, the examples of wind turbines used in the industry are examined to determine the length ratio between the turbine blade and the tower. Later, the wind turbine tower is tried to be modeled according to ASCE (American Civil Engineering Association) standards for the

offshore conditions. The design wind load calculated with the help of this standard was used in fatigue, buckling, and stress analyses in the Ansys Structural module.

Dynamic properties, one of the most important parameters in the preliminary design of the wind turbine tower, are mentioned in the last part of the thesis. The Baumeister Method was used to determine the natural frequency of the tower. The turbine operating frequencies, and the resonance criteria of the tower natural frequency were explained. Lastly, it will be observed whether the model of the turbine tower is suitable for the design load considering structural analysis and dynamic properties.

DEDICATION

This thesis is dedicated to my family, Saniye, Suleyman Guduk, Derya Parlak, and Kamil Balyer, and my life partner Selin Guner. Without their love, patience, guidance, encouragement, and constant support, my graduate study would not be possible.

ACKNOWLEDGEMENTS

I would like to express my sincere appreciation to my committee chair and advisor Prof. Jeffrey Falzarano for his unlimited knowledge and patience. I am grateful to him for every new thing I have learned through him. It has always made me feel lucky to know that he supports me.

I would like to thank my committee members, Dr. David Allen and Prof. Hamn-Ching Chen, for their guidance and support throughout this research.

Thanks also go to my friends Tugay Gumus, Cuneyt Sakonder, Osman Erener, Hayden Smith, and other colleagues and the department faculty and staff for making my time at Texas A&M University a great experience.

CONTRIBUTORS AND FUNDING SOURCES

Contributors

This work was supervised by a thesis committee consisting of Prof. Jeffrey Falzarano and Dr. David Allen of the Department of Ocean Engineering and Prof. Hamn-Ching Chen of the Department of Civil & Environmental Engineering and Ocean Engineering.

Funding Sources

This work was supported by the Republic of Turkey Minister of National Education.

TABLE OF CONTENTS

	Page
ABSTRACT	ii
DEDICATION	iv
ACKNOWLEDGEMENTS	v
CONTRIBUTORS AND FUNDING SOURCES.....	vi
TABLE OF CONTENTS	vii
LIST OF FIGURES.....	x
LIST OF TABLES	xiv
1. INTRODUCTION.....	1
1.1. Components of a HAWT	4
1.1.1. Foundation.....	5
1.1.2. Tower.....	5
1.1.3. Nacelle.....	5
1.1.4. Rotor.....	6
1.1.5. Electrical system room	6
1.2. Literature review	6
2. AERODYNAMIC ANALYSIS OF THE WIND TURBINE BLADE.....	10
2.1. Overview of the wind turbine blade.....	10
2.2. Mathematical Model for the Simulation	13
2.3. Turbulence Modelling.....	14
2.4. Boundary Conditions	15
2.5. Meshing.....	17
2.6. Model Setup	19
2.7. Aerodynamics of Wind Turbines	20
2.8. Blade Velocity.....	23
2.9. Velocity Streamline.....	24
2.10. Pressure Contours.....	25
2.11. Torque	28
2.12. Verifications.....	28

2.12.1. Mass flow rate	28
2.12.2. Tip velocity.....	29
2.12.3. Power coefficient.....	29
3. STRUCTURAL ANALYSIS OF THE WIND TURBINE BLADE	31
3.1. Structural Model of the Blade	32
3.2. Start-up.....	35
3.3. Mesh.....	36
3.4. Model Setup	36
3.5. Pressure Loads.....	37
3.6. Total Deformation	38
3.7. Equivalent Stress	39
3.8. Force Reaction.....	41
3.9. Moment Reaction	42
3.10. Turbine Blade Categorization Based on Structural Zones	43
3.10.1. The blade root.....	43
3.10.2. The mid-span.....	43
3.10.3. The tip.....	43
4. CONCLUSIONS OF THE BLADE AERODYNAMIC AND STRUCTURAL ANALYSIS	45
5. TOWER STRUCTURE ANALYSIS CONSIDERING WIND LOAD	47
5.1. Types of Wind Turbine Tower.....	47
5.1.1. Lattice Towers.....	48
5.1.2. Cylindrical Steel Towers	49
5.1.3. Reinforced Concrete Towers.....	50
5.1.4. Hybrid Towers.....	51
5.2. Wind Turbine Tower Selection	52
5.3. Wind Model.....	56
5.4. Determination of Design Wind Load and Pressure.....	57
5.4.1. Velocity Pressure.....	58
5.4.2. Design Wind Loads	62
5.5. Overview of Structural Analysis of the Tower	65
5.5.1. Preliminary Analysis	66
5.5.2. Analysis Setup.....	68
5.5.3. Total Deformation	70
5.5.4. Equivalent Stress and Safety Factor	71
5.5.5. Fatigue Analysis	73
5.5.6. Buckling Analysis	75
5.5.7. Determination of the Tower Natural Frequency	78
5.5.8. Baumeister Method	79

5.5.9. Resonance Control of the Tower	80
6. CONCLUSIONS	82
7. REFERENCES	85
8. APPENDIX	88
9. APPENDIX B	94

LIST OF FIGURES

	Page
Figure 1-1: Change in hub height and rotor diameter of HAWTs and increase in their power generation (Victor Igwemezie at all, 2019)	2
Figure 1-2: Components of the HAWT and VAWT (T. Al-Shemmeri,2010).....	3
Figure 1-3: Components of a HAWT (Alper Kanbur,2014).....	4
Figure 2-1: NREL S818 airfoils (Dayton A. Griffin,2000).....	10
Figure 2-2: NREL S825 airfoil (Dayton A. Griffin,2000)	11
Figure 2-3: NREL S826 airfoil (Dayton A. Griffin,2000)	11
Figure 2-4: Blade geometry.....	12
Figure 2-5: Fluid Domain.....	13
Figure 2-6: Assumptions of periodicity (Acker, T., Hand, M.,2000)	16
Figure 2-7: Fluid domain modelling in ANSYS Fluent.....	17
Figure 2-8: Mesh of the fluid domain in Ansys	18
Figure 2-9: Mesh statics and meshing state	19
Figure 2-10: Wind turbine blade geometry in the fluid domain (Wireframe view).....	19
Figure 2-11: Stream tube of a HAWT (Neill, S. P., & Hashemi, M. R.,2018).....	21
Figure 2-12: A typical power curve for a wind turbine (E. Hau,2010).....	23
Figure 2-13: Blade velocity in ANSYS Fluent	24
Figure 2-14: Velocity Streamline in the Fluid Domain.....	25
Figure 2-15: Pressure contours in the front of the blade	25
Figure 2-16: Pressure contours in the front of the blade	26
Figure 2-17: Wind velocities and forces (Manwell, J.F,2010).....	27
Figure 2-18: Pressure contours over the airfoil	27

Figure 2-19: Torque calculation by using Ansys Fluent module	28
Figure 2-20: Flux report in Ansys Fluent.....	28
Figure 3-1: Blade structure used in finite element analysis (Rajendra Roul, 2020)	32
Figure 3-2: Thickness of blade surface and spar along the blade	33
Figure 3-3: Connection between CFD project and FEA project.....	35
Figure 3-4: Mesh statistics	36
Figure 3-5: Mesh for FEA analysis.....	36
Figure 3-6: Blade with varying thickness	37
Figure 3-7: Pressure load acting on the blade at 12 m/s.....	38
Figure 3-8: Total Deformation-Wind Speeds.....	39
Figure 3-9: Von Mises Stress-Wind Speed	40
Figure 3-10: Force reaction for the blade in ANSYS Mechanical.....	41
Figure 3-11: Moment reaction of the blade.....	42
Figure 3-12: Turbine blade regions considering aerodynamic and structural efficiency (Armen Sargsyan,2010).....	44
Figure 5-1: Lattice-type wind turbine tower (DNV/Risø, 2002)	49
Figure 5-2: Cylindrical steel tower type a) tower body b) flange (Kanbur, 2014).....	50
Figure 5-3: Tubular Reinforced Concrete Towers (DNV/Risø, 2002)	51
Figure 5-4: Example of hybrid tower (Anonym)	52
Figure 5-5: Blade diameter-hub height of common industrial wind turbines	53
Figure 5-6: Technical drawing of the wind turbine tower	54
Figure 5-7: Wind shear profile (Ryan Wass,2018)	56
Figure 5-8: Wind speed calculation for offshore conditions (53,64 m/s basic wind speed).....	57

Figure 5-9: Basic wind speed for Western Gulf of Mexico Coastline (ASCE 7-02, Figure 6-1a)	62
Figure 5-10: Start-up for the tower structural analysis	66
Figure 5-11: Mesh section taken from the inner surface of the tower	67
Figure 5-12: Blade and nacelle mass trend changes with the rotor diameter (Curran A. Crawford, 2007).....	68
Figure 5-13: Designed tower with varying thickness.....	68
Figure 5-14: Loads acting on the tower	69
Figure 5-15: Total deformation of the tower.....	70
Figure 5-16: Von-Misses stress on the tower.....	71
Figure 5-17: Stress safety factor analysis of the tower	72
Figure 5-18: Fatigue sensitivity of the tower	74
Figure 5-19: Fatigue safety factor analysis of the tower	75
Figure 5-20: Start-up for the eigenvalue buckling analysis	76
Figure 5-21: Buckling loads applied on the tower	77
Figure 5-22: Eigenvalue buckling analysis result	78
Figure 5-23: Tower mass calculated in Ansys Structural.....	80
Figure 8-1: Total deformation on the blade at 8 m/s (from top to bottom, E-Glass, S- Glass, Carbon Epoxy, and Carbon fiber, respectively)	88
Figure 8-2: Total deformation on the blade at 10 m/s.....	89
Figure 8-3: Total deformation on the blade at 12 m/s.....	90
Figure 8-4: Total deformation on the blade at 15 m/s.....	91
Figure 8-5: Total deformation on the blade at 18 m/s.....	92
Figure 8-6: Total deformation on the blade at 20 m/s.....	93
Figure 9-1: Equivalent stress on the blade at 8 m/s (from top to bottom, E-Glass, S- Glass, Carbon Epoxy, and Carbon fiber, respectively)	94

Figure 9-2: Equivalent stress on the blade at 10 m/s.....	95
Figure 9-3: Equivalent stress on the blade at 12 m/s.....	96
Figure 9-4: Equivalent stress on the blade at 15 m/s.....	97
Figure 9-5: Equivalent stress on the blade at 18 m/s.....	98
Figure 9-6: Equivalent stress on the blade at 20 m/s.....	99

LIST OF TABLES

	Page
Table 2-1: Blade geometry properties (Malcolm & Hansen 2006).....	12
Table 2-2: Skewness and orthogonal quality values (Cornell University, Project Guide, 2013)	18
Table 3-1: Material characteristics of Epoxy E-Glass (Ansys Composite_Materials.xml)	33
Table 3-2: Material characteristics of Epoxy S-Glass (Ansys Composite_Materials.xml)	34
Table 3-3: Material characteristics of Epoxy Carbon (Ansys Composite_Materials.xml)	34
Table 3-4: Material characteristics of Carbon Fiber (Ansys Composite_Materials.xml)	35
Table 3-5: Total deformation at various wind speed.....	39
Table 3-6: Von-Misses stress at various wind speed	40
Table 3-7: Radial force distribution	41
Table 3-8: Moment reaction.....	42
Table 5-1: Size specifications of common industrial wind turbines	53
Table 5-2: Tower dimensions and calculation of the moment of inertia	55
Table 5-3: Terrain exposure constants (ASCE 7-02, Table 6-2).....	59
Table 5-4: Importance factor, wind load (ASCE 7-02, Table 1-1)	60
Table 5-5: Wind directional factor (ASCE 7-02, Table 6-4)	61
Table 5-6: Force coefficient of structures for all height (ASCE 7-02, Figure 6-19).....	63
Table 5-7: Design wind load calculation of the wind tower for Corpus Christi, Tx.....	64
Table 5-8: Material properties of S355 Steel (Ansys General_Materials.xml).....	65
Table 5-9: Operating Frequencies for Different Sizes of Turbines (Lanier,2005).....	81

1. INTRODUCTION

The demand for renewable energy has developed increasingly due to the energy needs of the increasing human population, environmental consciousness of societies, and economic concerns. This rapid development and the fact that wind energy can be economically competitive with fossil energy sources make wind energy at the forefront among other renewable energy sources. Wind energy is forecast to generate 1.1 trillion kilowatt-hours of the total 3.3 trillion kWh of renewable energy anticipated by 2030. In addition, solar and wind are likely to supply cost-effective energy sources thanks to the investment of many developed countries. In contrast, other exotic renewable energy sources will probably still be pricey and untested [1].

Land, sea, and atmosphere have their own specific heats. The rays reaching the earth by the sun cause a temperature change in these regions because of the different specific heat of the regions. These temperature differences create pressure differences. Due to the pressure difference, the air gets activated and it always flows from the high-pressure zone to the low-pressure zone. This movement of air is defined as wind and the higher the pressure difference, the faster the wind blows. Lastly, wind energy resulting from this movement can be used by converting it into mechanical energy or electrical energy by wind turbines.

Investments made in wind turbine technology generally focus on improving the durability of wind turbines, increasing their efficiency, reducing their costs, and thus reducing the return time of the investment.

In addition, recent studies on design developments, which increase efficiency in these applications, are aimed to use wind energy more effectively. The main objectives of these studies carried out with the aim of reducing the average cost per kW can be summarized as increasing the reliability of the turbine components, increasing the size of the wind turbine rotors, and using new materials that will reduce the operation and maintenance costs.

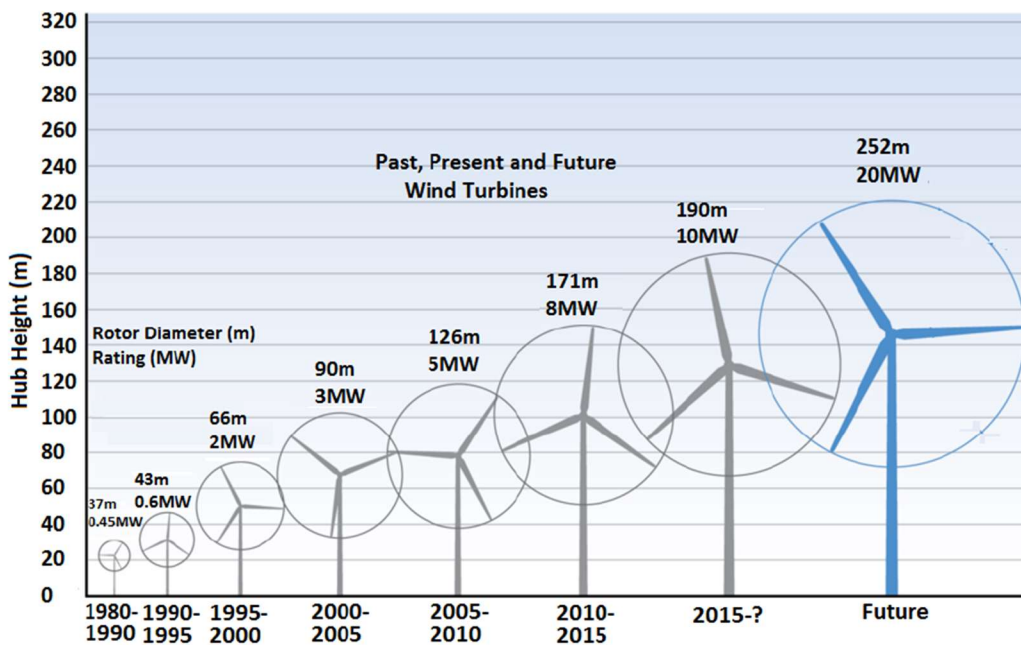


Figure 1-1: Change in hub height and rotor diameter of HAWTs and increase in their power generation (Victor Igwemezie et al., 2019)

The working principle of modern wind turbines is generally based on the conversion of kinetic energy obtained from the wind into mechanical energy and electrical energy. The kinetic energy of the wind is transmitted to the low-speed shaft by utilizing the rotational movement of the blades and converted into mechanical energy. Later, the

mechanical energy generated in the low-speed shaft is transmitted to the high-speed shaft and then to the generator by increasing the rotation speed and decreasing the torque with the help of the gearbox. Finally, in the generator unit, the mechanical energy is converted into electrical energy and transmitted to the grid circuit [2].

Wind turbines can be classified as horizontal and vertical axes wind turbines according to their rotation axes. Horizontal axis wind turbines, which dominate majority of the wind industry today, generally consist of a tower, generator, gearbox, hub, electrical-electronic elements, and blade (Figure 1-2).

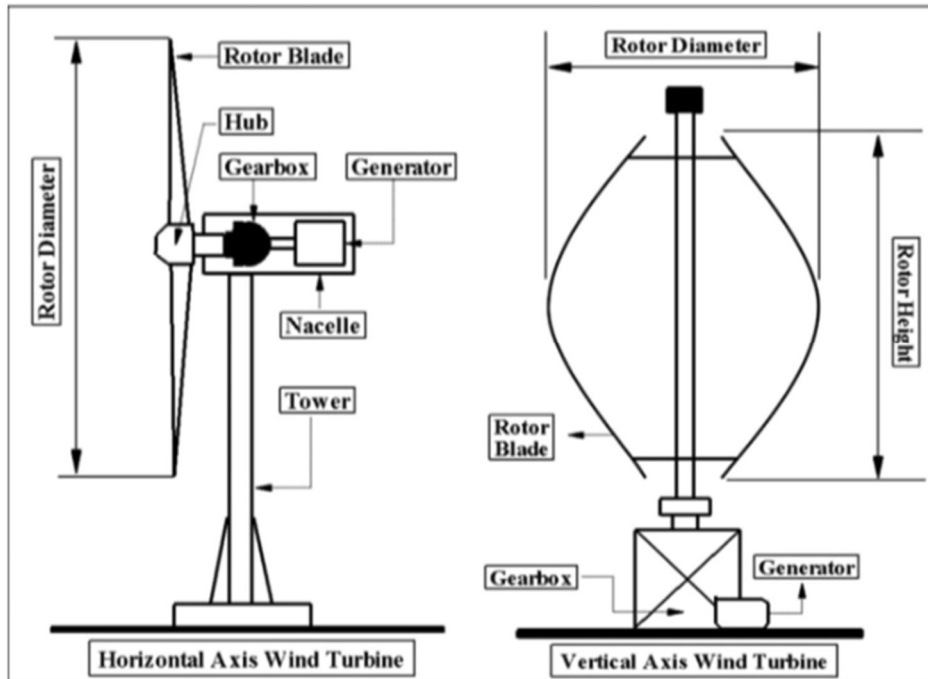


Figure 1-2: Components of the HAWT and VAWT (T. Al-Shemmeri,2010)

Horizontal axis wind turbines can be called the modernized design of windmills. In this structure, the rotor rotation axis is parallel to the ground and therefore the turbine blades are perpendicular to the direction of movement of the wind. In this way, it is aimed

to gain maximum energy from the wind. The nacelle is placed perpendicular to the turbine tower. Due to the force (thrust) that the wind acts on the blades, the turbine rotor is rotated, and the kinetic energy of the wind is converted into mechanical energy.

1.1. Components of a HAWT

Components of a horizontal axis wind turbine can be listed as a foundation, tower, nacelle, rotor, and electrical system room (Figure 1-3).

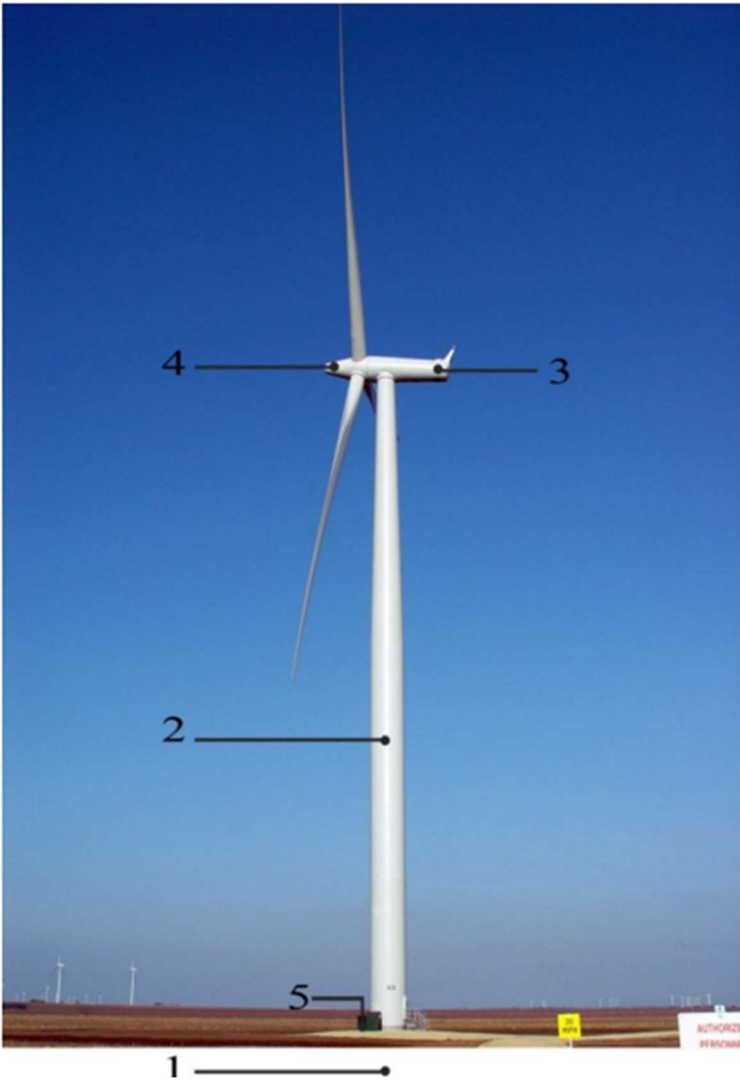


Figure 1-3: Components of a HAWT (Alper Kanbur,2014)

1.1.1. Foundation

The foundation, which provides continuity between the tower's base and the ground, is designed as reinforced concrete. The foundation is intended to resist the effects of rotation, overturning, and shear. For cylindrical steel towers, the connection of the turbine with the ground is provided by the base flange and the basket flange that will remain in the foundation.

1.1.2. Tower

Towers carry the rotor, blades, and nacelle's weight. They are structures designed to safely meet the wind effect coming on themselves and the wind loads caused by the operation of the propellers and transfer them to the foundation. The main segments are formed by welding the tower body parts, obtained by bending the steel plate sheets in the hot rolling mills. These segments are connected to each other with the help of flanges. Steel cylindrical towers are generally preferred in the industry. Other tower designs can be listed as reinforced concrete, hybrid (steel-reinforced concrete), or lattice type.

1.1.3. Nacelle

The nacelle is a wind turbine part of the tower that converts the wind energy coming from the propeller into electrical energy with the help of mechanical elements. It includes a gearbox, main bearing, rotating bearing, deflection mechanism, brake mechanism, generator, and hydraulic system.

Since the nacelle weight and the wind loads are transferred to the tower, these loads constitute an essential analysis subject for the tower design. In addition to different wind scenarios such as regular operation and braking, the nacelle weight has an important place

in the tower's design. The nacelle weight is also a point to be considered in terms of affecting the tower's natural frequency and local buckling.

1.1.4. Rotor

A rotor is a structure located on the tower's top, containing the blades and the hub in front of the blades. Today, systems with three blades are used, but some examples with two blades can also be seen. Blades are usually made of composite materials such as fiberglass and carbon fiber. The hub is the structure at the center of the propellers and can be designed as rigid or jointed [3].

1.1.5. Electrical system room

There are some electrical components in the electrical system room which is located under the wind turbine. These can be listed as cables, electronic converters, and power factor correction capacitors [3].

1.2. Literature review

Aerodynamic and mechanical properties are considered in the design of modern wind turbine blades. The aerodynamic properties of the blade determine the amount of power to be obtained from the turbine; mechanical properties affect the mechanical behavior of turbine elements. Since horizontal axis wind turbines, which are widely used today, are commercial products, information about horizontal axis wind turbine blades is limited.

Blade design information is obtained from the project and development made by such as DOWEC (Dutch Offshore Wind Energy Converter), Upwind (EU's Wind Energy

Research and Development Project) and DOE/NREL (US energy department/National renewable energy laboratory), Sandia laboratories (USA).

If some studies done by these research and development companies are examined, DOWEC was conducted with the aim of developing a large and economical offshore wind farm. With this project, a 64.5 m long wind turbine blade was designed and the blade's profile chord line lengths, profile placements, and the blade's geometric and rigidity properties were determined [4].

In another study which is conducted by NREL, an aeroelastic model including tower, blades, nacelle, power transmission and turbine control mechanism was developed for a 5 MW wind turbine and the structural and aerodynamic properties of the blade were evaluated [5].

While the Upwind project is a 20 MW economic wind turbine development project [6], in the Sandia study, the good and bad aspects of large-scale blades were investigated, and material properties of the blade were determined for a 100 m blade wind turbine [7].

Apart from these studies, the materials used in the turbine blade are another important subject. In many studies, the strength and damage mechanisms of composite materials have been investigated.

While the advantages of natural fibers used in wind turbine applications can be listed as low cost, ease of production and environmental friendliness; the disadvantages are high moisture uptake and low thermal stability of raw fibers [8].

Additionally, E-glass fibers (“electric glass” used for high electrical resistance) are used as the main reinforcement in composites used in turbine blades. In this way, the

hardness, tensile and compression strength of the blade can be increased, and weight reduction can be achieved [9].

Carbon fibers can be considered an important alternative when compared to glass fibers. The reason for this is that carbon fibers show much higher stiffness compared to glass fibers and they have lower density. In this way, they enable the production of thinner turbine blades, as well as allow lighter and more durable structures. Finally, despite all these positive features, they are less resistant to damage that may occur due to the pressure acting on the blades and have a lower ultimate strain. Their unit prices are much higher than E-glass fibers [10].

In the light of all these studies, the design methodology of wind turbine blades was evaluated considering design challenges such as suitable material selection according to turbine size and trends, total system cost, etc. NREL S-series 43.2 meters long blade was chosen, and the aerodynamic performance of the blade at optimum wind speed was investigated by fluid-structure interaction analysis using the Ansys Fluent module. Four different trend materials used in the wind turbine industry were chosen for structural analysis and the effects of material properties on the blade were examined for different wind speeds.

The blade in this study was created to be comparable in size to that of a GE 1.5xl turbine, which was utilized to validate the CFD results. The results of wind turbine aerodynamic analysis were compared to theoretical calculations.

The length ratio between the turbine blade and the tower is determined in the second part of the study, which examines samples of wind turbines utilized in the industry,

and the wind turbine tower design was attempted to be analyzed by Ansys Static Structural module. The design wind load used in the FEA analysis is calculated using ASCE (American Civil Engineering Association) standards for offshore conditions.

2. AERODYNAMIC ANALYSIS OF THE WIND TURBINE BLADE

2.1. Overview of the wind turbine blade

In the study, the blade model, which has NREL S-series airfoils, was examined to see its aerodynamic performance by using Ansys Fluent module. The blade is 43.2 meters long and S818, S825 and S826 airfoils were used for the cylindrical root, body, and tip parts, respectively. The pitch angle at the blade tip is 4 degrees, and it varies as a function of radius, which gives the blade a twist. The blade was designed to be similar to the GE 1.5XLE turbine in size by Cornell University [11].

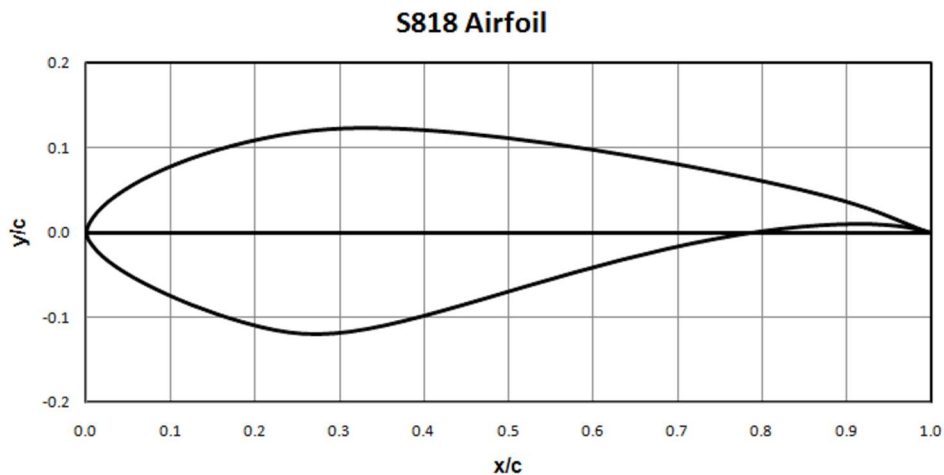


Figure 2-1: NREL S818 airfoils (Dayton A. Griffin,2000)

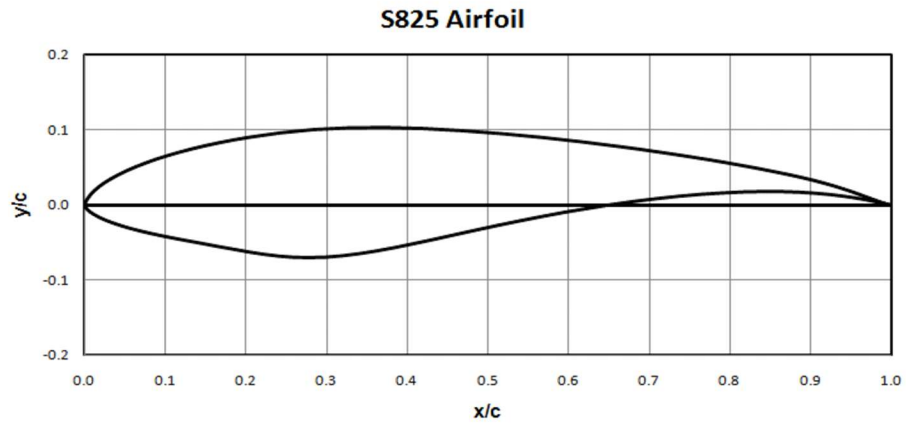


Figure 2-2: NREL S825 airfoil (Dayton A. Griffin,2000)

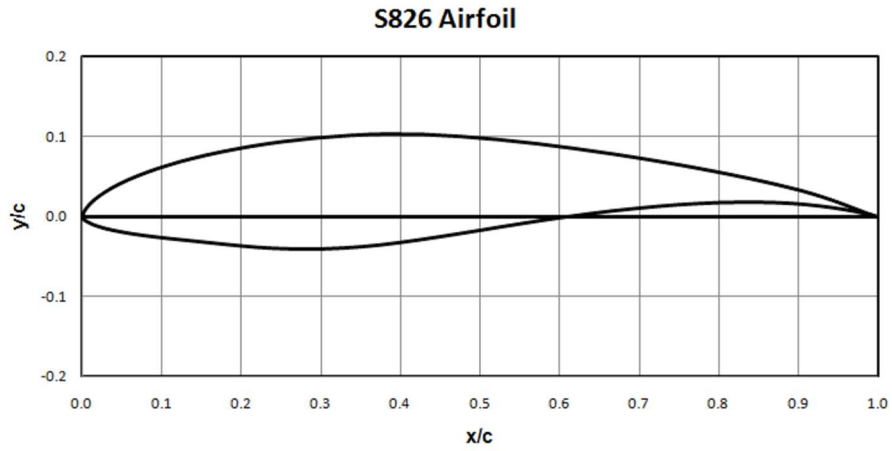


Figure 2-3: NREL S826 airfoil (Dayton A. Griffin,2000)

Blade geometry properties including the length of the span, twist, and chord length for S818, S825, and S826 type airfoils were shown in Table 2-1 below.

Relm (%span)	Span (m)	Twist (deg)	Chord (% span)	Chord (m)	Airfoil
0.075	3.09375	42	0.06140	2.5328	
0.125	5.15625	32	0.06826	2.8157	
0.175	7.21875	23	0.07452	3.0740	
0.225	9.28125	15	0.07782	3.2101	
0.275	11.34375	11.5	0.07543	3.1115	S818
0.325	13.40625	8.2	0.07188	2.9651	
0.375	15.46875	7	0.06832	2.8182	
0.425	17.53125	6	0.06479	2.6726	
0.475	19.59375	5	0.06126	2.5270	
0.525	21.65625	4	0.05771	2.3805	
0.575	23.71875	4.15	0.05415	2.2337	
0.625	25.78125	3.85	0.05062	2.0881	
0.675	27.84375	3.25	0.04707	1.9416	S825
0.725	29.90625	2.75	0.04360	1.7985	
0.775	31.96875	1.25	0.04024	1.6599	
0.825	34.03125	0.75	0.03704	1.5279	
0.875	36.09375	0.55	0.03385	1.3963	
0.925	38.15625	0.85	0.03066	1.2647	S826
0.975	40.21875	0.05	0.02747	1.1331	
1	41.25	0	0.02424	1	

Table 2-1: Blade geometry properties (Malcolm & Hansen 2006)

The blade begins with a circular root section. This circular root is followed by the S818 airfoil, which is then switched to the S825 airfoil, and finally, the S826 airfoil is used at the tip of the blade [11]. The turbine geometry used in the calculation, fluid domain volume, and its boundary created in Ansys Design Modeler can be seen in Figure 2-4 and 2-5 below.

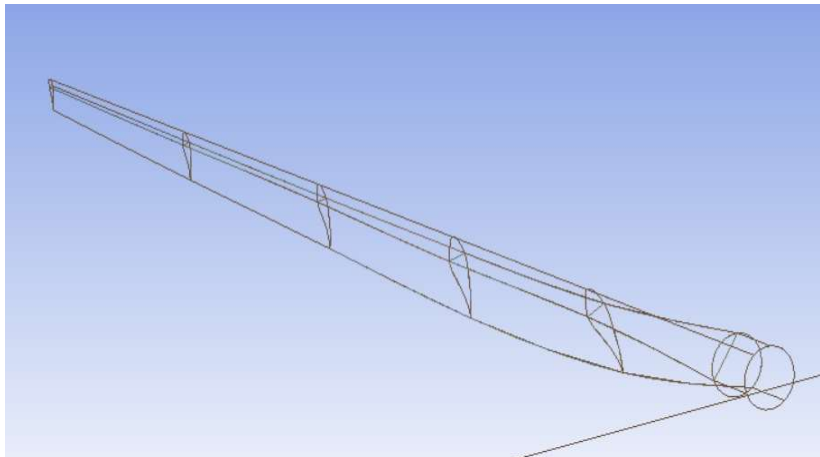


Figure 2-4: Blade geometry

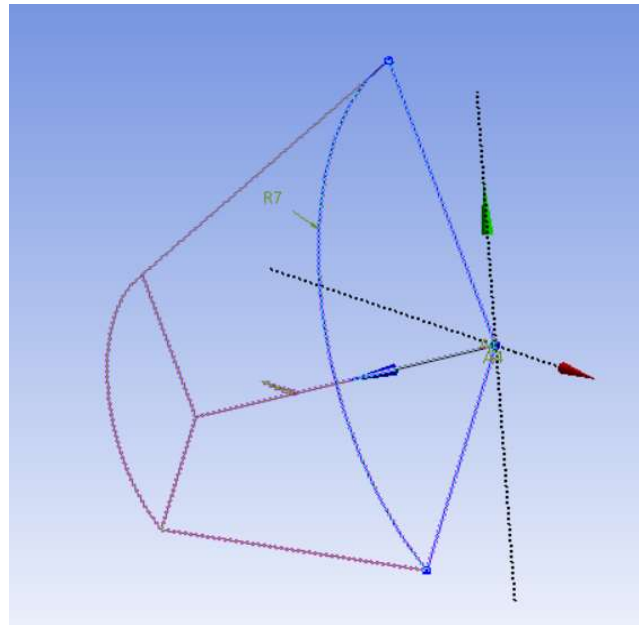


Figure 2-5: Fluid Domain

2.2. Mathematical Model for the Simulation

The blade used in the analysis has different thicknesses along the surface area, and it has a spar inside to be a stiff structure. At 12 m/s, the turbulent wind flows in a negative z-direction (into the page), which is a typical optimum wind speed for maximum power for a turbine of this size. The blade is supposed to rotate at an angular velocity of -2.22 rad/s around the z-axis due to the incoming flow (the blade is thus spinning clockwise when looking at it from the front, like most real wind turbines). The tip speed ratio (the ratio of the blade tip velocity to the incoming wind velocity) is equal to 8, which is a reasonable value for a large wind turbine [11].

The equations valid for the current calculation consist of the continuity equation, and the conservation of momentum equation and they can be expressed as [12].

Continuity equation:

$$\frac{\partial \rho}{\partial t} + \nabla(\rho \vec{V}) = 0 \quad (1)$$

Momentum equation:

$$\rho \left[\frac{D\vec{V}}{Dt} + \vec{V}\nabla\vec{V} \right] = -\nabla p + \frac{1}{3}\mu\nabla(\nabla\vec{V}) + \rho\vec{g} \quad (2)$$

Where \vec{V} is the velocity vector in the x, y, and z directions, p is the pressure, μ is the dynamic viscosity, and ρ is the density of the fluid.

2.3. Turbulence Modelling

The most widely used turbulence models for modeling flow around objects are the k- ϵ , k- ω , and SST turbulence models but it is not possible to specify a specific turbulence pattern for all flows.

The turbulence model selection should be considered the physical state of the flow, the desired level of accuracy, the computability of the values required for the model, and the time required for the simulation. To choose the most suitable model, the above-mentioned features, and the limitations of the model to be used should be taken into consideration.

The k- ω shear stress transport (SST k- ω) model is used to examine the flow turbulence in this study. To describe two turbulence properties of the fluid flow, this model combines two equations based on the k- ω model. The turbulent kinetic energy (k) is the first, while the specific dissipation rate (ω) is the second.

This two-equation model established by Menter, F. Zonal (1933) has the advantage of being able to move from a k- ω turbulence model, which is suitable for simulating far-

field flows, to a $k-\omega$ turbulence model [13], which is suitable for modeling the boundary layer.

The Menter SST $k-\omega$ turbulence model provides a more precise solution for the boundary layer problems and in the blade region, which is called the bottom of the wall region. This model has been widely used for wind turbine blades analysis with positive results [14]. Therefore, ANSYS FLUENT is utilized to investigate turbulence modeling using this transport equation for the SST model to determine the turbulent kinetic energy (k) and the specific dissipation rate (ω).

2.4. Boundary Conditions

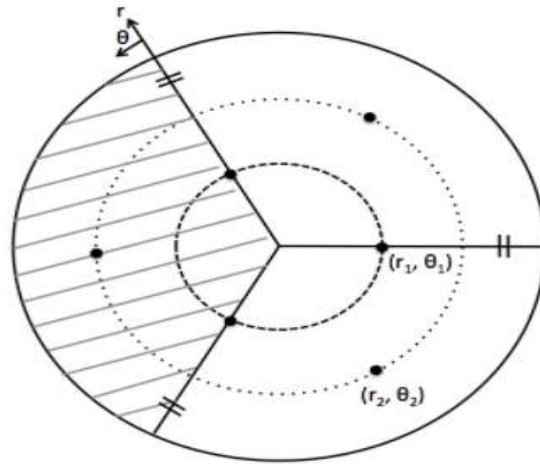
To reduce computation time, only 1/3 volume is represented using periodicity assumptions instead of the entire flow domain. The velocity distribution at angles of 0 and 120 degrees is the same for the entire volume, assuming periodicity (see below). As a result, the velocity distributions at 0 and 120 degrees are the same and this method can be used to reduce the computation time.

$$\vec{u}_r(r_1, \theta) = \vec{u}_r(r_1, \theta - 120^\circ n) = 0 \quad (3)$$

with $n=1,2,3\dots$ where θ is the rotating angle.

Equation 3 means that the velocity profiles at the angle of $\theta=0$, $\theta_1=120^\circ$, $\theta_2=240^\circ$ and $\theta_3=360^\circ$ are the same. If we use θ_1 and θ_2 to represent the two periodic boundaries of the 1/3 domain, then we have the expression below.

$$\vartheta(r_i, \theta_1) = \vartheta(r_i, \theta_2) \quad (4)$$



$$\begin{aligned}\bar{v}(r_1, \theta) &= \bar{v}(r_1, \theta_1 - 120^\circ n) \quad \text{For } n = 1, 2, 3\dots \\ &= \bar{v}(r_1, 240^\circ - 120^\circ(1)) = \bar{v}(r_1, 120^\circ) \\ &= \bar{v}(r_1, 240^\circ - 120^\circ(2)) = \bar{v}(r_1, 0^\circ)\end{aligned}$$

$$\begin{aligned}\bar{v}(r_2, \theta) &= \bar{v}(r_2, \theta_2 - 120^\circ n) \quad \text{For } n = 1, 2, 3\dots \\ &= \bar{v}(r_2, 180^\circ - 120^\circ(1)) = \bar{v}(r_2, 60^\circ)\end{aligned}$$

Figure 2-6: Assumptions of periodicity (Acker, T., Hand, M.,2000)

One of the most important things for obtaining the correct result of the problem is that the boundary conditions must be defined completely and accurately. The boundary conditions on the fluid domain are as follows:

Inlet: Velocity of 12 m/s (optimum velocity for maximum power) with the turbulent intensity of 5% and turbulent viscosity ratio of 10 (default settings for Ansys Fluent Module)

Outlet: Pressure (1 atm). Since the system pressure is opened to the atmospheric environment, the pressure outlet has been selected and the atmospheric boundary condition has been defined.

Blade: Wall (No-slip). For a surface with a wall boundary condition on which the fluid cannot pass through the wall, the nominal value of the velocity along the surface will be zero. In addition, the tangential component of the velocity on the surface due to the no-slip condition is also accepted as zero.

Two Side Boundaries: Periodic boundary condition. The flow field variables along the boundary surface are numerically coupled to another surface of the same shape. Thus, the flow leaving the first surface is considered as entering the second surface with the same properties.

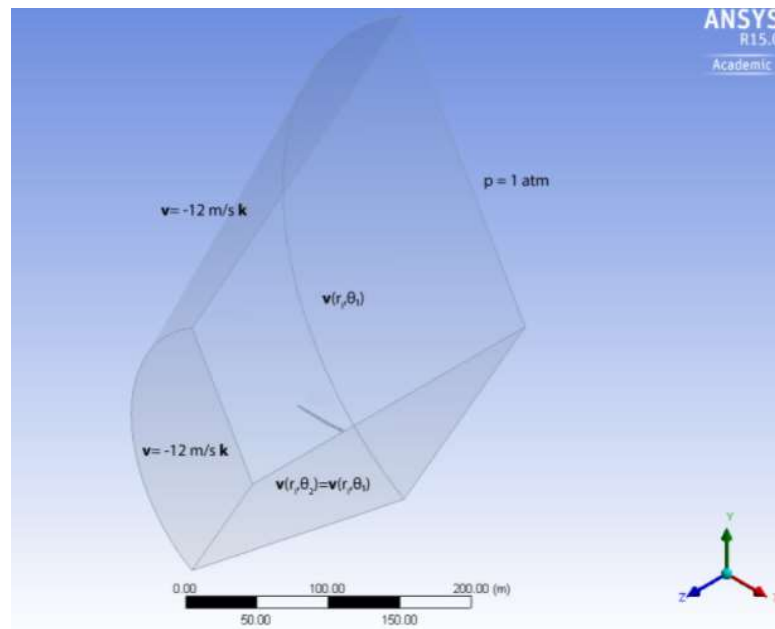


Figure 2-7: Fluid domain modelling in ANSYS Fluent

2.5. Meshing

Local mesh settings (face sizing, match control, inflation, and body sizing) are used to produce more precise results and increase mesh quality, particularly near the blade

region. These mesh settings influence a specific area of the mesh (around the blade).

Figure 2-8 shows that there are around 350000 elements.

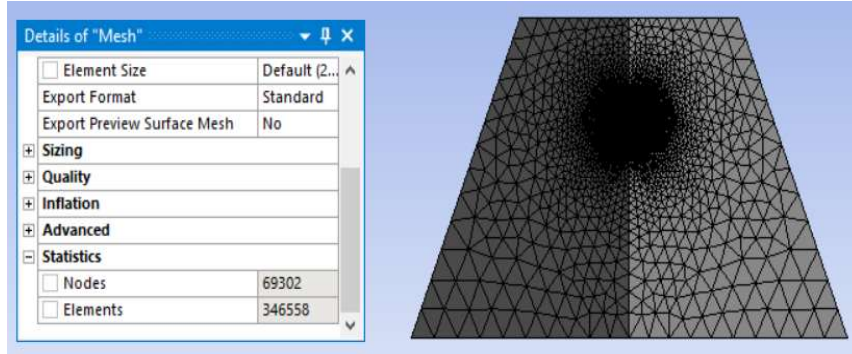


Figure 2-8: Mesh of the fluid domain in Ansys

Two important metrics are used to check mesh quality (less skewed elements). They are skewness and orthogonal quality. It is generally advised to keep the minimum orthogonality greater than 0.15 and maximum skewness lower than 0.95. Bad cells or elements can lead to incorrect simulation results. When mesh statistics and meshing state are examined, it can be seen mesh quality is quite good in figure 2-9.

Skewness:

Outstanding	Very Good	Good	Sufficient	Bad	Inappropriate
0-0.25	0.25-0.50	0.50-0.80	0.80-0.95	0.95-0.98	0.98-1.00

Orthogonal quality:

Inappropriate ↕	Bad ↕	Sufficient ↕	Good ↕	Very Good ↕	Outstanding ↕
0-0.001	0.001-0.15	0.15-0.20	0.20-0.70	0.70-0.95	0.95-1.00

Table 2-2: Skewness and orthogonal quality values (Cornell University, Project Guide, 2013)

Mesh Metric	Skewness	Mesh Metric	Orthogonal Quality
<input type="checkbox"/> Min	3.7942e-004	<input type="checkbox"/> Min	3.3188e-002
<input type="checkbox"/> Max	0.96681	<input type="checkbox"/> Max	0.99187
<input checked="" type="checkbox"/> Average	0.26738	<input checked="" type="checkbox"/> Average	0.73193
<input type="checkbox"/> Standard Deviation	0.1227	<input type="checkbox"/> Standard Deviation	0.12187

Figure 2-9: Mesh statics and meshing state

2.6. Model Setup

To begin, viscous parameters are adjusted in the Ansys Fluent module, and the SST $k-\omega$ model is used to study turbulence. Fluid is considered air and is taken as incompressible. The density and viscosity of air are assumed to be 1.225 kg/m^3 and $1.7894 \times 10^{-4} \text{ kg/ms}$, respectively. Finally, boundary conditions are implemented to each face of the model (inlet, inlet top, outlet, periodic 1-2, and blade).

In the next step, the three-blade turbine rotor has been visualized by changing the number of graphical instances to 3 instead of 1.

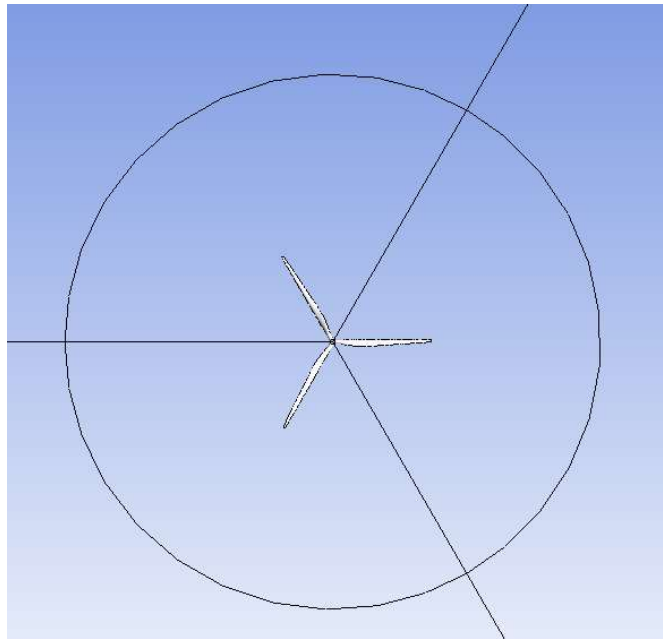


Figure 2-10: Wind turbine blade geometry in the fluid domain (Wireframe view)

2.7. Aerodynamics of Wind Turbines

The most fundamental challenge in wind turbine designs is how much of the kinetic energy of the wind will be captured by the turbine blades. While the blades cause the kinetic energy of the wind to decrease by preventing the passage of the wind, they enable the mechanical energy to be generated by making the rotor move.

The aerodynamics of horizontal axis wind turbines are very similar to the hydrodynamics of horizontal axis tidal turbines. Below is a brief overview of this topic [15].

Suppose a wind turbine with swept area A and diameter D is examined. The wind speed u and the available or 'theoretical' wind kinetic energy per unit time (wind power, P_t) can be calculated as follows.

$$P_t = \frac{\partial}{\partial t} \left(\frac{1}{2} \rho m u^2 \right) = \frac{1}{2} \frac{\partial m}{\partial t} u^2 = \frac{1}{2} \rho Q u^2 \quad (5)$$

Where Q is the wind's volumetric flow rate and ρ is the density of the air. When Q is replaced by Au , the wind power is:

$$P_t = \frac{1}{2} \rho A u^3 \quad (6)$$

A wind turbine can capture only a fraction of the available/theoretical energy. The power coefficient (C_p ; or turbine efficiency) can be defined as the ratio of the power extracted (electricity produced) to the available wind power as follows.

$$C_p = \frac{P_e}{P_t} \quad (7)$$

Where P_e is the power can be extracted. A combination of aerodynamic, mechanical, and electrical efficiency determines P_e , hence power coefficient. The maximum power

coefficient of a horizontal axis wind turbine can be calculated theoretically to be 59 percent, which is known as the *Betz limit/law* [16].

Figure 2-11 shows a stream tube, which is traditionally used to analyze wind turbines using momentum disk theory. Momentum disk theory is used to determine the wind power that can be held by the rotor. According to this theory, instead of the turbine rotor placed in the free flow, it is assumed that there is an infinitely thin disk of the same diameter and the change in the momentum of the air passing through this disk area in the flow is examined.

Turbine blades reduce wind velocity at the turbine (or disk), as well as in the wake of the turbine, by partially blocking and extracting energy from the flow by turbine rotor. Using the steady-state continuity equation ($Q = Au$), this flow reduction indicates that the flow area at the turbine will increase, and even more at the wake shown in the figure below.

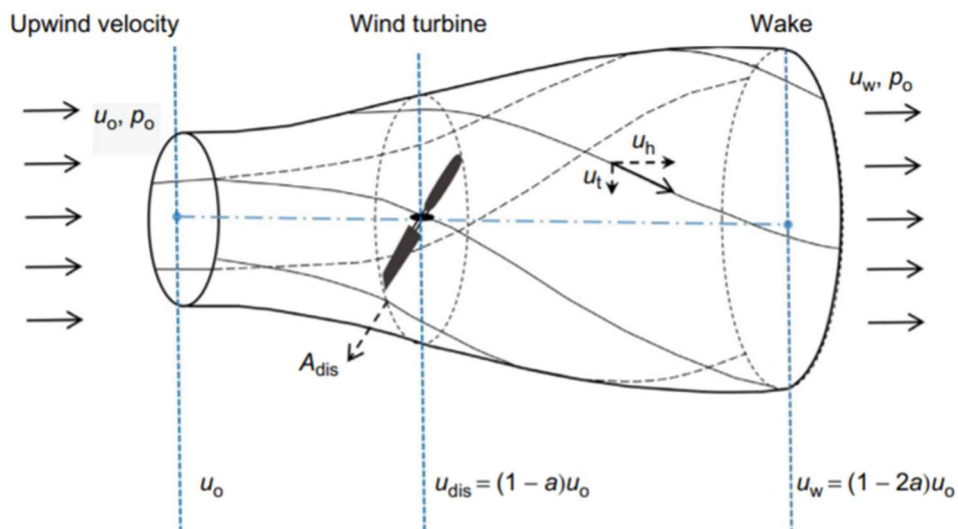


Figure 2-11: Stream tube of a HAWT (Neill, S. P., & Hashemi, M. R.,2018)

The axial flow induction factor (a) can be used to express the average wind velocity at the turbine. A wind turbine with an induction factor of 1 has no effect on upwind velocity ($u_{dis} = u_o$), whereas a turbine with an induction factor of 0 fully blocks/stops the wind ($u_{dis} = 0$).

In practice, the induction factor ranges from 0 to 1. The power coefficient may be demonstrated to be a function of the flow induction factor as follows:

$$C_p = \frac{P_e}{P_t} = 4a(1 - a)^2 \quad (8)$$

At this point, the maximum power coefficient can be easily calculated by taking the derivative of both sides of the above equation.

$$\frac{dC_p}{da} = 4(1 - a)^2 - 8a(1 - a) = 0 \rightarrow a = \frac{1}{3} \text{ and } C_p = \frac{16}{27} \quad (9)$$

Therefore, the maximum power coefficient is $16/27 = 0.593$, corresponding to $a = 1/3$. This limit, calculated above, was revealed by the German scientist Albert Betz, who pioneered wind turbine technology, and is also called the Betz limit, after him [16].

Lastly, wind turbine efficiency, or power coefficient, is not constant and is affected by wind speed. A power curve depicts how a wind turbine's output varies with wind speed. Figure 2-12 indicates a typical power curve. This power curve shows the power coefficient of a typical turbine is at the max range with a rated output wind speed of 12-14 m/s which is the inlet boundary condition of the aerodynamic analysis used in this study.

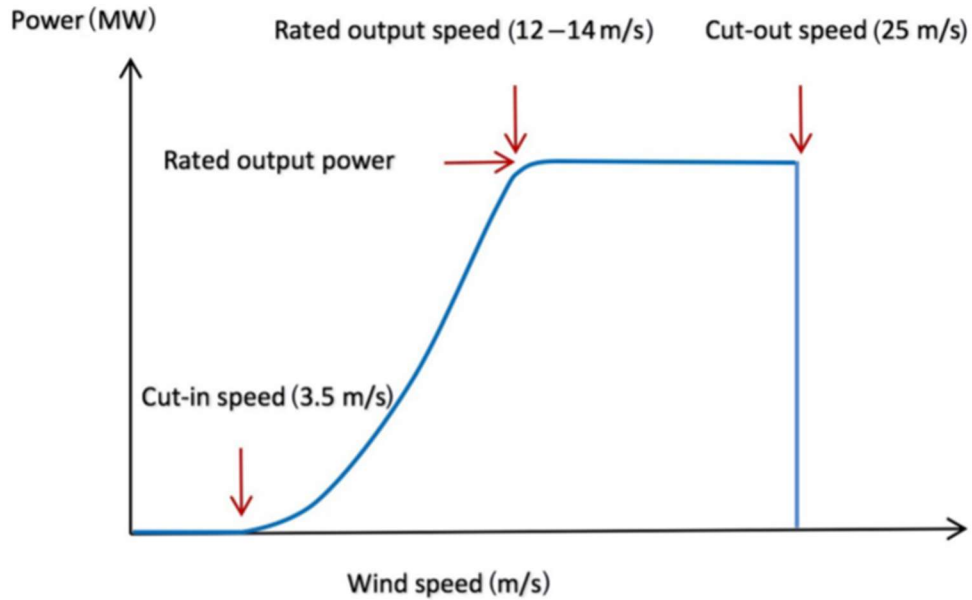


Figure 2-12: A typical power curve for a wind turbine (E. Hau,2010)

2.8. Blade Velocity

The blade speed is shown in Figure 2-13 with colored arrows, which represent the magnitude of rotational speed. As expected, the local blade velocity increases with radius, reaching the maximum value of 98 m/s at the tip of the blade. To calculate the speed on the blade by hand calculation:

$$V = r \times \omega \tag{10}$$

Using angular velocity in problem definition, which is -2.22 rad/s and the blade length of 43.2 and adding extra 1 meter for distance from the root to the hub, tip velocity can be calculated as 98.124 m/s as shown below:

$$V = -2.22 \text{ rad/s} \times -44.2 \text{ m} = \mathbf{98.124 \text{ m/s}}$$

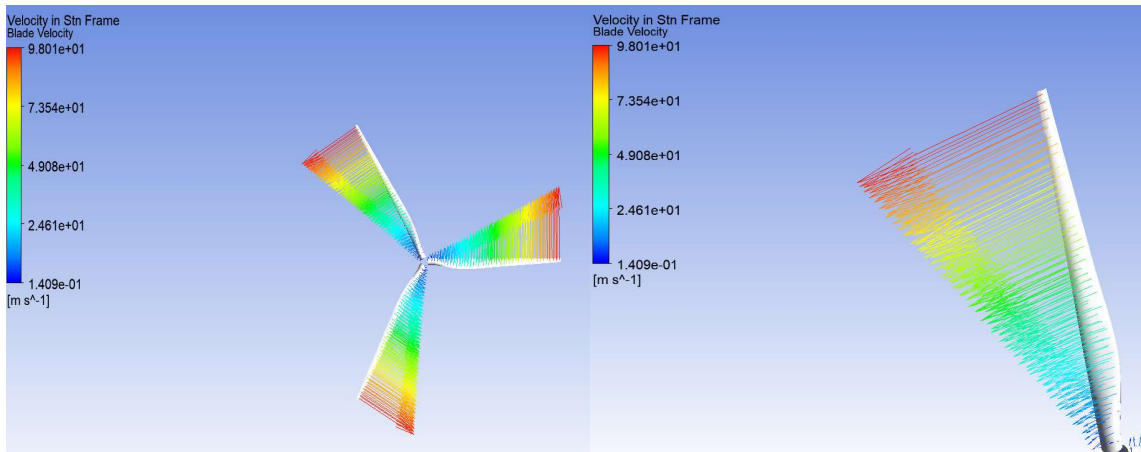


Figure 2-13: Blade velocity in ANSYS Fluent

2.9. Velocity Streamline

Figure 2-14 shows the flow rate in a fixed volume domain. In the simulation, as seen in the figure, the wind comes from the inlet and side surfaces. The wind speed decreases after hitting the turbine blades. In the horizontal direction the velocity is almost evenly distributed; however, the wind speed decreases around the turbine blade.

Inlet has a yellow color, and it is graded 12 m/s (V_0) as it is specified. There is a clear drop in velocity behind the turbine. It indicates the wake behind the turbine ($V_3=10\text{m/s}$). Finally, there is a clear acceleration of flow around the wake, and this is shown by the orange color. This is what is expected from mass and momentum balance.

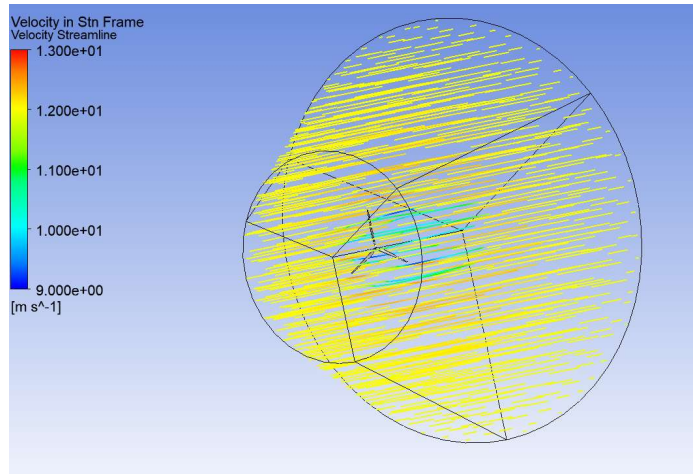


Figure 2-14: Velocity Streamline in the Fluid Domain

2.10. Pressure Contours

The pressure contour of the turbine blade front is shown in Figure 2-15. In comparison to the near root, pressure near the tip is high. It can be also seen that the pressure is higher towards the edges, but lower near the rotor's trailing edge.

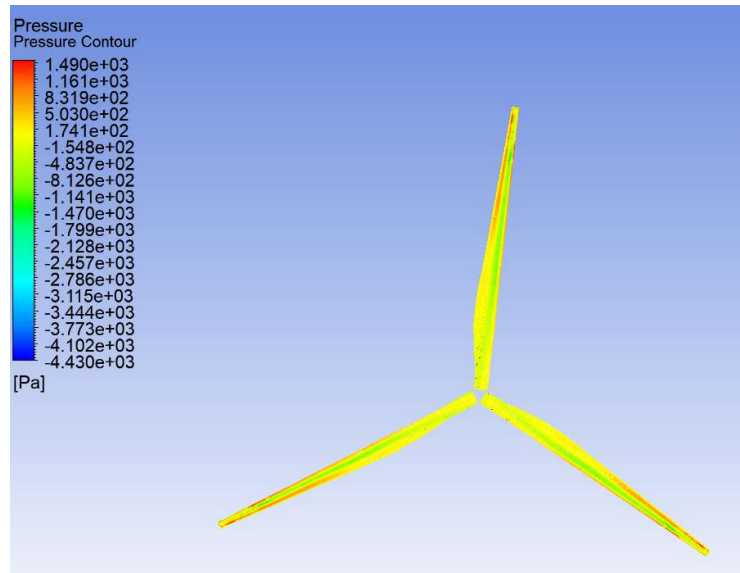


Figure 2-15: Pressure contours in the front of the blade

In Figure 2-16, the pressure contour on the rear of the blade is visualized. This indicates that the pressure in front of the blade is higher but then it drops. Both figures explain that the pressure at the blade tip is greater than the pressure on the side closer to the rotor. The dynamic pressure is greater close to the tip due to the rotation of the blade, which explains why the pressure at the blade tip is greater.

Secondly, the pressure is lower on the back surface of the blade compared to blade front surface since the wind slows down after hitting the blade front surface. This difference between front and back surfaces creates a lift force and the component of the lift in the negative z-direction has a large effect on blade deflection.

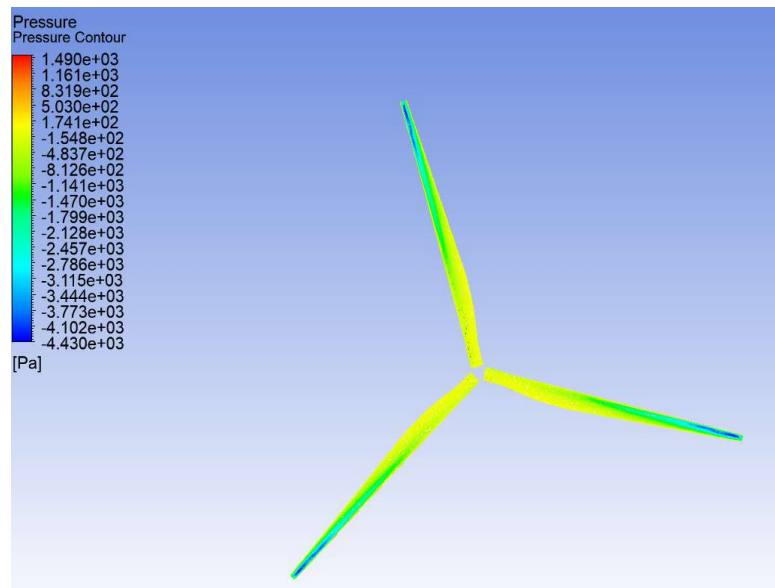


Figure 2-16: Pressure contours in the front of the blade

Pressure contours on the Y-Z plane are displayed to see pressure distribution around the airfoil. While the red color represents a high-pressure zone, the blue color shows a

low-pressure zone. The velocity vector in the Y-Z plane is shown to view the lift force on the airfoil and the lift force is perpendicular to the direction of the velocity stream.

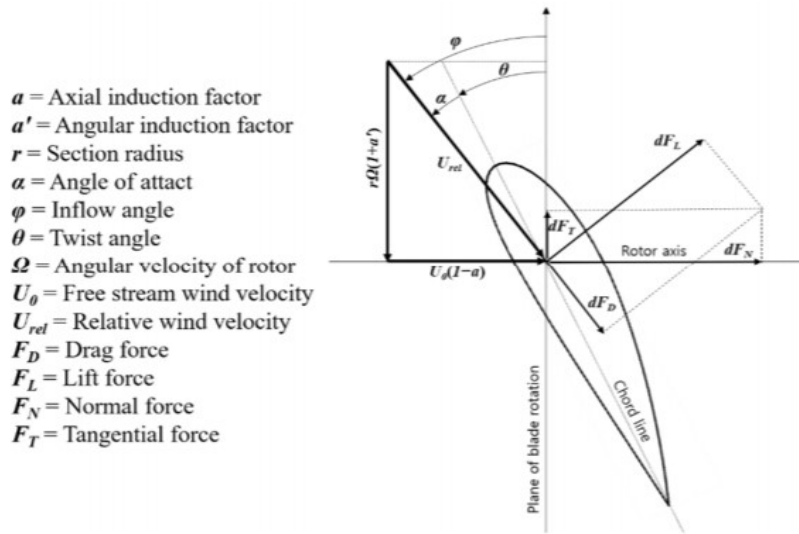


Figure 2-17: Wind velocities and forces (Manwell, J.F,2010)

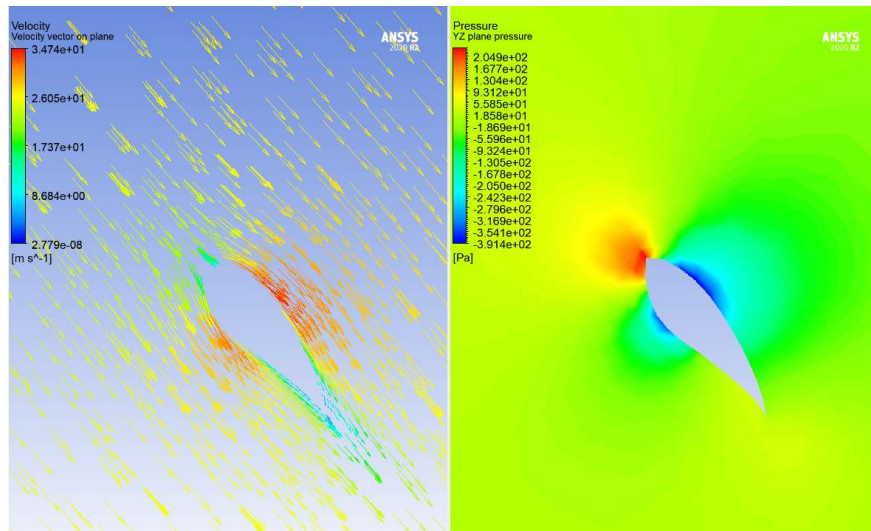


Figure 2-18: Pressure contours over the airfoil

2.12.2. Tip velocity

According to equation 10: $V = r \times \omega = 44.2 \text{ m} \times 2.22 \text{ rad/s} = 98.124 \text{ m/s}$

Analysis result in figure 2-13 shows tip velocity is 98.01 m/s.

Hand-calculation (m/s)	CFD analysis (m/s)	error (%)
98.124	98.01	0.116179528

2.12.3. Power coefficient

Power coefficient can be calculated by equation 11 below.

$$C_p = \frac{P_{rated}}{P_{Wind}} = \frac{P_{rated}}{\frac{1}{2} \rho A V_{rated}^3} \quad (11)$$

$P_{rated} = 1.5 \text{ MW}$ (from turbine specification), $\rho = 1.225 \text{ kg/m}^3$ the rated wind speed to be 11.5 m/s and the rotor diameter to be 82.5 m . Therefore, $C_p = 0.3$ (hand calculation)

Power coefficient (C_p), can also be calculated by using the induction factor (a) as:

$$C_p = 4a(1 - a)^2 \quad (12)$$

Where (a) is the induction factor, the fractional decrease in wind velocity between the free stream and rotor plane can be expressed in terms of an axial induction factor:

$$a = (\vartheta_0 - \vartheta) / \vartheta_0 \quad (13)$$

Where ϑ is the velocity at the disk, and it is defined by:

$$\vartheta = \frac{1}{2} (\vartheta_0 + \vartheta_3) \quad (14)$$

V_0 and V_3 are free streams and downstream velocities, respectively. The amount of axial induction factor determines the amount of power extracted by turbine [17]. From the topic of velocity streamline, $V_3 = 10 \text{ m/s}$ and $V_0 = 12 \text{ m/s}$. Using the equation for induction factor, $C_p = 0.324$.

Hand-calculation	CFD analysis	error (%)
0.3	0.324	8

When the CFD results and mathematical calculations are compared, the results match very well. All these verifications indicate that the blade's aerodynamic analysis has been done successfully.

3. STRUCTURAL ANALYSIS OF THE WIND TURBINE BLADE

Optimum weight and aerodynamic performance are the criteria to be considered for wind turbine blade designs. For this reason, material selection, production technology and the use of advanced design tools are very important in blade design.

The mechanical properties of the selected material are effective on the fatigue life, resistance to stresses caused by high wind load, the prevention of damages that may occur due to excessive loading, and the deformation at the tip. In addition, since the blade weight is proportional to the density of the material used, it also affects the efficiency of the turbine by affecting its aerodynamic performance.

When the literature studies are examined, the rotor efficiency greatly affects the wind turbine efficiency. The geometry of the modeled blade, the material used are extremely important in the rotor efficiency and therefore in the turbine efficiency.

Bechly and Clausen [18] designed the wind turbine blade with glass fiber material to increase the efficiency of the wind turbine and carried out the numerical analysis of this design by developing the Fortran finite element program software. At the end of this study, the most suitable blade design was revealed to reduce the maximum stress on the blade and the deflection at the blade tip under the design conditions with the software they designed.

In another study, Kensche [19] used glass fiber reinforced plastics (GFRP) in his blade model and revealed that composite materials should be used to provide the long fatigue life condition required in blade design.

In parallel with the studies in the literature, in this section, composite materials widely used in the wind turbine industry, such as Epoxy E-Glass, Epoxy S-Glass, Carbon Epoxy and Carbon fiber materials, were used to calculate the Von-Misses stress acting on blade with varying wind speed along 8-20 m/s and deformation on the blade due to the wind pressure. Then, these values obtained by the structural analysis were tabulated and examined with the help of graphics. Lastly, the effect of the mechanical properties of the materials on the deformation of the turbine blade was observed.

3.1. Structural Model of the Blade

The blade generally has two parts called an inner spar and outer surface, as can be seen in the figure. The thickness of the outside surface linearly decreases from 0.1 m at the root to 0.005 m at the tip and the spar has a similar behavior from 0.1 m at the root and 0.03 m at the tip. These thicknesses are actually very close to what can be encountered on a real turbine.

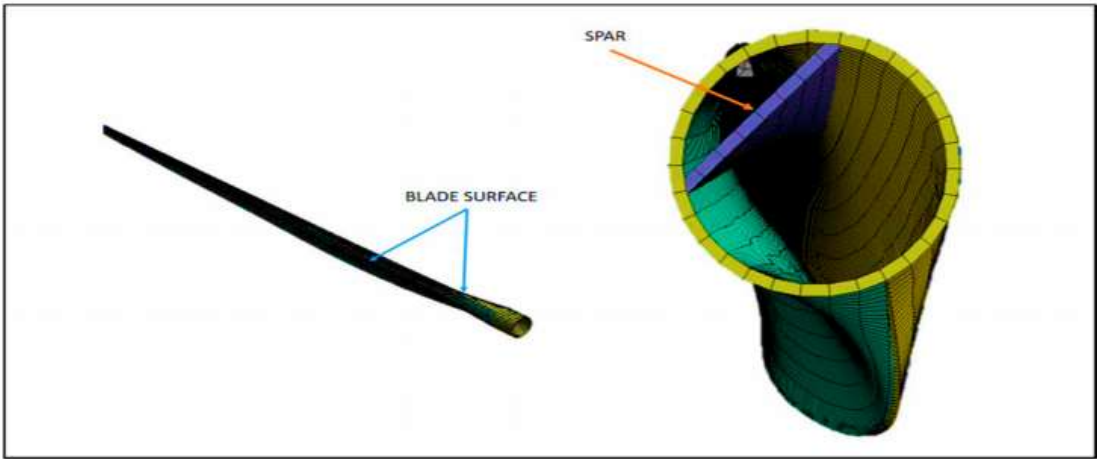


Figure 3-1: Blade structure used in finite element analysis (Rajendra Roul, 2020)

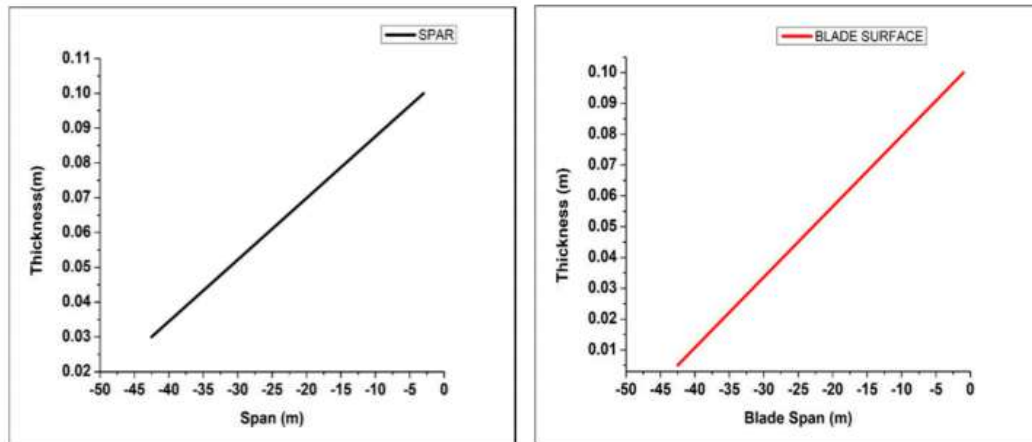


Figure 3-2: Thickness of blade surface and spar along the blade

Wind turbine blades are generally made of composite materials to reduce their weight. Also, in this study, four composite materials are used for the structural analysis, and their mechanical properties, such as elastic modulus, and density, are shown in the tables below. These values are representative of the mechanical properties of composite materials found in real wind turbine blades and defined in Ansys engineering data.

Properties of Outline Row 7: Epoxy E-Glass UD			
	A	B	C
1	Property	Value	Unit
2	Density	2000	kg m ⁻³
3	Orthotropic Elasticity		
4	Young's Modulus X direction	4.5E+10	Pa
5	Young's Modulus Y direction	1E+10	Pa
6	Young's Modulus Z direction	1E+10	Pa
7	Poisson's Ratio XY	0.3	
8	Poisson's Ratio YZ	0.4	
9	Poisson's Ratio XZ	0.3	
10	Shear Modulus XY	5E+09	Pa
11	Shear Modulus YZ	3.8462E+09	Pa
12	Shear Modulus XZ	5E+09	Pa

Table 3-1: Material characteristics of Epoxy E-Glass (Ansys Composite_Materials.xml)

Properties of Outline Row 8: Epoxy S-Glass UD			
	A	B	C
1	Property	Value	Unit
2	Density	2000	kg m ⁻³
3	Orthotropic Elasticity		
4	Young's Modulus X direction	50000	MPa
5	Young's Modulus Y direction	8000	MPa
6	Young's Modulus Z direction	8000	MPa
7	Poisson's Ratio XY	0.3	
8	Poisson's Ratio YZ	0.4	
9	Poisson's Ratio XZ	0.3	
10	Shear Modulus XY	5000	MPa
11	Shear Modulus YZ	3846.2	MPa
12	Shear Modulus XZ	5000	MPa

Table 3-2: Material characteristics of Epoxy S-Glass (Ansys Composite_Materials.xml)

Properties of Outline Row 6: Epoxy Carbon UD (230 GPa) Prepreg			
	A	B	C
1	Property	Value	Unit
2	Density	1490	kg m ⁻³
3	Orthotropic Elasticity		
4	Young's Modulus X direction	1.21E+11	Pa
5	Young's Modulus Y direction	8.6E+09	Pa
6	Young's Modulus Z direction	8.6E+09	Pa
7	Poisson's Ratio XY	0.27	
8	Poisson's Ratio YZ	0.4	
9	Poisson's Ratio XZ	0.27	
10	Shear Modulus XY	4.7E+09	Pa
11	Shear Modulus YZ	3.1E+09	Pa
12	Shear Modulus XZ	4.7E+09	Pa

Table 3-3: Material characteristics of Epoxy Carbon (Ansys Composite_Materials.xml)

Properties of Outline Row 4: Carbon Fiber (230 GPa)			
	A	B	C
1	Property	Value	Unit
2	Density	1800	kg m ⁻³
3	Orthotropic Elasticity		
4	Young's Modulus X direction	2.3E+11	Pa
5	Young's Modulus Y direction	2.3E+10	Pa
6	Young's Modulus Z direction	2.3E+10	Pa
7	Poisson's Ratio XY	0.2	
8	Poisson's Ratio YZ	0.4	
9	Poisson's Ratio XZ	0.2	
10	Shear Modulus XY	9E+09	Pa
11	Shear Modulus YZ	8.2143E+09	Pa
12	Shear Modulus XZ	9E+09	Pa

Table 3-4: Material characteristics of Carbon Fiber (Ansys Composite_Materials.xml)

3.2. Start-up

Firstly, a static structural analysis system was chosen, and material properties shown in the table were put in the Engineering Data. Then, the blade geometry was copied to new project to use for the new analysis.

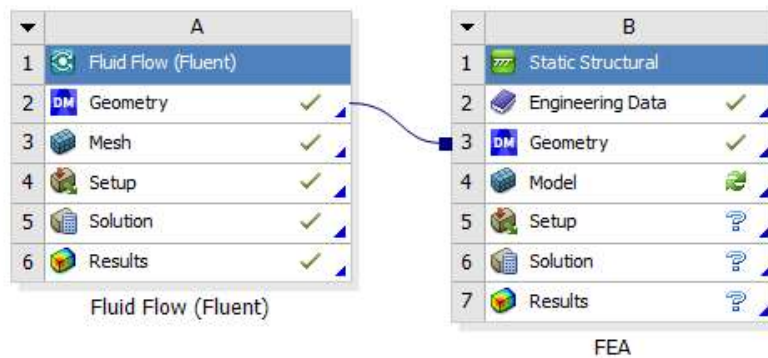


Figure 3-3: Connection between CFD project and FEA project

3.3. Mesh

Name selection was created for spar and blade surfaces before creating the mesh. Local mesh settings (face meshing and face sizing) are implemented to improve mesh quality. After mesh generation, there are around 5000 components, which is significantly less than in the aerodynamic section. However, the aerodynamic model involves complex wind turbine blade geometry and flow physics, orthogonal quality is close to 1, which means mesh is pretty good.

Statistics		Mesh Metric	Orthogonal Quality
<input type="checkbox"/> Nodes	5079	<input type="checkbox"/> Min	0.7706
<input checked="" type="checkbox"/> Elements	5227	<input type="checkbox"/> Max	1.
		<input type="checkbox"/> Average	0.98666
		<input type="checkbox"/> Standard Devi...	2.2448e-002

Figure 3-4: Mesh statistics

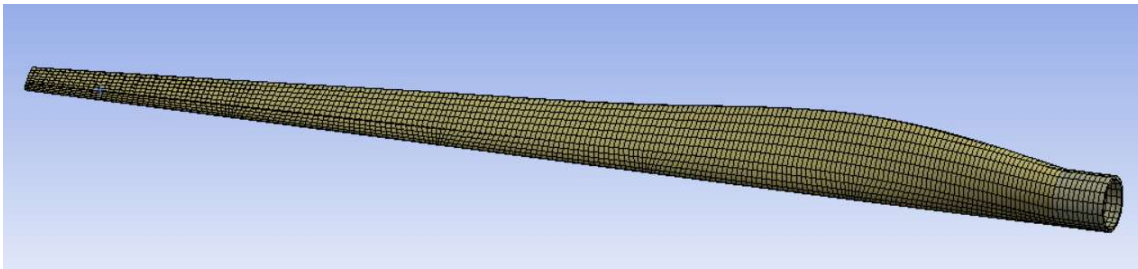


Figure 3-5: Mesh for FEA analysis

3.4. Model Setup

To begin, rotational velocity was added as -2.22 rad/s in the z-component, and aerodynamic loads obtained from the Fluent module were transferred into the structural analysis. Later, the material properties were implemented, and thickness values shown in problem statement were inserted linearly from 0.1 m to 0.005m for blade surface. A similar

process has been done for spar as well, from 0.1 to 0.03m by using a tabular section in the thickness definition.

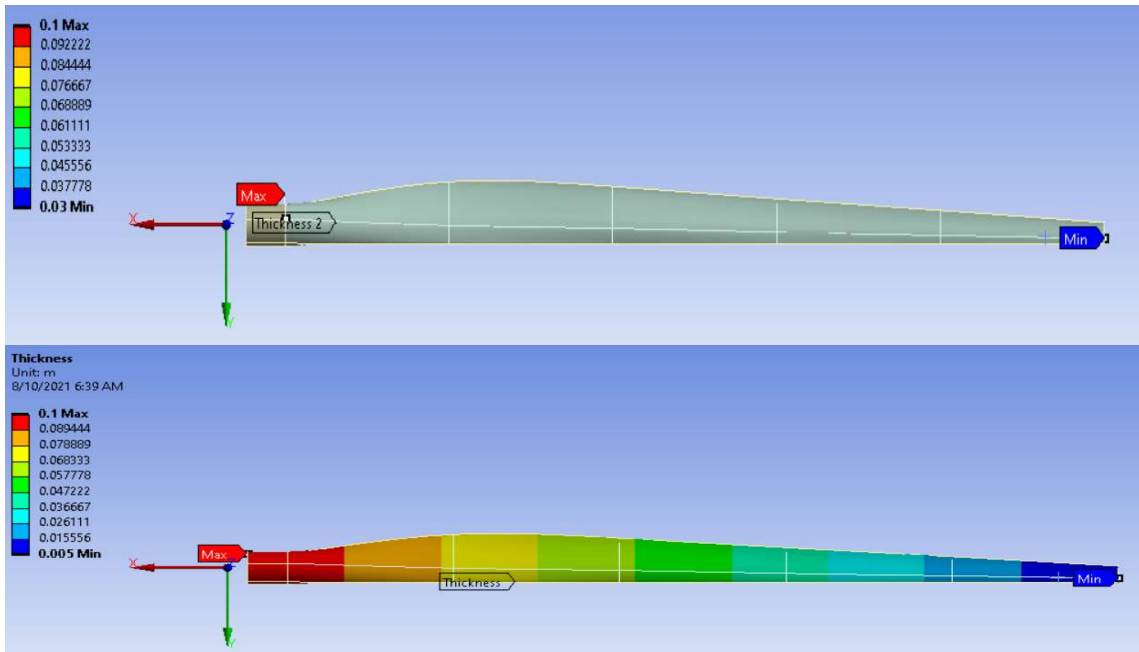


Figure 3-6: Blade with varying thickness

3.5. Pressure Loads

In the next step, the pressure load was imported from Fluent to Mechanical. One good takeaway from Figure 3-27 is that the region of low fluid pressures contributes enormously to the pressure load experienced by the blade. Therefore, the blade will tend to be forced toward the side that has lower pressure.

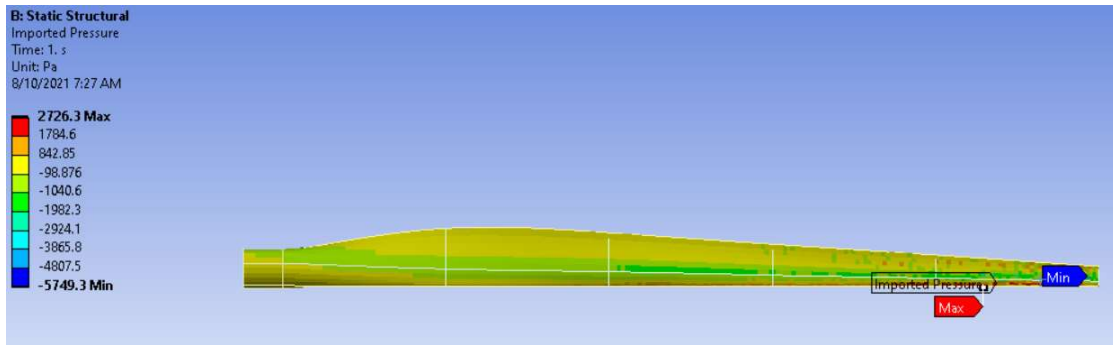


Figure 3-7: Pressure load acting on the blade at 12 m/s

3.6. Total Deformation

Given the pressure load, the blade appears to be deflecting as expected. Actual wind turbine blades deform away from the incoming wind. The maximum deformation occurs at the blade tip, whereas the deformation of the blade near the hub is almost insignificant. The deformation values of the blade, in which four different composite materials are applied (E-Glass, S-Glass, Epoxy Carbon, and Carbon Fiber, respectively), can be seen below figures. The analysis was run repeatedly at speeds of 8-10-12-15-18-20 m/s, and the total deformation at all these speeds was calculated separately.

The expectation before the analysis is that E-Glass material, which has the lowest Elastic modulus, will have the largest tip deformation, followed by S-Glass, Carbon Epoxy, and Carbon fiber materials, respectively.

Secondly, the deformation and equivalent stress will increase as the wind speed increases. The results will be discussed with the help of tables and graphs in the conclusion part.

The total deformation on the blade due to the wind load at different speeds was provided in Appendix A.

Table 3-5 and figure 3-8 show the total deformation for all wind speed and materials below.

Wind Speed (m/s)	Epoxy E-Glass (m)	Epoxy S Glass (m)	Epoxy Carbon (m)	Carbon Fiber (m)
8	0.4748	0.4418	0.2194	0.1205
10	0.6544	0.6092	0.3054	0.1669
12	0.8074	0.7504	0.3806	0.2075
15	1.0022	0.9088	0.4672	0.2545
18	1.0727	0.9957	0.5001	0.2724
20	1.1189	1.0487	0.52	0.2835

Table 3-5: Total deformation at various wind speed

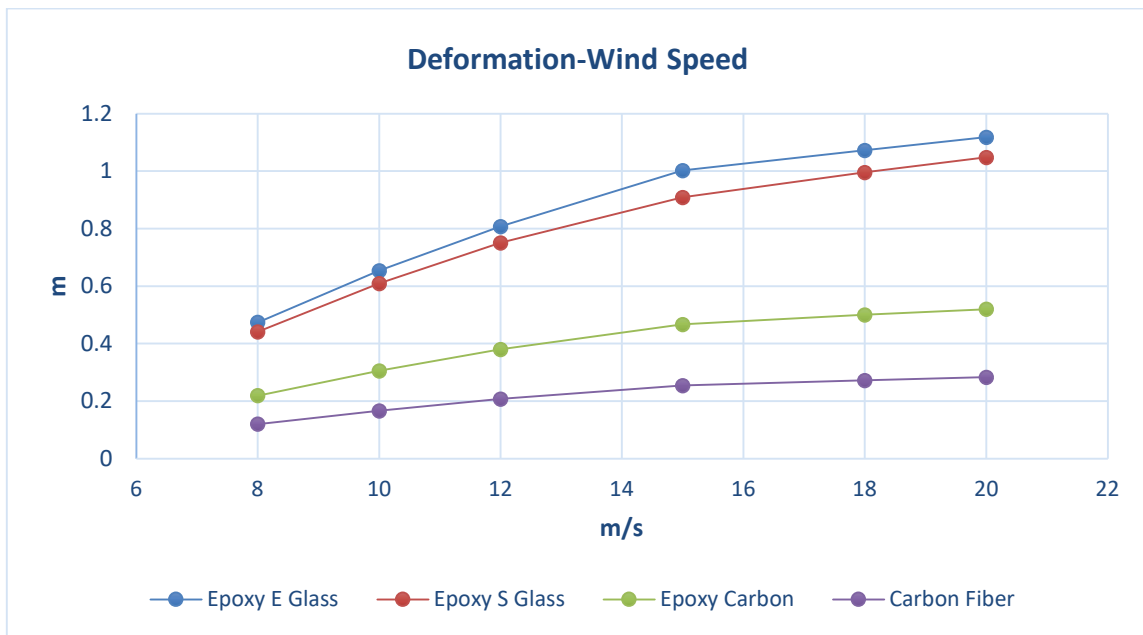


Figure 3-8: Total Deformation-Wind Speeds

3.7. Equivalent Stress

It is important to show and detect where the maximum stresses occur. When the stress distribution of the blade is examined, it shows that the stress at the trailing edge of

the wind turbine blade is smaller than on the leading edge. The maximum stress is located close to leading edge. Similar calculations for deformation were also done for von-Mises stress.

In Appendix B, von Mises stresses the blade due to the wind load at different speeds were provided.

Wind Speed (m/s)	Epoxy E-Glass (mPa)	Epoxy S-Glass (mPa)	Epoxy Carbon (mPa)	Carbon Fiber (mPa)
8	2565	2585	2544	2847
10	3153	3192	3247	3577
12	3652	3695	4242	4275
15	4229	4300	5438	5467
18	4463	4654	5837	5867
20	4629	4820	6083	6113

Table 3-6: Von-Misses stress at various wind speed

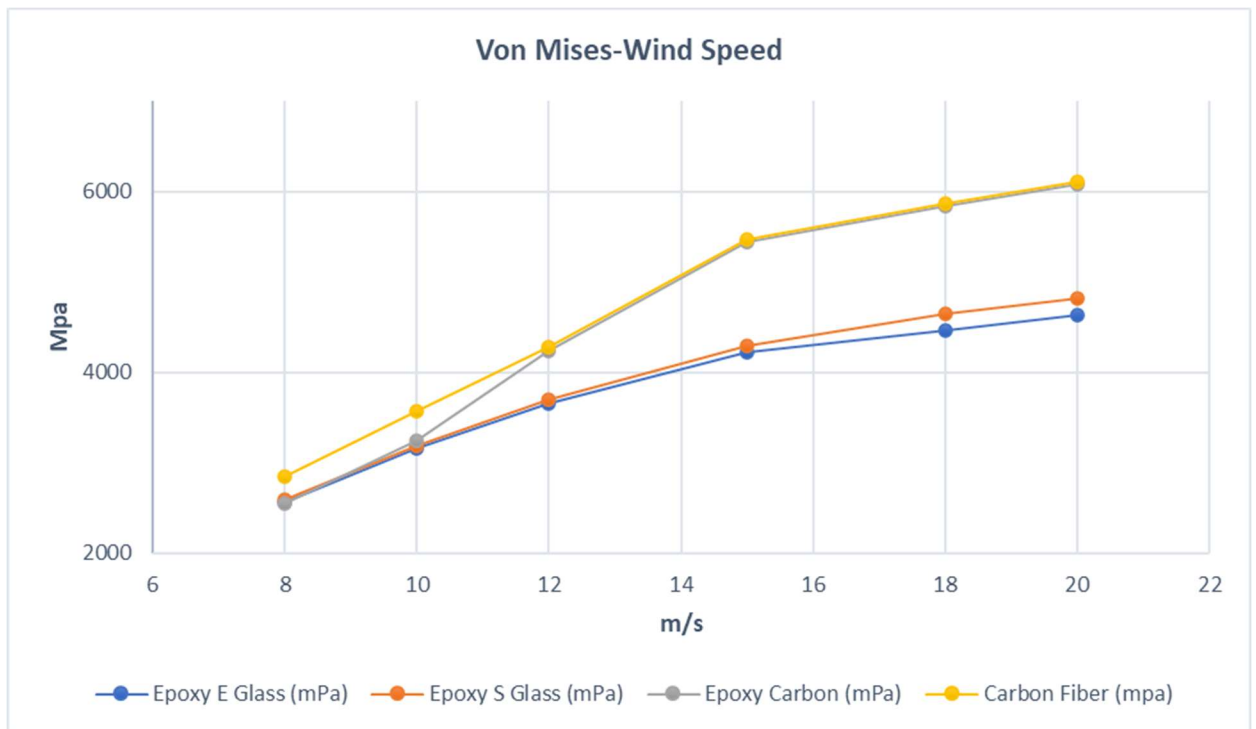


Figure 3-9: Von Mises Stress-Wind Speed

3.8. Force Reaction

Force and moment reaction calculations were made at 12 m/s. Almost all the force reaction is in the x-direction and considering the centripetal acceleration acting on this blade, and it is sensible.

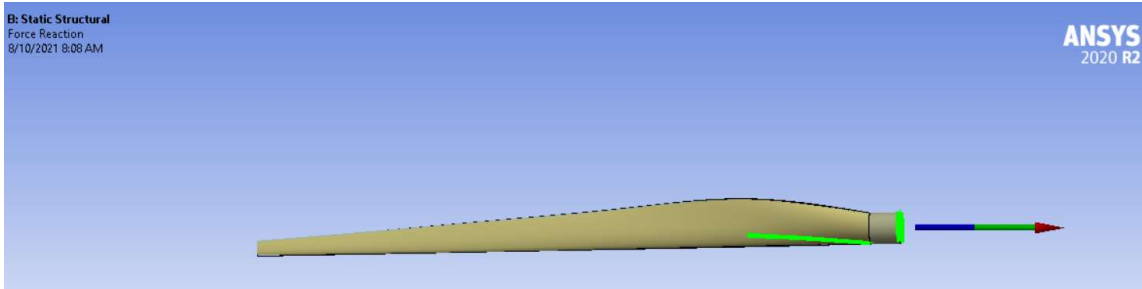


Figure 3-10: Force reaction for the blade in ANSYS Mechanical

After checking solution information for force reaction, the blade weight is calculated 22,537 kg and its center of mass (X, Y, Z) is located at the coordinate (-14.229 m, -0.2085 m, 0.162 m). Using these values, force reaction calculated by the Ansys, and hand calculation will be compared, and calculations will be verified.

TOTAL MASS = 22537.	
The mass principal axes coincide with the global Cartesian axes	
CENTER OF MASS (X,Y,Z)=	-14.229 -0.20852 0.16235
Maximum Value Over Time	
<input type="checkbox"/> X Axis	1.5812e+006 N
<input type="checkbox"/> Y Axis	16539 N
<input type="checkbox"/> Z Axis	67238 N
<input type="checkbox"/> Total	1.5827e+006 N

Table 3-7: Radial force distribution

The blade is oriented so that the x-axis points along the radial direction of the blade.

Plugging in these values in the radial force equation below:

$$F_{radial} = -mr\omega^2 \tag{15}$$

$$F_{radial} = -(22537 \text{ kg}) \times (-14.229\text{m}) \times (-2.22 \text{ rad/s})^2 = 1580 \text{ kN}$$

Accurate calculation of radial forces is a critical design consideration for anything involving circular motion. Correctly determining of redial forces play an important role in the efficiency, safety, and service life of the equipment. When the results of the hand calculation and the numerical results are compared, they appear to be very similar.

Hand-calculation (kN)	Static analysis (kN)	error (%)
1580	1582.7	0.170886076

3.9. Moment Reaction

Most of the response bending moment appears to be centered on the y-axis. This is to be expected, given the pressure on this blade and how it deforms. 2.36 KN.m was determined as the total moment reaction.

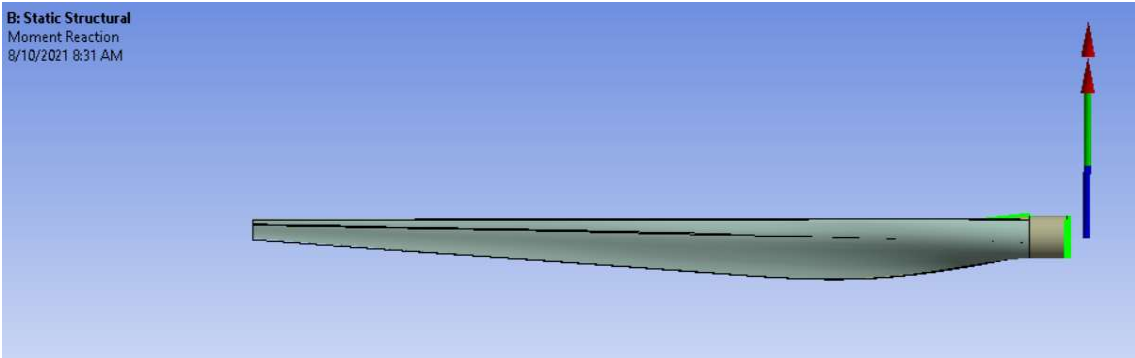


Figure 3-11: Moment reaction of the blade

Maximum Value Over Time	
<input type="checkbox"/> X Axis	22686 N·m
<input type="checkbox"/> Y Axis	2.3557e+006 N·m
<input type="checkbox"/> Z Axis	1.3804e+005 N·m
<input type="checkbox"/> Total	2.3599e+006 N·m

Table 3-8: Moment reaction

3.10. Turbine Blade Categorization Based on Structural Zones

A wind turbine blade can be divided into three categories based on their aerodynamic and structural functions, and information below should be considered when a wind turbine model is created.

3.10.1. The blade root

This segment carries the highest load as it transitions from the circular mount to the first airfoil shape. Due to a low relative wind velocity in this part, there is less aerodynamic lift, and it results in long chord lengths. As a result, the blade profile at the rotor hub becomes large. It is necessary to use thick airfoil sections to improve structural integrity in this load-intensive location. As a result, thick airfoil designs with low aerodynamic efficiency will often be found at the blade's root area.

3.10.2. The mid-span

Aerodynamic efficiency is significant at this section. Therefore, the thinnest airfoil should be considered while this section is modeled as structural limits allow.

3.10.3. The tip

Since the lift to drag ratio will be maximized, aerodynamic efficiency is critical at this part. Thus, it is crucial to use slender airfoils and specially designed tip geometries to reduce noise and losses in this section [20].

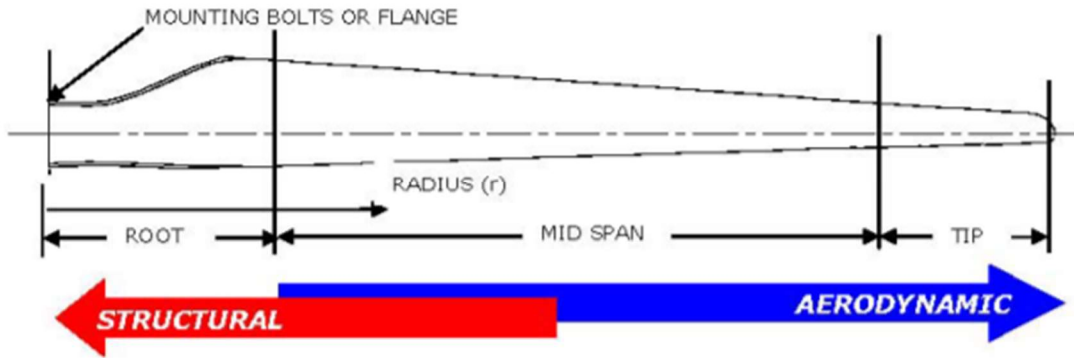


Figure 3-12: Turbine blade regions considering aerodynamic and structural efficiency (Armen Sargsyan,2010)

4. CONCLUSIONS OF THE BLADE AERODYNAMIC AND STRUCTURAL ANALYSIS

In this first step of the study, the NREL S-series 43.2 meters long wind turbine blade has been chosen. Aerodynamic and static analyses were studied by using computational fluid dynamics methods for the blade. The obtained CFD results are compared with the mathematical calculation.

The blade velocity increases with radius, and the velocity at the tip reaches the highest velocity, which is about 98,01 meters per second. This result matches perfectly with mathematical calculations. The power coefficient (C_p) was calculated (0.324) using velocity streamline, and this result was verified with hand calculation. Thanks to pressure contours, pressure distribution around airfoil and lift forces were visualized. Lastly, torque analysis was made, and the contribution of pressure difference and viscous forces to torque was provided by the Fluent.

The pressure load calculated in the aerodynamic analysis was used in the structural analysis. The deformation caused by the pressure load acting on the blade was visualized for four different composite materials. Deformation analysis was performed repeatedly at speeds of 8-10-12-15-18-20 m/s, and the total deformation at all these speeds was calculated separately for all materials. Figures in Appendix A show that the deformation of the blade near the hub is insignificant, and the maximum deformation occurs at the blade tip.

The deformation occurring in the blade was assumed as elastic. According to a typical stress-strain curve, the larger the elastic modulus of the material, the more rigid the

material. The smaller the elastic module, the more deformation on the material. That means the material with a bigger elastic module shows less deformation with stress.

E-Glass has the smallest young module, followed by S-Glass, Carbon Epoxy, and Carbon Fiber, respectively. Based on this information, it is expected that the blade that has the biggest deformation will be made of E-Glass material and then S-Glass, Epoxy Carbon, and Carbon Fiber, respectively. In addition, as the wind speed increases, the force and deformation on the blade will also increase.

Figure 3-8 and Table 3-5, which are obtained from the analysis, confirm the information above. In addition, in parallel with the expectation before the analysis, the total deformation gets larger as the wind speed increased since the wind load acting on the blade also increased. Therefore, this part of the study has achieved its purpose.

In the next step, the stress distribution of the blade was provided. The maximum stress is located close to the leading edge. Also, as the wind speed increased, the von-Mises stress on the blade increased for all material types according to Figure 3-9, as expected.

Lastly, the force and momentum reaction of the turbine blade was examined. While all the force reaction is in the x-direction, the most reaction bending moment is about the y-axis.

In this part of the study, only the static performance of the composite materials used in the blade was investigated according to the deformation rates, but this is not the only criterion in material selection. Many other factors, such as the density of the material, fragility, hardness, price, etc., play a role in material selection.

5. TOWER STRUCTURE ANALYSIS CONSIDERING WIND LOAD

In the second part of the study, the length ratio between the turbine blade and the tower was determined by using examples from wind turbines used in the industry. Access to the geometries of the sample turbines is not possible due to confidentiality, and academic studies do not mention a specific blade-to-tower ratio. For these reasons, while deciding on the turbine tower dimensions, the wind turbine towers used in the industry were examined.

The wind turbine tower was tried to be modeled for offshore conditions using ASCE (American Civil Engineering Association) standards. Design wind loads calculation coming directly to the tower, and the explanation of calculation stages specified in the "Minimum Design Loads for Buildings and Other Structures" ASCE 7-02 (2006) standard are the scopes of this part of the thesis.

The main objective of the design is to test whether the structure is suitable for the calculated design wind load for offshore conditions by performing fatigue, buckling, and stress analysis.

5.1. Types of Wind Turbine Tower

Wind turbine towers are available in a variety of construction systems and materials. Towers are composed of reinforced concrete or structural steel as a material, and they are generally in the industry with four different building systems. According to the towers construction systems, towers can be classified as lattice types, cylindrical towers in which

structural steel is used, cylindrical towers in which reinforced concrete material is used, and finally, hybrid towers in which two main materials are used together.

5.1.1. Lattice Towers

Historically, lattice towers were popular in the industry until 1980s [21]. Lattice-type towers generally consist of angle sections, and the connection of the joint elements to the main bearing legs and the connection of the main bearing legs to each other is provided by bolts.

They provide a price advantage compared to other tower types since the manufacturing parts and setup are more manageable. In addition, the smaller surface area compared to cylindrical steel towers provides less wind force on the tower [15]. However, this situation creates a disadvantage for lattice-type towers by creating difficulties in maintenance and repair works in cold weather.



Figure 5-1: Lattice-type wind turbine tower (DNV/Risø, 2002)

5.1.2. Cylindrical Steel Towers

Cylindrical steel towers are the most preferred tower type. The high strength it provides plays an important role in the preference. Steel cylindrical towers consist of body and flange connections with prestressed bolts. The body elements connect vertically and consist of 2-3m cylindrical cones (Figure 5-2). These truncated cones are combined with the help of welding to form their main segments [15].

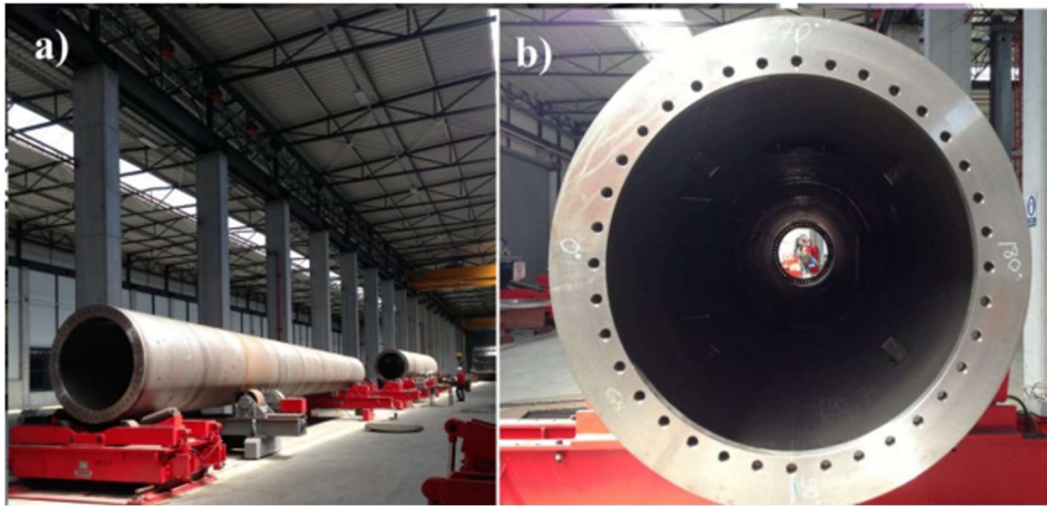


Figure 5-2: Cylindrical steel tower type a) tower body b) flange (Kanbur, 2014)

Diameter values decrease towards the upper regions of the tower, and the wall thickness varies with height. These features provide a significant economic advantage for this type of tower. It is a big advantage that cylindrical steel towers require fewer connection elements than lattice-type towers and, therefore, less maintenance. In addition, providing a safer climbing area compared to lattice-type towers is one of the main reasons for their preference [3]. The high strength demand that arises with the increasing tower height can be met by increasing the thickness.

5.1.3. Reinforced Concrete Towers

Concrete, which is used as the primary material in most products in the construction sector, has been overshadowed by structural steel in the wind energy sector. However, the resonance tendency of cylindrical steel towers in high-scale wind turbines has increased the demand for reinforced concrete towers [22].

They are formed by combining reinforced concrete panels on site. The usage of reinforced concrete structures is more common than structural steel in many areas of civil engineering. Therefore, transportation of reinforced concrete wind turbine towers is more economical [23].

Cracks do not occur under service loads. Thus, they have high fatigue strength. In addition, local buckling, which can affect the design of steel towers, is not seen in reinforced concrete towers, and these are advantages of this type of tower [24].



Figure 5-3: Tubular Reinforced Concrete Towers (DNV/Risø, 2002)

5.1.4. Hybrid Towers

Hybrid towers are towers in which steel and reinforced concrete construction systems are used together (Figure 5-4). They are designed as a reinforced concrete tower at the bottom and a cylindrical steel tower at the top, and they take advantage of both

construction systems. The transportation and construction problems that hinder the design of high towers are eliminated with this tower type.



Figure 5-4: Example of hybrid tower (Anonym)

Lanier (2005) stated that for an all-reinforced concrete 100-meter-height tower, the large single foundation requirement and demand for high strength and higher cranes to lift precast segments would incur extra costs. If the upper part is a cylindrical steel tower in a hybrid tower, overall weight will reduce. Thus, all three problems are eliminated, and weight reduction also helps reduce earthquake loads [24].

5.2. Wind Turbine Tower Selection

A cylindrical steel tower design was chosen by considering the design wind load and since this type of tower is commonly used in offshore-onshore models due to their high strength. According to the comparison of common industrial wind turbines, 60m hub

height can be considered suitable for the blade whose static and aerodynamic analyses were done before.

Blade Length (m)	Blade Diameter(m)	Rated Power (5 MW)	Hub Height (m)	Turbine Type
31.25	62.5	5	90	Semisubmersible
31.25	62.5	5	87.5	Tensile Leg
31.25	62.5	5	77.6	Fixed
44.5	89	10	119	Fixed
60	120	15	150	Fixed
17.625	35.25	1.5	64.7	GE 1.5S
19.25	38.5	1.5	80	GE 1.5 SLE
20.5	41	1.65	70	Vestas V82
22.5	45	1.8	80	Vestas V90
27.5	55	2	95	Vestas V110
28	56	3	84	Vestas V112
23.25	46.5	2.3	80	Siemens

Table 5-1: Size specifications of common industrial wind turbines

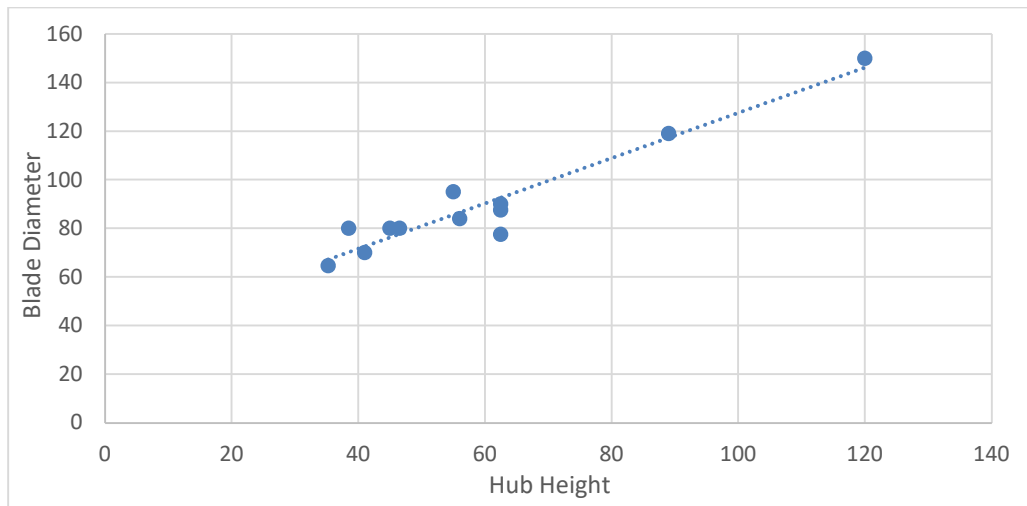


Figure 5-5: Blade diameter-hub height of common industrial wind turbines

The cylindrical tower will be made up of four blocks and thirty-two sections connected by internal flange-bolt connections. Furthermore, bolts link the tower to the foundation (the foundation can be onshore or offshore). The tower's height is 60m, and

the outer diameter of the tower varies between 2.4m and 3.36m. All dimensions of the modeled turbine can be seen in the technical drawing below.

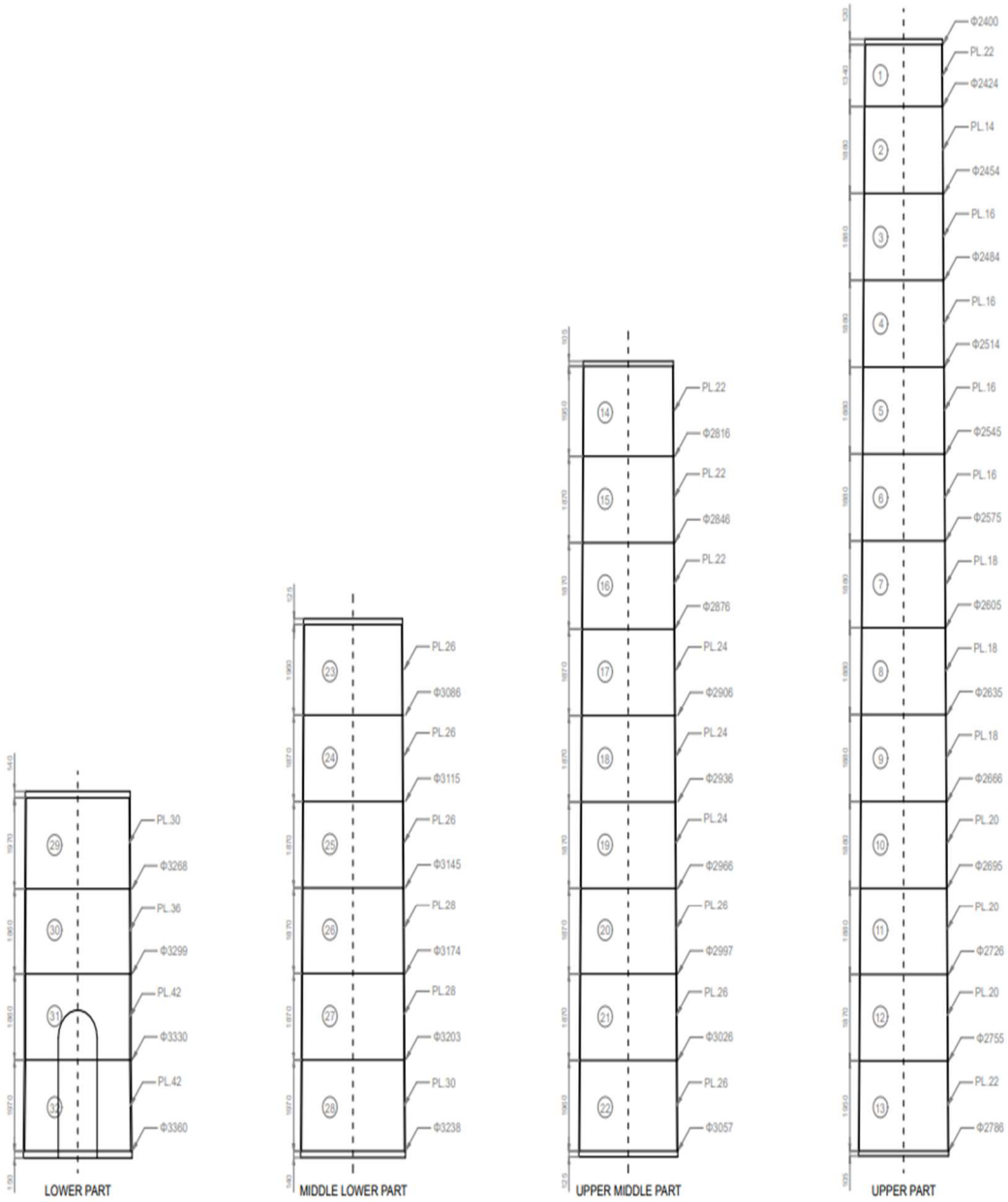


Figure 5-6: Technical drawing of the wind turbine tower

Section	Height (m)	Diameter (m)	Section Height (m)	Projected Area (m²)	Thickness (m)	Moment of Inertia	
Rotor+Nacelle	60.00	2.400					
1	58.66	2.424	1.34	3.22	0.022	0.1231	Section 1-13 Upper Part
2	56.78	2.454	1.88	4.59	0.014	0.0813	
3	54.90	2.484	1.88	4.64	0.016	0.0963	
4	53.02	2.514	1.88	4.70	0.016	0.0999	
5	51.15	2.545	1.88	4.75	0.016	0.1036	
6	49.27	2.575	1.88	4.81	0.016	0.1073	
7	47.39	2.605	1.88	4.86	0.018	0.1249	
8	45.52	2.635	1.88	4.92	0.018	0.1294	
9	43.64	2.666	1.88	4.97	0.018	0.1339	
10	41.76	2.695	1.88	5.03	0.02	0.1538	
11	39.89	2.726	1.88	5.08	0.02	0.1590	
12	38.01	2.755	1.87	5.14	0.02	0.1643	
13	36.06	2.786	1.95	5.40	0.022	0.1868	
14	34.11	2.816	1.95	5.46	0.022	0.1929	Section 14-22 Upper Middle
15	32.24	2.846	1.87	5.30	0.022	0.1991	
16	30.37	2.876	1.87	5.35	0.022	0.2055	
17	28.50	2.906	1.87	5.41	0.024	0.2314	
18	26.62	2.936	1.87	5.46	0.024	0.2385	
19	24.75	2.966	1.87	5.52	0.024	0.2460	
20	22.88	2.997	1.87	5.57	0.026	0.2748	
21	21.02	3.026	1.87	5.63	0.026	0.2830	
22	19.05	3.057	1.96	5.97	0.026	0.2917	
23	17.09	3.086	1.96	6.03	0.026	0.3002	Section 23-28 Middle Lower
24	15.23	3.115	1.87	5.79	0.026	0.3087	
25	13.36	3.145	1.87	5.84	0.026	0.3176	
26	11.49	3.174	1.87	5.90	0.028	0.3518	
27	9.63	3.203	1.87	5.95	0.028	0.3614	
28	7.66	3.238	1.97	6.33	0.03	0.3998	
29	5.69	3.268	1.97	6.39	0.03	0.4112	Section 29-32 Lower Part
30	3.83	3.299	1.86	6.11	0.036	0.5077	
31	1.97	3.330	1.86	6.17	0.042	0.6089	
32	0.00	3.360	1.97	6.59	0.042	0.6257	

Table 5-2: Tower dimensions and calculation of the moment of inertia

5.3. Wind Model

To determine design wind load, an approximation of the wind speed at every given height is necessary. The wind velocity profile as it approaches a wind turbine might resemble the diagram below. The log law and the power law are two typical wind shear models that may be used to determine the wind profile at any given height [3].

$$\frac{U(z)}{U(z_r)} = \left(\frac{z}{z_r}\right)^\alpha \quad (16)$$

$U(z)$ = target height wind speed (m/s)

$U(z_r)$ = reference height wind speed (m/s),

z = target height (m),

z_r = reference height (m)

α = power law exponent

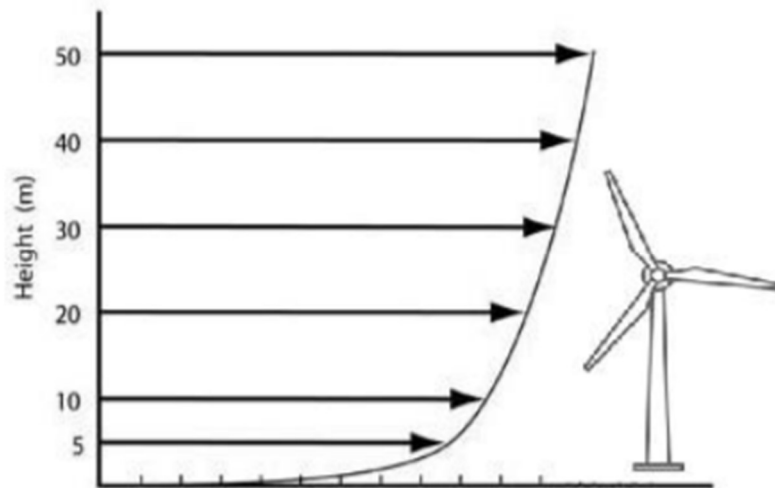


Figure 5-7: Wind shear profile (Ryan Wass,2018)

The wind speed calculation according to offshore conditions using the power law for every tower section can be seen below. These values will be used in further calculations.

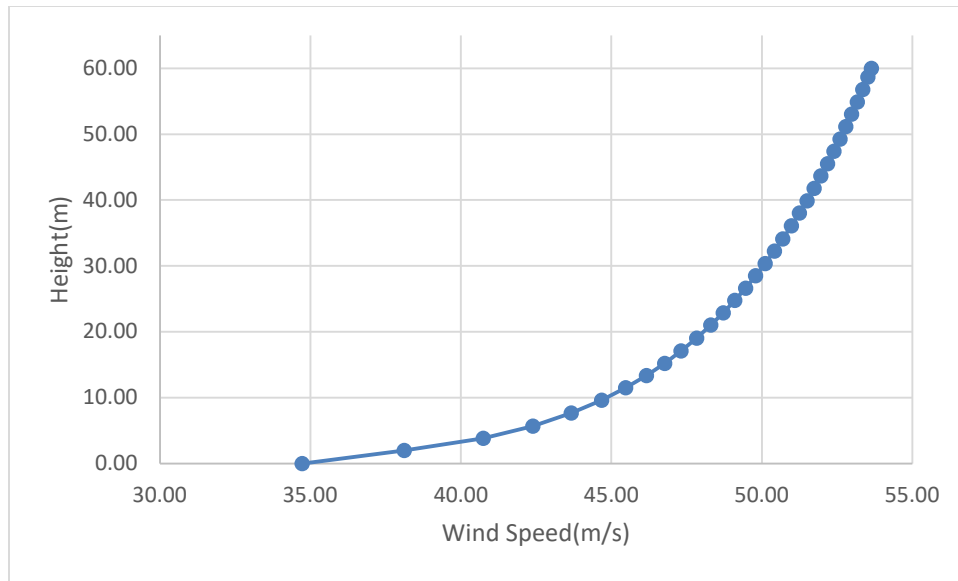


Figure 5-8: Wind speed calculation for offshore conditions (53,64 m/s basic wind speed)

5.4. Determination of Design Wind Load and Pressure

It is complicated to predict the wind loads acting on the structures during the operation period of the structure. Therefore, the standards allow calculating possible wind loads affecting the structure and the wind forces acting on the building surface economically and safely. Using the maximum wind speed to calculate the wind load affecting the structure will give unnecessary and uneconomical data.

Standard documents generally contain data about structures, past experiences, and information obtained from research. Many standards have been developed thanks to the work of related companies and government departments. In developing a standard, joint decisions and opinions of engineers working in various units are used.

It is necessary to determine the design wind speed, wind speed distribution, turbulence intensity, and statistical data to obtain the maximum wind load for the ultimate

wind speed (storm) required by the wind turbine tower structure design, as well as the wind load and fatigue load during power generation.

According to ASCE 7-02 “Minimum Design Loads for Buildings and Other Structures” standards, the design wind load was calculated step by step in the following stages of the study.

5.4.1. Velocity Pressure

The Bernoulli Equation is used in the velocity pressure calculation given below.

$$q = \frac{1}{2} \rho V^2 \quad (17)$$

In Equation 17, when the unit of velocity is m/s, the specific gravity of the air is kg/m³, and the acceleration of gravity is m/s²:

$$q_z = 0,613V^2 \quad (18)$$

Here, q_z is the velocity pressure at height z from the ground.

$$q_z = 0,613 \cdot K_z \cdot K_{zt} \cdot K_d \cdot I \cdot V^2 \quad (19)$$

Here: K_z = Velocity pressure expose coefficient depends on height, K_d = wind directional factor, K_{zt} = topographic factor, I = Importance factor, V = basic wind speed. These coefficients are examined one by one below [25].

5.4.1.1. Velocity Pressure Expose Coefficient, K_z

K_z values vary depending on the terrain roughness, land category, and building height. Offshore conditions will be considered for land category. The exposure coefficients that change depending on the height of the building are given in Table 5-3. The values of K_z can be calculated using Equation 20 and Equation 21 given below.

In the following equations, z_g represents the nominal height. Nominal height values are given in Table 5-3.

For $15 \text{ ft (4.6 m)} \leq z \leq z_g$,

$$K_z = 2,01 \left(\frac{z}{z_g} \right)^{2/a} \quad (20)$$

For $z \leq 15 \text{ ft (4,6 m)}$,

$$K_z = 2,01 \left(\frac{15}{z_g} \right)^{2/a} \quad (21)$$

Exposure	α	z_g (ft)	\hat{a}	\hat{b}	$\bar{\alpha}$	\bar{b}	c	l (ft)	$\bar{\epsilon}$	z_{\min} (ft)*
B	7.0	1200	1/7	0.84	1/4.0	0.45	0.30	320	1/3.0	30
C	9.5	900	1/9.5	1.00	1/6.5	0.65	0.20	500	1/5.0	15
D	11.5	700	1/11.5	1.07	1/9.0	0.80	0.15	650	1/8.0	7

Table 5-3: Terrain exposure constants (ASCE 7-02, Table 6-2)

According to standard, Exposure D should be considered for flat, unobstructed areas, water surfaces, and areas where the storm is active. Considering Exposure Type D and the height of the tower 60m, values of a should be chosen 11.5 and Equation 20 and 21 used for velocity pressure expose coefficient (K_z).

5.4.1.2. Importance Factor, I

It is a factor that explains the degree of danger to the human living environment and damages properties around the structure. The classification of the importance factor of the buildings is given in Table 5-4.

Category	Non-Hurricane Prone Regions and Hurricane Prone Regions with V = 85-100 mph and Alaska	Hurricane Prone Regions with V > 100 mph
I	0.87	0.77
II	1.00	1.00
III	1.15	1.15
IV	1.15	1.15

Table 5-4: Importance factor, wind load (ASCE 7-02, Table 1-1)

According to the standard, buildings and other structures designated for power generation should be considered as Category IV. Therefore, for the tower importance factor (I) is 1.15.

5.4.1.3. Topographic Factor, K_{zt}

It expresses the change of the wind increasing speed on the rocks or hill. K_{zt} can be accepted as 1.0 for a flat open area.

5.4.1.4. Wind Directional Factor, K_d

The wind direction coefficient (K_d) is a load reduction factor. Its value varies between 0.85 and 0.95 depending on the structure type. Round structures take the wind in every direction. According to the table below, for a round cylinder tower, K_d is 0.95.

Structure Type	Directionality Factor K_d^*
Buildings Main Wind Force Resisting System Components and Cladding	0.85 0.85
Arched Roofs	0.85
Chimneys, Tanks, and Similar Structures Square Hexagonal Round	0.90 0.95 0.95
Solid Signs	0.85
Open Signs and Lattice Framework	0.85
Trussed Towers Triangular, square, rectangular All other cross sections	0.85 0.95

Table 5-5: Wind directional factor (ASCE 7-02, Table 6-4)

5.4.1.5. Basic Wind Speed, V

The basic wind speed, V , is used to determine the design wind loads on buildings and other structures. The wind maps in the standard are used to determine the basic wind speed. Corpus Christi, Texas, is chosen as the region where the wind turbine tower is located. According to Figure 5-9, the basic wind speed is acceptable as 120 mph for the Corpus Christi region.

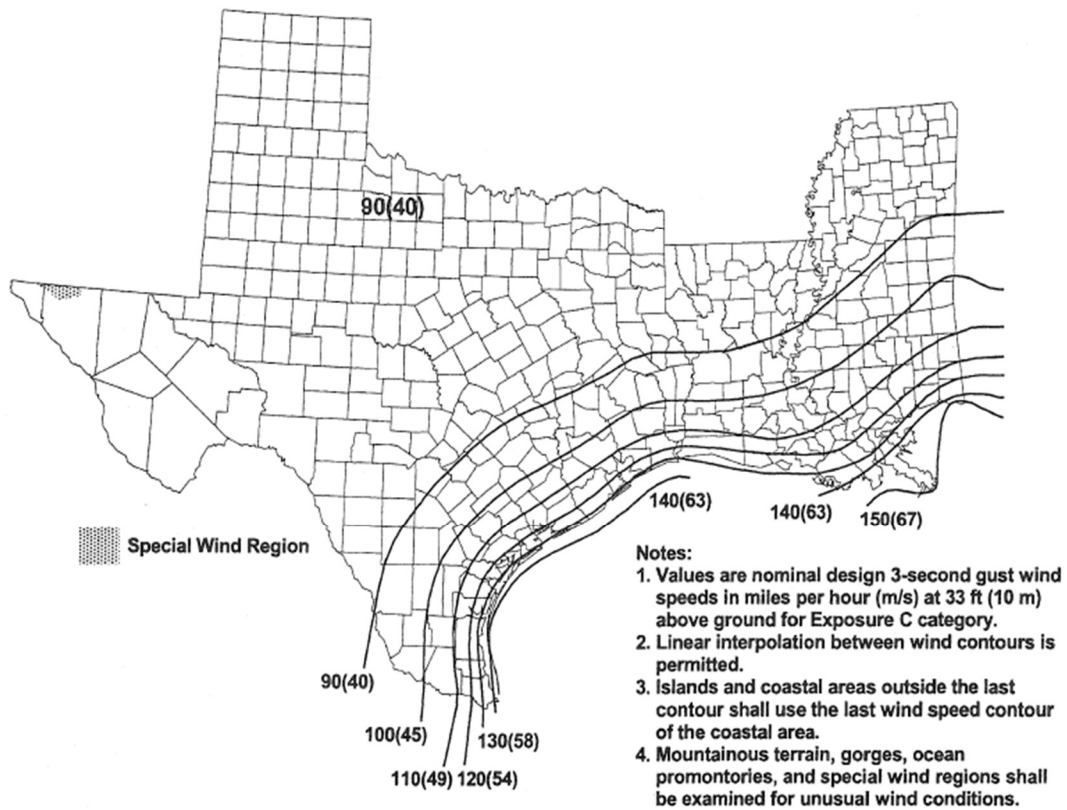


Figure 5-9: Basic wind speed for Western Gulf of Mexico Coastline (ASCE 7-02, Figure 6-1a)

5.4.2. Design Wind Loads

For calculations of design wind loads equation 22 below is used according to the standard.

$$F = q_z \cdot G \cdot C_f \cdot A_f \quad (22)$$

In the above equation, A_f represents the structure's surface projected area, C_f is the force coefficient, and G is the gust effect factor. Gust effect factor is accepted as 0.85 for the rigid structures.

5.4.2.1. Force Coefficient, C_f

The model tower height is 60m and the average outer diameter is 2.88 m. The ratio of tower height to diameter is approximately 21. Therefore, with the help of interpolation, C_f should be selected as 0.672 for the round shape tower.

Cross-Section	Type of Surface	h/D		
		1	7	25
Square (wind normal to face)	All	1.3	1.4	2.0
Square (wind along diagonal)	All	1.0	1.1	1.5
Hexagonal or octagonal	All	1.0	1.2	1.4
Round ($D\sqrt{q_z} > 2.5$) ($D\sqrt{q_z} > 5.3$, D in m, q_z in N/m^2)	Moderately smooth	0.5	0.6	0.7
	Rough ($D'/D = 0.02$)	0.7	0.8	0.9
	Very rough ($D'/D = 0.08$)	0.8	1.0	1.2
Round ($D\sqrt{q_z} \leq 2.5$) ($D\sqrt{q_z} \leq 5.3$, D in m, q_z in N/m^2)	All	0.7	0.8	1.2

Table 5-6: Force coefficient of structures for all height (ASCE 7-02, Figure 6-19)

5.4.2.2. Projected Area, A_f

The projected area is defined as the area where the wind pressure will act vertically. It will be calculated for a 60m height tower in the following steps by using the trapezoidal area calculation. The tower height on the z-axis is 60m, and the outer diameter varies between 2.4m and 3.36m.

The design wind load of the 60m long wind turbine tower is calculated below. In the following stages, it will be used in the fatigue, buckling, and stress analyses. Finally, the modeled tower will be examined if it is suitable for the design wind load.

Wind Load Calculation									
z(m)	z(ft)	Kz	qz	V	$p=0.00256*V^2$	Projected Area(Af)		$F=qz*G*Cf*Af$	F
			(lb/ft2)	(mph)	(lb/ft2)	m2	ft2	(lbf)	(kN)
60.00	196.85	1.61	52.59	120.00	29.86	-	-	-	-
58.66	192.47	1.61	52.38	119.73	36.86	3.22	34.70	1042.30	4.64
56.78	186.30	1.60	52.09	119.34	36.70	4.59	49.36	1476.98	6.57
54.90	180.13	1.59	51.78	118.94	36.46	4.64	49.95	1486.09	6.61
53.02	173.97	1.58	51.47	118.53	36.22	4.70	50.56	1495.36	6.65
51.15	167.80	1.57	51.15	118.10	35.96	4.75	51.15	1503.79	6.69
49.27	161.64	1.56	50.82	117.66	35.71	4.81	51.74	1511.72	6.72
47.39	155.48	1.55	50.47	117.20	35.44	4.86	52.33	1518.89	6.76
45.52	149.33	1.54	50.12	116.73	35.17	4.92	52.91	1525.51	6.79
43.64	143.17	1.53	49.76	116.24	34.88	4.97	53.53	1532.41	6.82
41.76	137.02	1.51	49.38	115.73	34.59	5.03	54.11	1537.81	6.84
39.89	130.87	1.50	48.98	115.20	34.29	5.08	54.72	1543.19	6.86
38.01	124.72	1.49	48.58	114.65	33.97	5.14	55.30	1547.21	6.88
36.06	118.32	1.48	48.13	114.04	33.65	5.40	58.17	1614.08	7.18
34.11	111.91	1.46	47.67	113.41	33.30	5.46	58.81	1616.91	7.19
32.24	105.77	1.45	47.20	112.77	32.93	5.30	57.08	1554.06	6.91
30.37	99.63	1.43	46.71	112.10	32.56	5.35	57.63	1553.89	6.91
28.50	93.49	1.42	46.20	111.39	32.17	5.41	58.24	1554.16	6.91
26.62	87.35	1.40	45.66	110.64	31.76	5.46	58.82	1552.36	6.90
24.75	81.21	1.38	45.08	109.83	31.33	5.52	59.43	1549.89	6.89
22.88	75.08	1.36	44.47	108.97	30.88	5.57	59.99	1544.86	6.87
21.02	68.95	1.34	43.82	108.05	30.40	5.63	60.59	1539.24	6.85
19.05	62.51	1.32	43.08	107.00	29.89	5.97	64.22	1607.43	7.15
17.09	56.08	1.30	42.27	105.84	29.31	6.03	64.86	1595.85	7.10
15.23	49.95	1.27	41.43	104.62	28.68	5.79	62.31	1504.52	6.69
13.36	43.83	1.24	40.50	103.26	28.02	5.84	62.90	1488.44	6.62
11.49	37.70	1.21	39.45	101.72	27.30	5.90	63.47	1468.11	6.53
9.63	31.58	1.17	38.25	99.93	26.49	5.95	64.05	1443.40	6.42
7.66	25.13	1.13	36.76	97.68	25.57	6.33	68.13	1488.76	6.62
5.69	18.68	1.07	34.92	94.82	24.42	6.39	68.82	1445.18	6.43
3.83	12.57	1.03	33.61	91.14	23.02	6.11	65.82	1312.73	5.84
1.97	6.46	1.03	33.61	91.14	23.02	6.17	66.44	1275.40	5.67
0	0.00	1.03	33.61	91.14	23.02	6.59	70.93	1361.70	6.06

Table 5-7: Design wind load calculation of the wind tower for Corpus Christi, Tx

5.5. Overview of Structural Analysis of the Tower

In this part of the study, the stress analysis, fatigue, and buckling analysis of the wind turbine tower will be performed. Analyzes will be carried out by considering the design wind load, the wind turbine blade, and nacelle weight. Lastly, the study will be finalized by examining the conformity of the tower design according to ASCE standards.

S355 steel, one of the structural steels widely used in the wind turbine tower, was chosen as the construction material. Different from wind turbine blade analysis, strain-life parameters are needed since fatigue analysis of the structure will also be examined. All this information is defined in the “Engineering Data” section of the Ansys program.

Properties of Outline Row 3: S355 Steel			
	A	B	C
1	Property	Value	Unit
2	Material Field Variables	Table	
3	Density	2540	kg m ⁻³
4	Isotropic Secant Coefficient of Thermal Expansion		
6	Isotropic Elasticity		
7	Derive from	Young's Modulus and Po...	
8	Young's Modulus	2.1E+05	MPa
9	Poisson's Ratio	0.3	
10	Bulk Modulus	1.75E+11	Pa
11	Shear Modulus	8.0769E+10	Pa
12	Strain-Life Parameters		
13	Display Curve Type	Strain-Life	
14	Strength Coefficient	9.2E+08	Pa
15	Strength Exponent	-0.106	
16	Ductility Coefficient	0.213	
17	Ductility Exponent	-0.47	
18	Cyclic Strength Coefficient	1E+09	Pa
19	Cyclic Strain Hardening Exponent	0.2	
20	S-N Curve	Tabular	
21	Interpolation	Log-Log	
22	Scale	1	
23	Offset	0	Pa
24	Tensile Yield Strength	2.5E+08	Pa
25	Compressive Yield Strength	2.5E+08	Pa
26	Tensile Ultimate Strength	4.6E+08	Pa
27	Compressive Ultimate Strength	0	Pa

Table 5-8: Material properties of S355 Steel (Ansys General_Materials.xml)

5.5.1. Preliminary Analysis

In the analyses made for the wind turbine blade, the wind load on the blade was calculated with the help of Ansys Fluent, and then the total deformation and Von-misses stress on the blade due to this wind load were calculated.

There is no need to use the Ansys Fluent module for the tower, as the wind load was previously calculated in the earlier stages of the study with the help of the standard. Instead, the average of the wind load calculated for each section will be taken separately, and the wind pressure will be entered manually in the Static Structural module.

The External Model option was used to start the analysis since Space Claim or Design Modeler, Ansys geometry creation systems, were not used in the creation of the tower geometry. Thanks to the External Model option, the geometry was imported to Ansys, then it was dragged to the Model tab as shown below to be used in the static structural analysis.

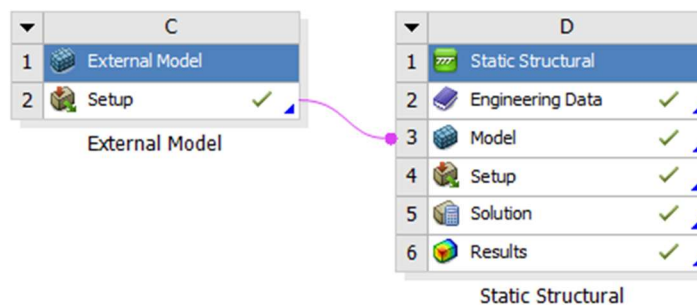


Figure 5-10: Start-up for the tower structural analysis

The application named “Coreform Cubit” was used both in the modeling and meshing of the tower. In the modeling, two vertical support structures were added to the tower geometry to avoid buckling.

To decide whether the mesh quality is good, it is examined whether the cells on different surfaces have common starting or ending points. In the figure below, especially the inner and outer surfaces of the tower and the mesh cells on the support elements can be seen. After this review, it was ensured that the mesh was correctly set, and calculations were started in the Ansys.

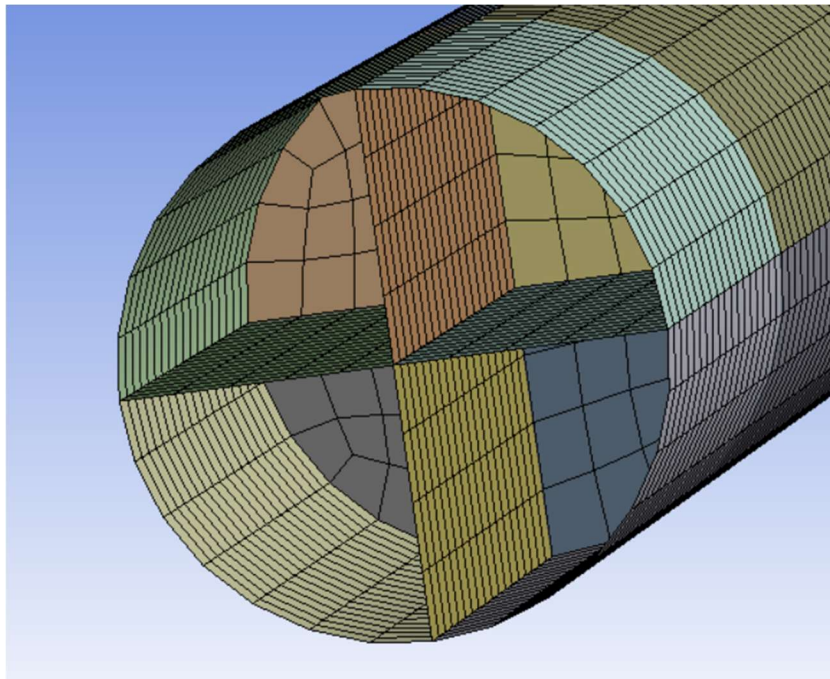


Figure 5-11: Mesh section taken from the inner surface of the tower

Another load to be added in the analysis is the weight of the blade and nacelle, which are two of the wind turbine elements. About a study by Curran A. Crawford [26], the mass of each turbine blade is approximately 10 tons, and the nacelle weight is calculated as 80 tons for the 86-m-diameter wind turbine.

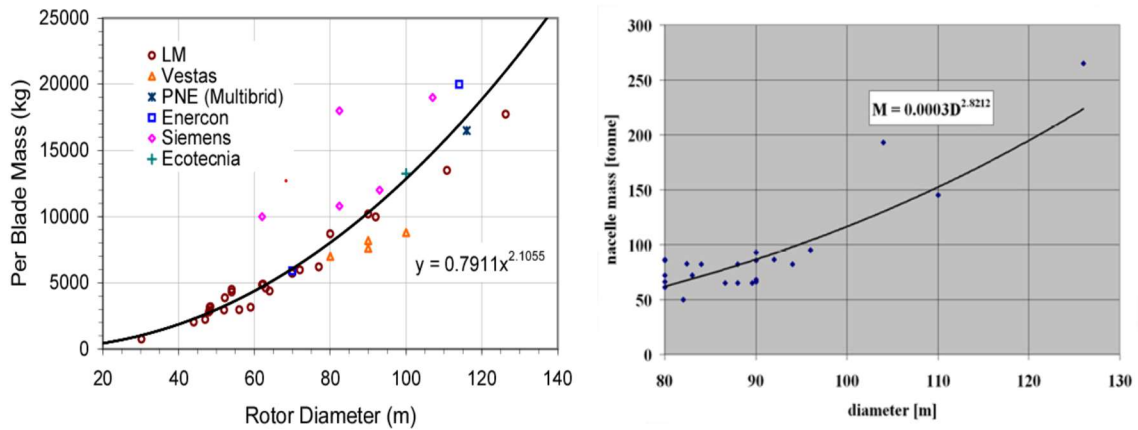


Figure 5-12: Blade and nacelle mass trend changes with the rotor diameter (Curran A. Crawford, 2007)

5.5.2. Analysis Setup

Before starting the analysis, the material properties for S355 steel were applied, and then the thickness values shown in the tower dimensions (Table 5-2) were applied.

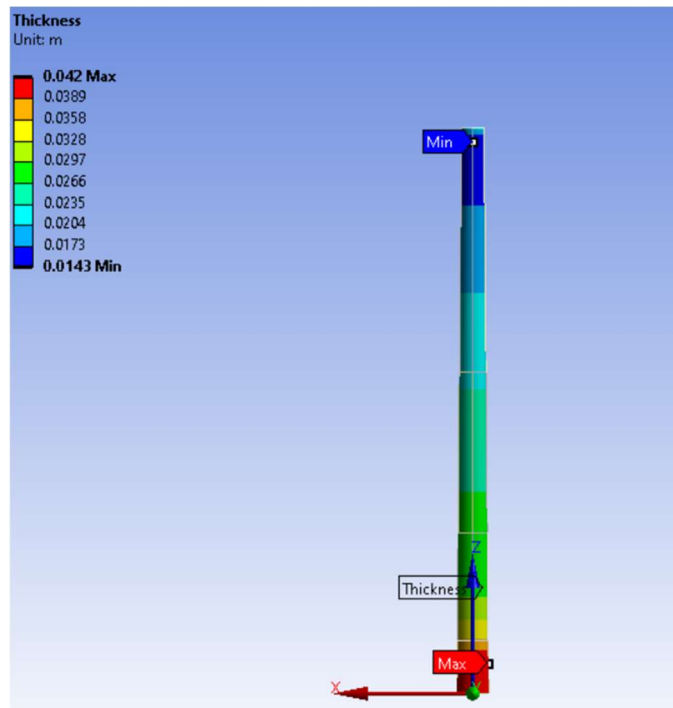


Figure 5-13: Designed tower with varying thickness

Finally, design wind load, blade and nacelle mass, boundary conditions were applied, and analysis conditions were met. The load caused by the nacelle and blade mass is applied to the upper surface of the tower, and the design wind load is applied to the tower's surface only on the windward side.

Since there is no rotational movement in the tower, “fixed support” condition should be added to the lower face of the tower as a limit condition.

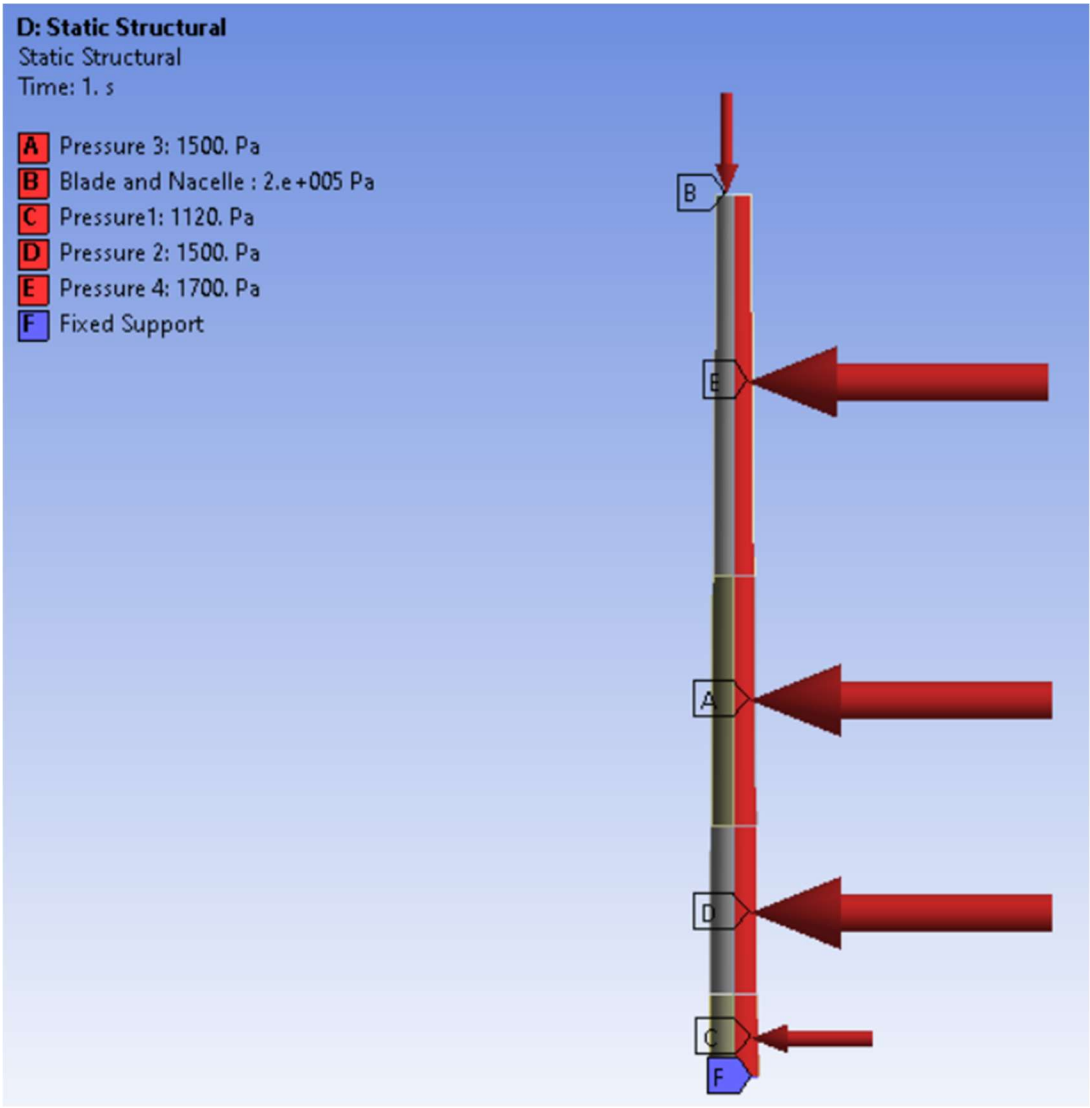


Figure 5-14: Loads acting on the tower

5.5.3. Total Deformation

The deformation in the tower should be as low as possible, as it may cause excessive deformation fractures and imbalance in the movements of the turbine blade. As expected, the tower is deformed (+x) towards the axis affected by the design wind load, and while it is around 12 cm at the top of the tower (%0.2), it is too small to be considered in the lower part where fixed support condition is applied. To avoid buckling failures, Chien and Jang (2009) suggest that the ratio of the displacement due to loading to the tower length should not be more than %1 [27]. %0.2 total deformation (12cm) will not cause buckling failure.

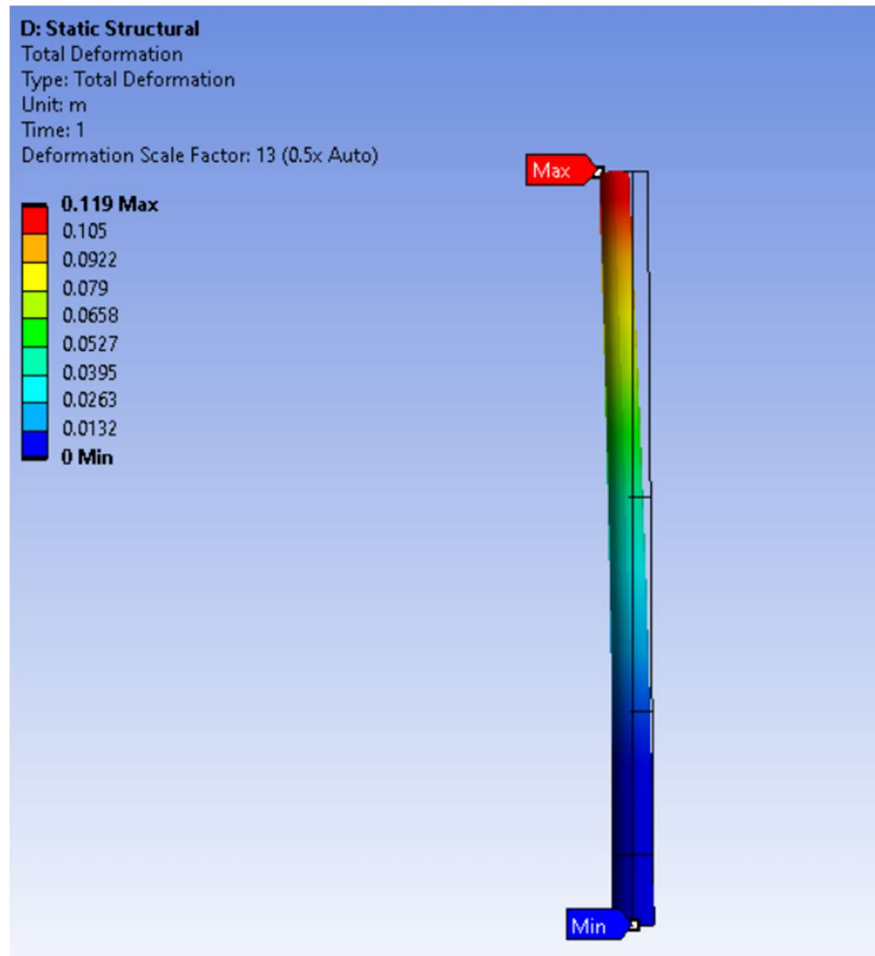


Figure 5-15: Total deformation of the tower

5.5.4. Equivalent Stress and Safety Factor

While modeling the tower, it is crucial to determine where the maximum stresses are concentrated in the structure. When the figure below is examined, it can be observed that the maximum stress is in the lower part of the tower and on the opposite side of the surface affected by the wind load. This shows that the Von-Mises stress reaches its maximum in the areas affected by the compressive stress. To prevent damage in this area, the sheet thickness in the lower sections of the tower should be chosen to be thicker, like the modeled tower.

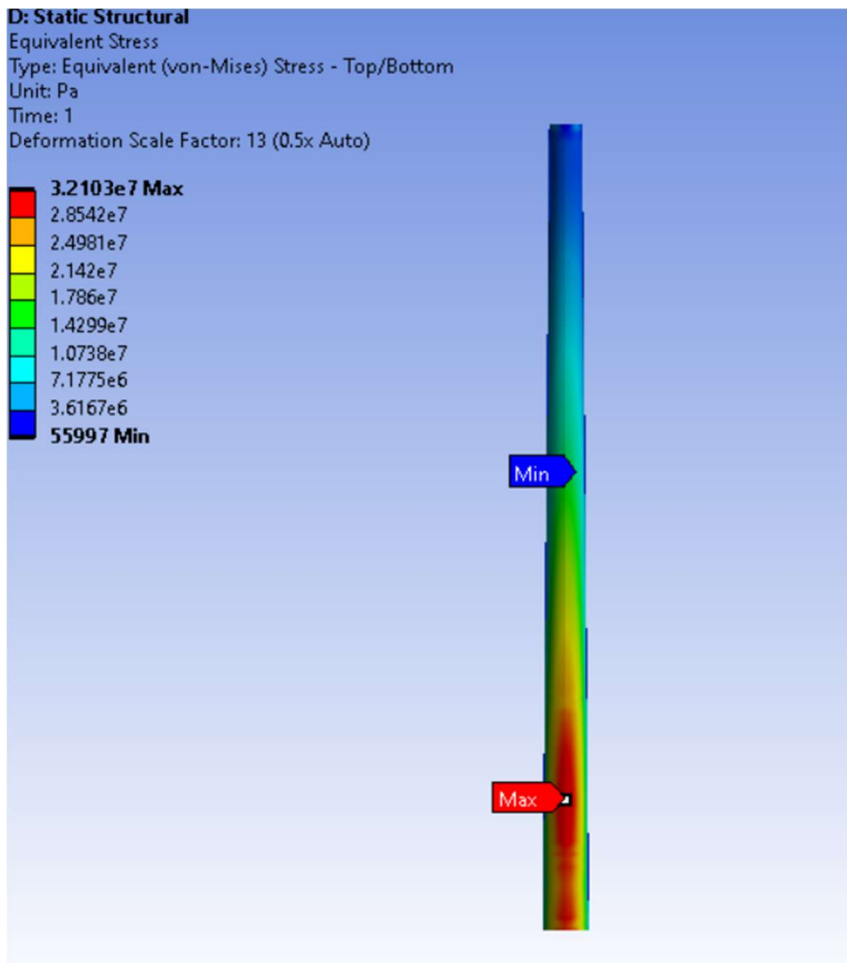


Figure 5-16: Von-Mises stress on the tower

To understand if the tower's design is safe, a safety factor analysis should be carried out using the "Stress Tool" in the Ansys Mechanical module. Safety factor analysis helps to understand if the design is failing or where it is failing and how to improve the modeling to avoid failing. In an FEA analysis, the safety factor can be calculated as follows.

$$\text{Safety factor} = \frac{\text{Limit Stress}}{\text{Maximum von Misses stress}} \quad (23)$$

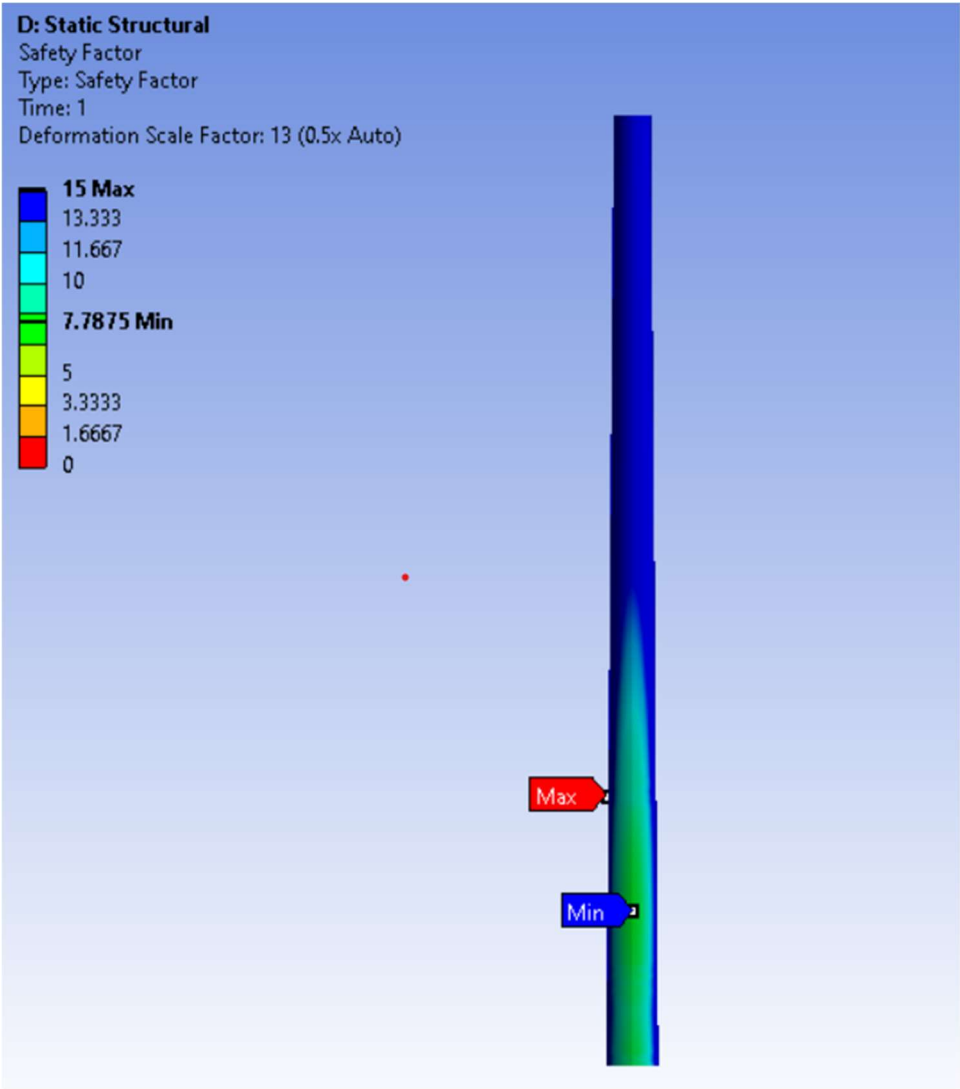


Figure 5-17: Stress safety factor analysis of the tower

A structure with a safety factor of 1 is only strong enough to support the design load. An unexpected extra load on the structure will cause the structure to be damaged. For this reason, a safety factor between 1.5 and 2 is an acceptable value for many designs. The analysis shows that the model tower can withstand a load of more than seven times the design load. It indicates that the design is safe enough.

5.5.5. Fatigue Analysis

In steel structures, the repetitive loading that the structure will be exposed to throughout its life causes cracks that start at the micro-level. These cracks grow over time, reducing the strength of the structure and finally causing irreversible damage to the structure.

It is inevitable for a wind turbine tower to be under repetitive loads. For this reason, determining the fatigue design criteria of the tower is one of the design safety criteria. In a wind turbine, the number of repetitions of wind loads (n) that will occur during the project's life is as significant as the stress intervals ($\Delta\sigma$) they create in the tower element sections.

In the fatigue analysis, *the design wind load* calculated in the earlier stage was used to determine the number of cycles until the part will fail due to fatigue, and then the fatigue safety factor was calculated. The fatigue safety factor is the safety factor for fatigue failure at a given design life. According to the "*Fatigue Tool*" used for the analysis, the Maximum Safety Factor is 15. Values less than one for Fatigue Safety Factor indicate failure before the design life is reached.

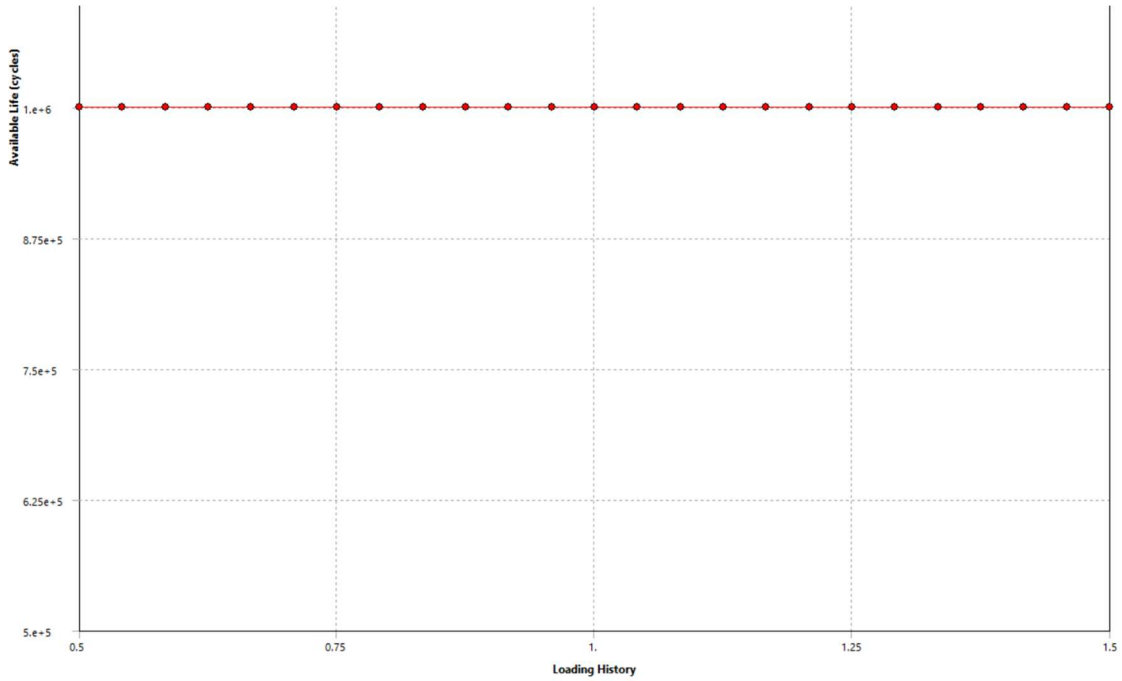


Figure 5-18: Fatigue sensitivity of the tower

The tower has a fatigue life of at least 100000 cycles even under a repeated load 1.5 times the design wind load, and the fatigue safety factor was calculated as 2.67. The results show that the tower model has a sufficiently high fatigue strength against the wind load that it will be exposed to throughout the project life.

The gravitational force which leads to compression and tension in each cycle of blade rotation, the centrifugal force due to the blade rotation, and other cyclic force that occurs due to wind turbulence are other forces that can lead to fatigue damage. In the study, only the design wind load affecting the tower was considered for the fatigue analysis.

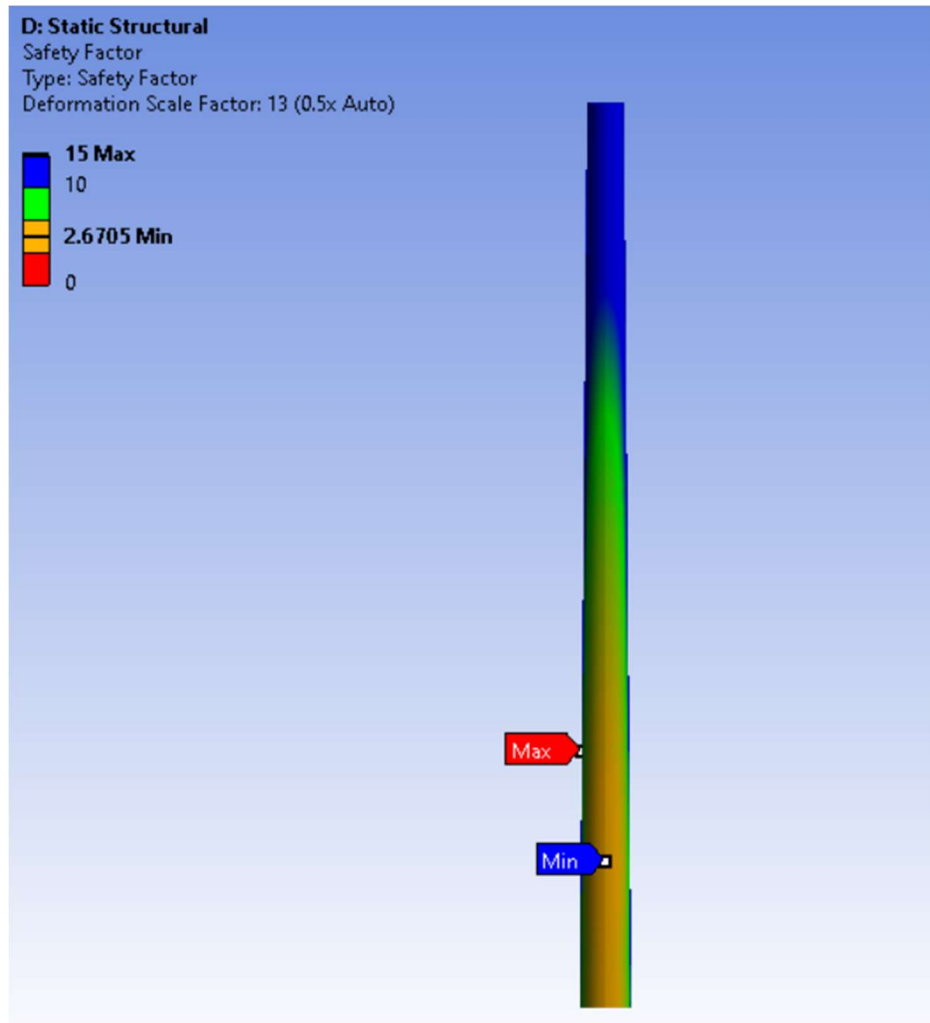


Figure 5-19: Fatigue safety factor analysis of the tower

5.5.6. Buckling Analysis

Buckling is an essential factor in designing structures operating under compression. If a structural member whose length is much greater than its other dimensions, it can be damaged in buckling if forced to press. If the load on the structure exceeds the critical load value, the material will be buckling.

In the last part of the study, the critical buckling force will be calculated using the Ansys "Eigenvalue Buckling" module. This value will be compared with the design load, and it will be examined whether the model is safe in buckling. The data obtained in the structural analysis, the tower geometry, and material properties were dragged to the module used for buckling analysis.

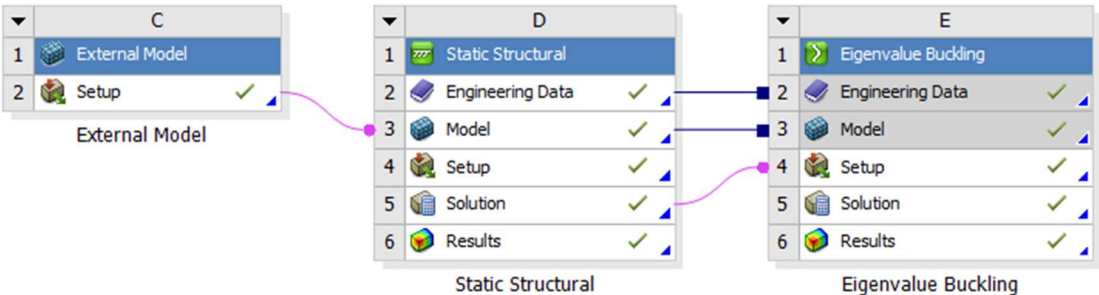


Figure 5-20: Start-up for the eigenvalue buckling analysis

The analysis aims to calculate the load multiplier. Later, critical buckling force can be calculated by multiplying this value by the force is applied to the structure. The calculated buckling force indicates when the model will buckle. Two buckling loads, 1000 N in the z-direction and 1000 N in the x-direction, were used in the analysis.

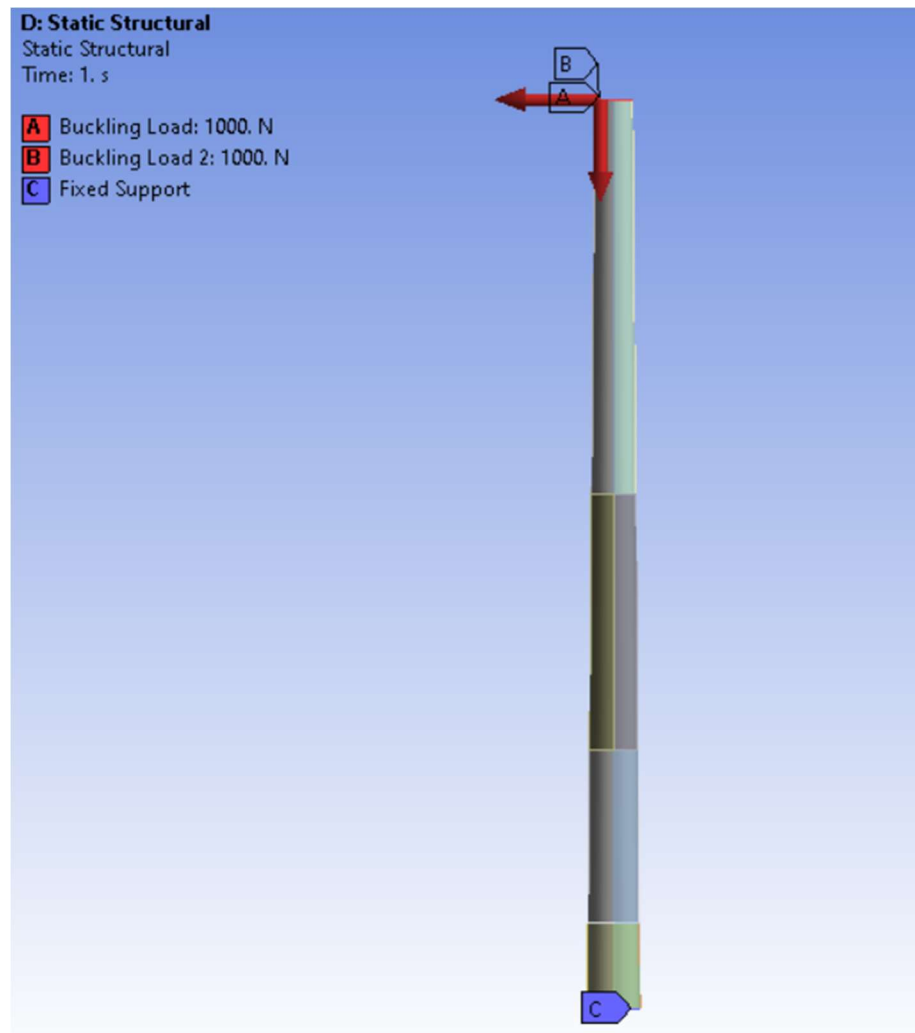


Figure 5-21: Buckling loads applied on the tower

As a result of the analysis, the smallest load multiplier was calculated as 5430. After multiplying this value with the applied force, the critical buckling load is approximately 7500 KN.

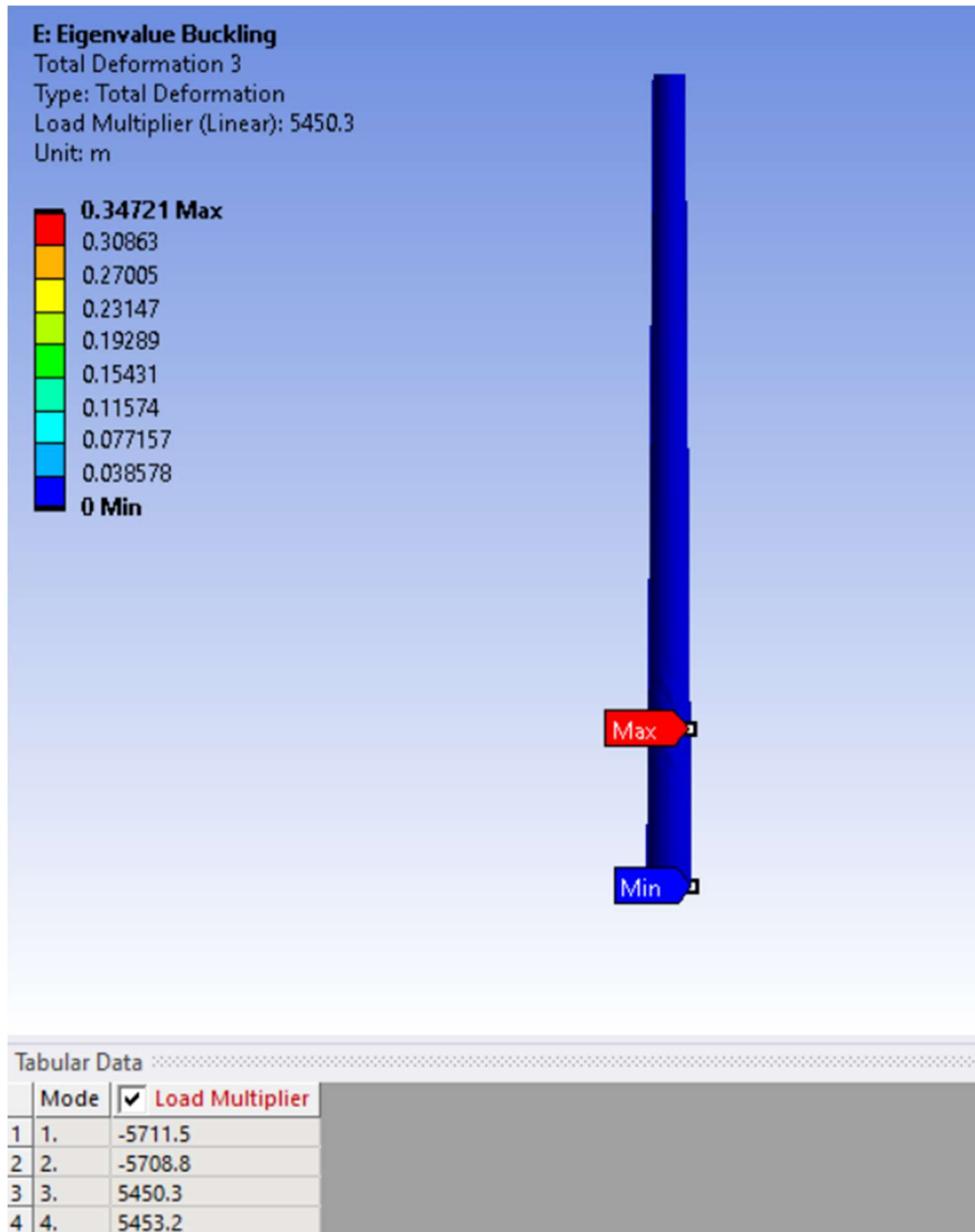


Figure 5-22: Eigenvalue buckling analysis result

5.5.7. Determination of the Tower Natural Frequency

Dynamic characteristics, which are one of the main factors in the design of wind turbine towers, should be determined. It is important to determine the natural frequency

of the tower considering the dynamic loads acting on the tower. The tower's natural (1st Mode) frequency will affect the behavior of the tower under dynamic loads according to the magnitude relationship with the blade passing frequency (P) and the rotational frequency (3P) values.

According to Manwell et al. (2009):

- Soft-soft towers have a natural frequency below than the blade passing frequency, $n_1 < f_b$
- Soft towers have a natural frequency between the blade passing and rotational frequencies, $f_b < n_1 < f_r$
- Stiff towers have a natural frequency higher than the rotational frequency, $f_r < n_1$ [3].

Dynamic effects create significant loads, especially in very soft and soft towers, but stiff towers are more expensive as they require more mass and material.

5.5.8. Baumeister Method

It is a method developed by Baumeister that is used when determining the natural frequency of the tower [28]. The empirical formula is based on tower height, tower mass, and rotor mass. Since the tower cross-section varies along the z-axis, an average moment of inertia (I) will be used, which is calculated in Table 5-2 (0.2506).

The natural frequency (f_n) of the tower can be obtained with the following formula.

$$f_n = \frac{1}{2\pi} \sqrt{\frac{3EI}{(0.23 \text{ tower} + m_{rotor})h^3}} \quad (24)$$

E: Tower material modulus of elasticity $E = 2.1 \times 10^8 \text{ kN/m}^2$

I: Tower section moment of inertia, $I = 0.2506 \text{ m}^4$

m_{tower} : Tower weight, $m_{tower}= 64,92$ tons

m_{rotor} : Nacelle and rotor weight, $m_{rotor} \approx 110$ tons (Figure 5-12)

h: Tower length, h =60.00 m

```
TOTAL MASS = 64920.  
The mass principal axes coincide with the global Cartesian axes  
CENTER OF MASS (X,Y,Z)= -0.41153E-16 -0.14010E-16 25.733
```

Figure 5-23: Tower mass calculated in Ansys Structural

Using this information, natural frequency of the tower calculated as $f_{n\ Baumeister}=0.3845$ Hz.

5.5.9. Resonance Control of the Tower

Wind turbine operating frequencies are calculated based on the turbine operating angular speed, W (rpm), obtained from the turbine designer. For a turbine with three blades:

- Blade passing frequency (P) = $\frac{W}{60}$ (25)

- Rotational frequency (3P).

Due to possible errors and uncertainties in the natural frequency calculations of the tower, a tolerance of $\pm 5\%$ should be considered in the natural vibration frequency of the tower [29]. While modeling a tower, the location of the center of gravity of the nacelle and blades, and ground effects are conditions that should be considered in the natural frequency calculation.

Manwell et al. (2009), in their study, considering the possible errors and uncertainties in the natural frequency calculation, suggested that the rotor operating frequencies (1P and

3P) values should not fall within the limits of 95% or 105% of the tower natural vibration frequency [3].

Lanier (2005) predicted the uncertainty as $\pm 10\%$ and stated that keeping the tower's natural frequency between the desired turbine operating frequencies (1.1P and 2.7P) will reduce the unwanted resonance effects [24]. He also mentioned the magnitude relations of the natural frequencies of different tower types with the operating frequencies of a wind turbine. The resonance analysis will be performed between operating frequencies in the range of 1.1P and 2.7P, taking the example of this study.

Turbine	Operation Speed		3P(op) Hz	Working Freq. 1		Design Tower		
	rpm	Hz		Hzx1.1	Hzx2.6	Hybr.(Hz)	Conc.(Hz)	Stl(Hz)
1.5 MW(EQ)	20.5	0.342	1.025	0.376	0.888	0.4848	0.4355	0.4059
1.5 MW(Wind)	20.5	0.342	1.025	0.376	0.888		0.3774	
3.6 MW(EQ)	13.2	0.220	0.660	0.242	0.572	0.4813	0.4431	0.3693
3.6 MW(Wind)	13.2	0.220	0.660	0.242	0.572		0.3768	
5.0 MW(EQ)	11.2	0.187	0.560	0.205	0.485	0.4835	0.4621	0.3973
5.0 MW(Wnd)	11.2	0.187	0.560	0.205	0.485		0.384	

Table 5-9: Operating Frequencies for Different Sizes of Turbines (Lanier,2005)

According to Lanier blade passing frequency is 0.376, and the rotational frequency is 0.888 for a 1.5 MW wind turbine with a 20.5 rpm operation speed. The natural frequency of the designed tower was found to be $f_{n\ Baumeister}=0.3845$ Hz. Therefore, tower natural frequency remains between the desired operating frequencies (1.1P, 2.7P) according to Lanier. Accordingly, the tower and the wind turbine do not present any danger in terms of resonance.

6. CONCLUSIONS

In the last part of the study, the wind turbines in the industry were examined, the tower size was decided, and the tower's design was made by considering the design wind load affecting the tower and the dynamic loads resulting from the operation of the wind turbine.

For the wind turbine with three blades of 43.2m, a 60m cylindrical steel tower design was deemed appropriate. The tower, whose geometry is prepared with the Coreform Cubit application, consists of four main segments and the surface wall thickness decreases from the base to the top. By designing the tower as a truncated conical instead of a full cylindrical one, it is aimed to reduce the body thickness upwards and use less material so that the tower can be constructed economically.

The basic wind speed for the Corpus Christi, Texas region was determined (53,64 m/s), and the change of wind speed according to tower height is explained by the power law. Then, the design wind calculations specified in the ASCE 7-02 standard are explained theoretically, and the design wind load was calculated as specified in the standard.

The studies showing the variation of the mass of the tower elements according to the rotor diameter were examined. The nacelle and blade masses were determined for the wind turbine with a rotor diameter of 86.4 m. As a result of all these findings, the static and wind load of the tower was calculated, and the stress, fatigue, and buckling analyses required for tower design were performed using the Ansys structural module.

According to the stress analysis, the Von-Mises stress reaches its maximum at the bottom surface of the tower. This area is affected by compressive stress. It explains that

the wall thickness in the lower parts of the tower should be thicker than in the upper part to avoid damage in this area. In the stress analysis, the stress safety factor was calculated as 7.78 using the stress tool, and the design was proven to be safe. Finally, the total deformation was calculated as a maximum of 12 at the top of the tower. It was concluded that this deformation, which corresponds to %0.2 of the turbine length, would not cause buckling failure.

In the fatigue analysis, it was seen that even when the tower is exposed to a load 1.5 times the cyclic loading used in the analysis, it will resist more than 100000 cycles. Later, the fatigue safety factor was calculated as 2.67. When the results are evaluated, it is seen that the design is safe in terms of fatigue.

In the eigenvalue buckling analysis, which is the last stage of the static analysis, two buckling loads, 1000 N in the z-direction and 1000 N in the x-direction, were used. The smallest load multiplier was found as 5450. By multiplying the loads used in the analysis with the load multiplier, it was concluded that the tower would buckle with a bigger force than 7500 KN. The forces acting on the tower were found to be a total of 1400 KN in the vertical direction and a design wind load of 215 KN in the horizontal direction. These structural analyses show that the turbine design is suitable for the fatigue, buckling, and stress safety conditions.

Wind turbine towers are structures where static loads and dynamic loads are seen. For this reason, it should be designed to prevent resonance due to dynamic loads that will occur on the tower during operation. The natural frequency of the designed wind turbine tower should be between the desired operating frequencies of the wind turbine (1.1P and

2.7P) to prevent resonance arising from calculation uncertainties and will make the design safer.

In the last part of the study, the natural frequency of the tower was calculated as 0.3845 using the Baumeister method and it was observed that this value remained between the operating frequencies corresponding to the 20.5 rpm operating speed. This result proves there will be no danger in terms of the resonance due to the wind turbine operation for the tower.

The effects of earthquake forces can be added to the study in future studies. In addition, if the ground where the wind turbine will be installed will be the sea surface, corrosion due to saltwater may be another issue that needs to be analyzed for the tower.

7. REFERENCES

- [1] G. A. M. Van Kuik, “The Lanchester-betz-joukowsky Limit”, *Wind Energy*, vol. 10, no. 3, pp. 289–291, 2007.
- [2] M.C. Senel, “Design Principles of Power Transmission Mechanisms in Wind Turbines”, 2012.
- [3] J. Manwell, J. McGowan, and A. Rogers, "Wind Energy Explained: Theory, design, and application, ch. 6 Wind Turbine Design", 2009.
- [4] Hendriks, H. B., at all, "Application of an Advanced Cost Model in Different Design Phases of and Offshore Wind Turbine", Energy Research Center of Netherlands, 2015.
- [5] Jonkman, J., Butterfield, S.Musial, W., Scott, G, “Definition of a 5-MW Reference Wind Turbine for Offshore System Development, Technical Report”, National Renewable Energy Laboratory, 2009.
- [6] Peerigna, J.,at all, “Upwind 20 MW Wind Turbine Pre-Design: Blade Design and Control”, Energy Research Centre of Netherlands, 2011.
- [7] Griffith, T. & Ashwill, T. D, “The Sandia 100-meter All- Glass Baseline Wind Turbine Blade: SNL100-00, Sandia National Laboratories”, 2011.
- [8] Kalagi G., Patil R., Nayak N. “Natural Fiber Reinforced Polymer Composite Materials for Wind Turbine Blade Applications”, 2016.
- [9] Mishnaevsky L & Jr., Brøndsted P. “Statistical modelling of compression and fatigue damage of unidirectional fiber reinforced composites”, 2008.
- [10] Grande J.A. “Wind Power Blades Energize Composites Manufacturing”, 2008.

- [11] Calvin Phelps & John Singleton, “Wind Turbine Blade Design”, Cornell University, Sibley School of Engineering, 2012.
- [12] Anderson J. D., “Computational Fluid Dynamics; The Basics with Applications”, 1995.
- [13] Wilcox, D.C., “Formulation of the k- ω Turbulence Model Revisited”, 2008.
- [14] Sørensen, J. N., Shen, W. Z., and Hansen, M. O. L., “A Vorticity-velocity Formulation of the 3D Navier-Stokes Equations in Cylindrical Coordinates”, 2002.
- [15] T.Burton, N.Jenkins, D.Sharpe, E.Bossanyi, “Wind Energy Handbook”, 2011.
- [16] Neill, S. P., & Hashemi, M. R. “Offshore Wind. Fundamentals of Ocean Renewable Energy Chapter 4”, 2018.
- [17] Armen Sargsyan, “Simulation and modeling of flow field around a horizontal axis wind turbine (HAWT) using RANS method”, 2010.
- [18] Bechly, M.E., Clausen, P.D., “Structural Design of a Composite Wind Turbine Blade Using Finite Element Analysis, Computers & Structures”, 1997.
- [19] Christoph W. Kensche, “Fatigue of Composites for Wind Turbines”, International Journal of Fatigue, 2006.
- [20] Peter J. Schubel & Richard J. Crossley, “Wind Turbine Blade Design”, 2012.
- [21] Wood, D. H., “An improved determination of the tower height that maximizes the power output per unit cost of a small wind turbine”, 2001.
- [22] Harte, R. & Zijl, V., “Structural stability of concrete wind turbines and solar chimney towers exposed to dynamic wind action”, 2007.

- [23] Lewin, T. J., “An investigation of design alternatives for 328-ft (100-m) tall wind turbine towers”, 2010.
- [24] Lanier, M. W., “LWST Phase I Project Conceptual Design Study: Evaluation of Design and Construction Approaches for Economical Hybrid Steel/Concrete Wind Turbine Towers”, 2005.
- [25] American Society of Civil Engineering Standards, “ASCE 7-02, Minimum Design Loads for Buildings and Other Structures”, 2006.
- [26] Curran A. Crawford, “The Path from Functional to Detailed Design of a Coning Rotor Wind Turbine Concept”, 2007.
- [27] Chien, C.W. & Jang, J.J., “A study of wind-resistant safety design of wind turbines tower system”, 2009.
- [28] Baumeister, T., “Standard Handbook for Mechanical Engineers, 8th edition”, 1978.
- [29] Germanischer Lloyd, “Regulation for the Certification of Wind energy Conversion Systems, Rules and Regulations Section IV, Non-Marine Technology, Part 1 Wind Energy”, 1993.

8. APPENDIX A

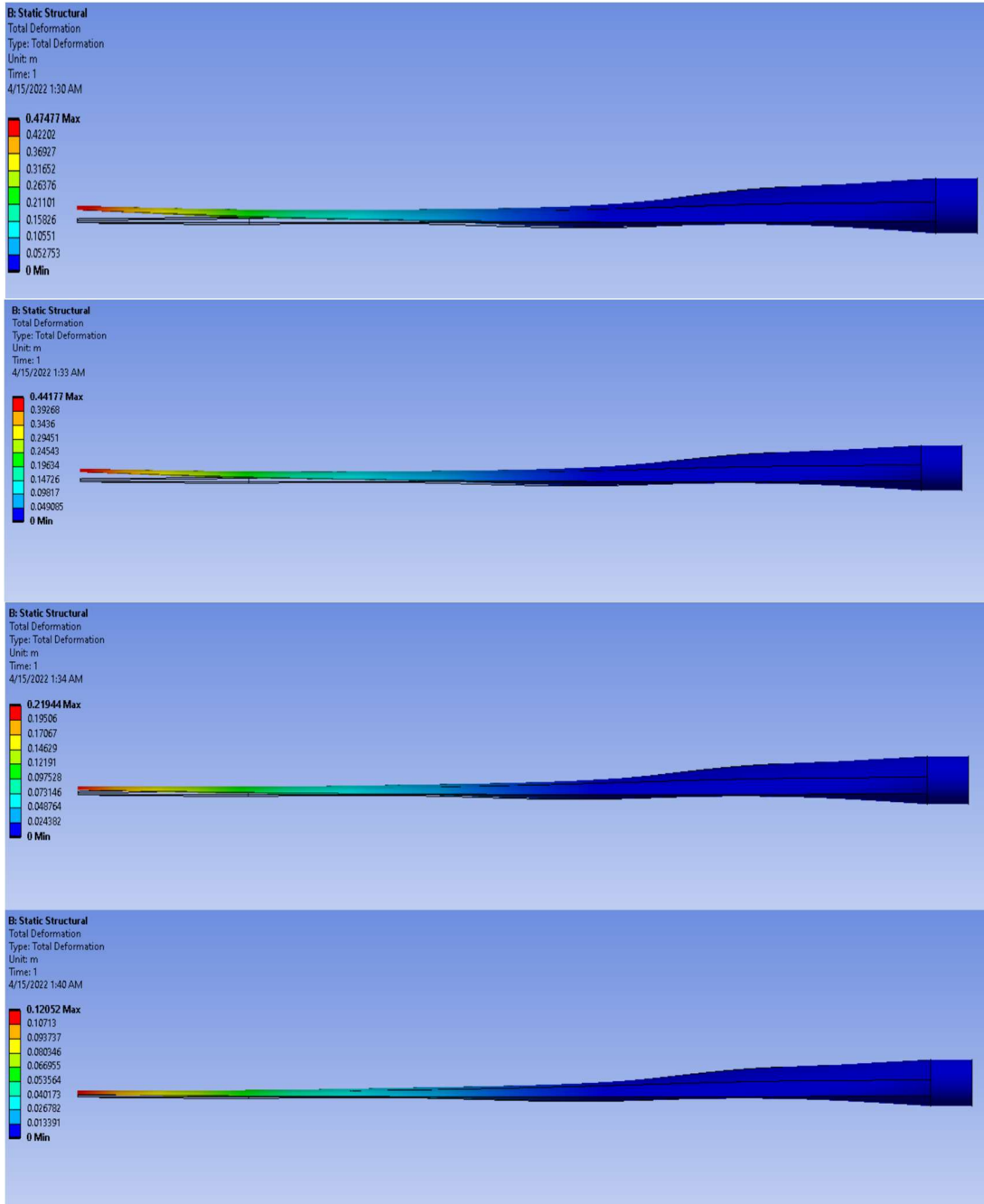


Figure 8-1: Total deformation on the blade at 8 m/s (from top to bottom, E-Glass, S-Glass, Carbon Epoxy, and Carbon fiber, respectively)

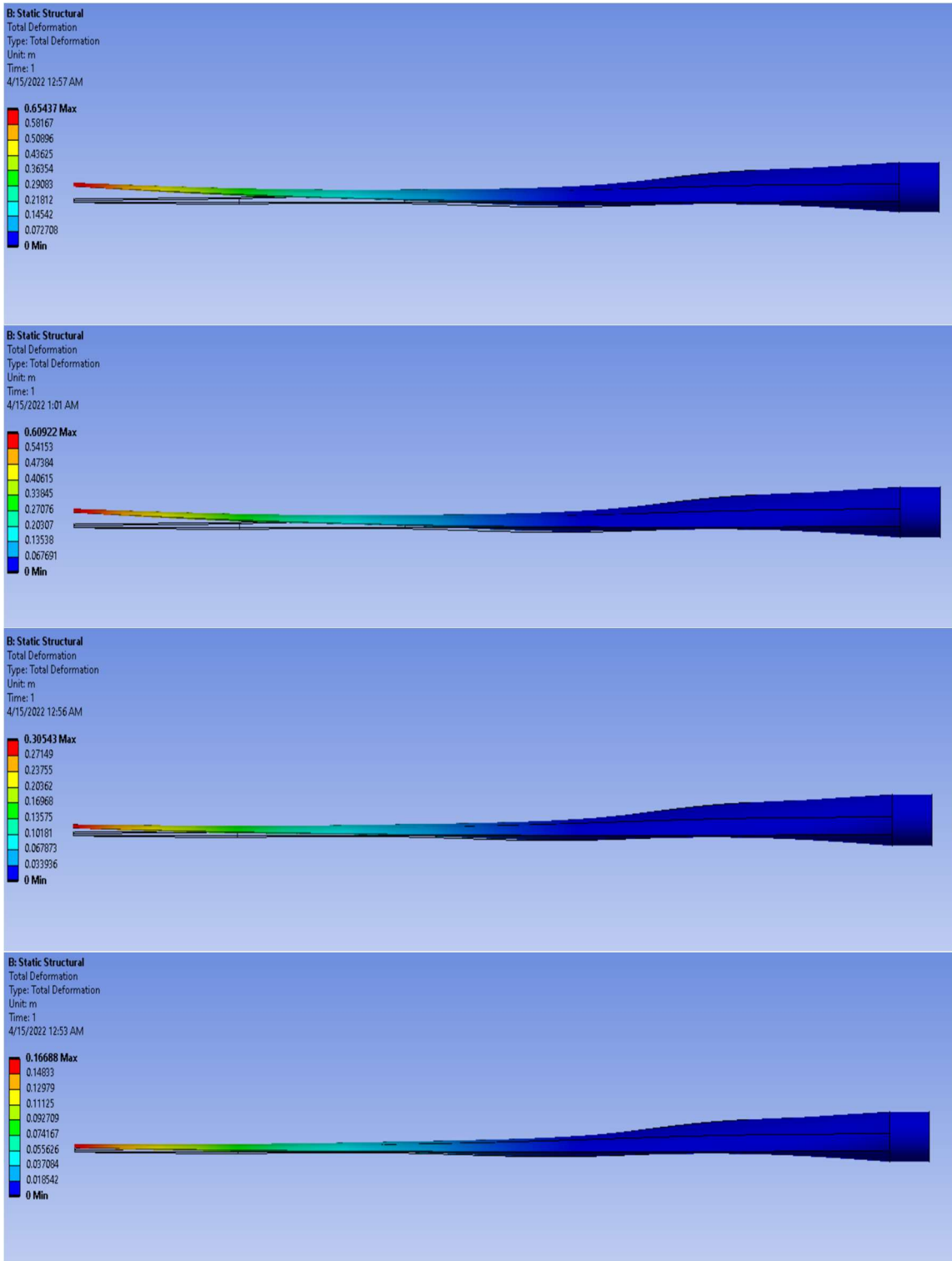


Figure 8-2: Total deformation on the blade at 10 m/s

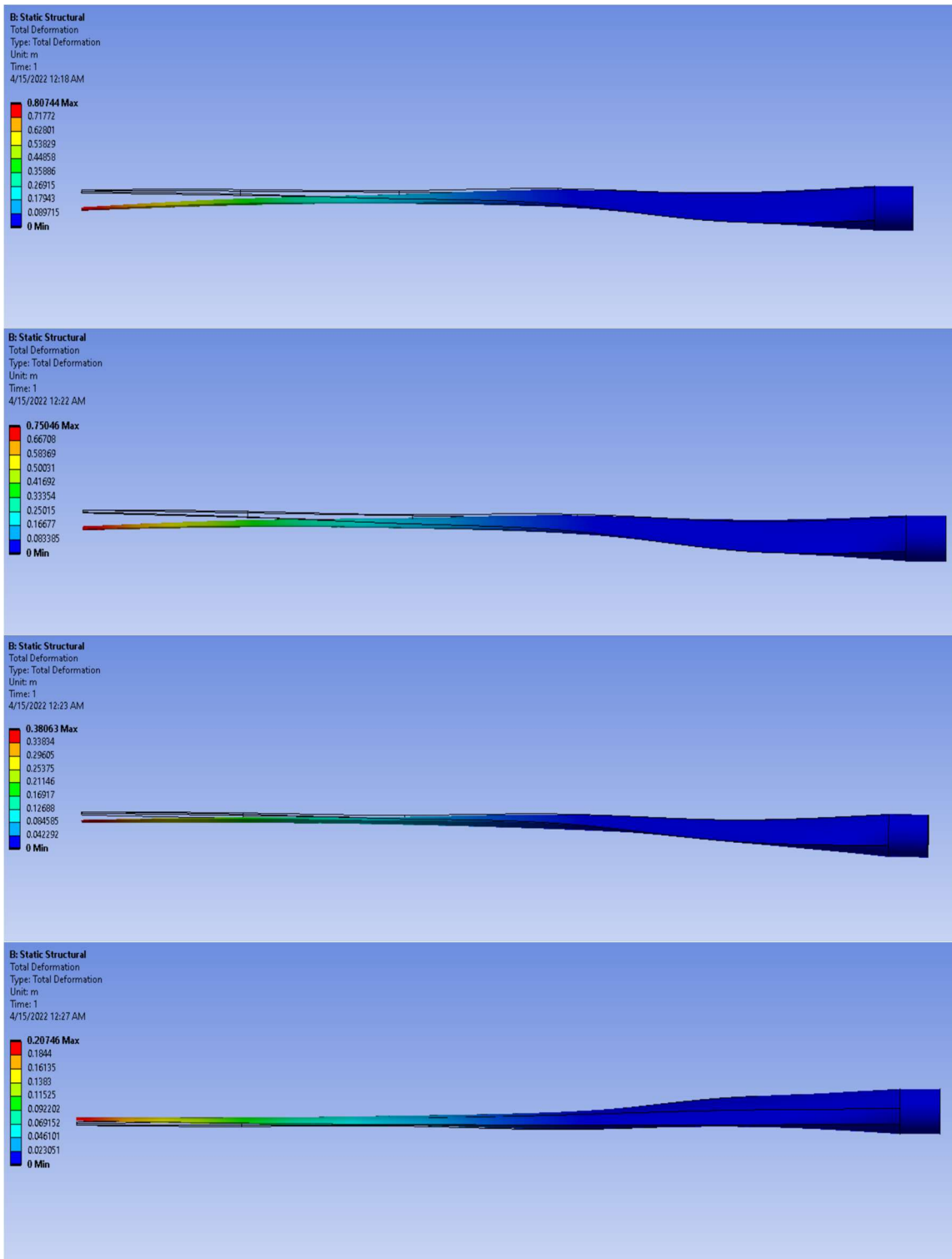


Figure 8-3: Total deformation on the blade at 12 m/s

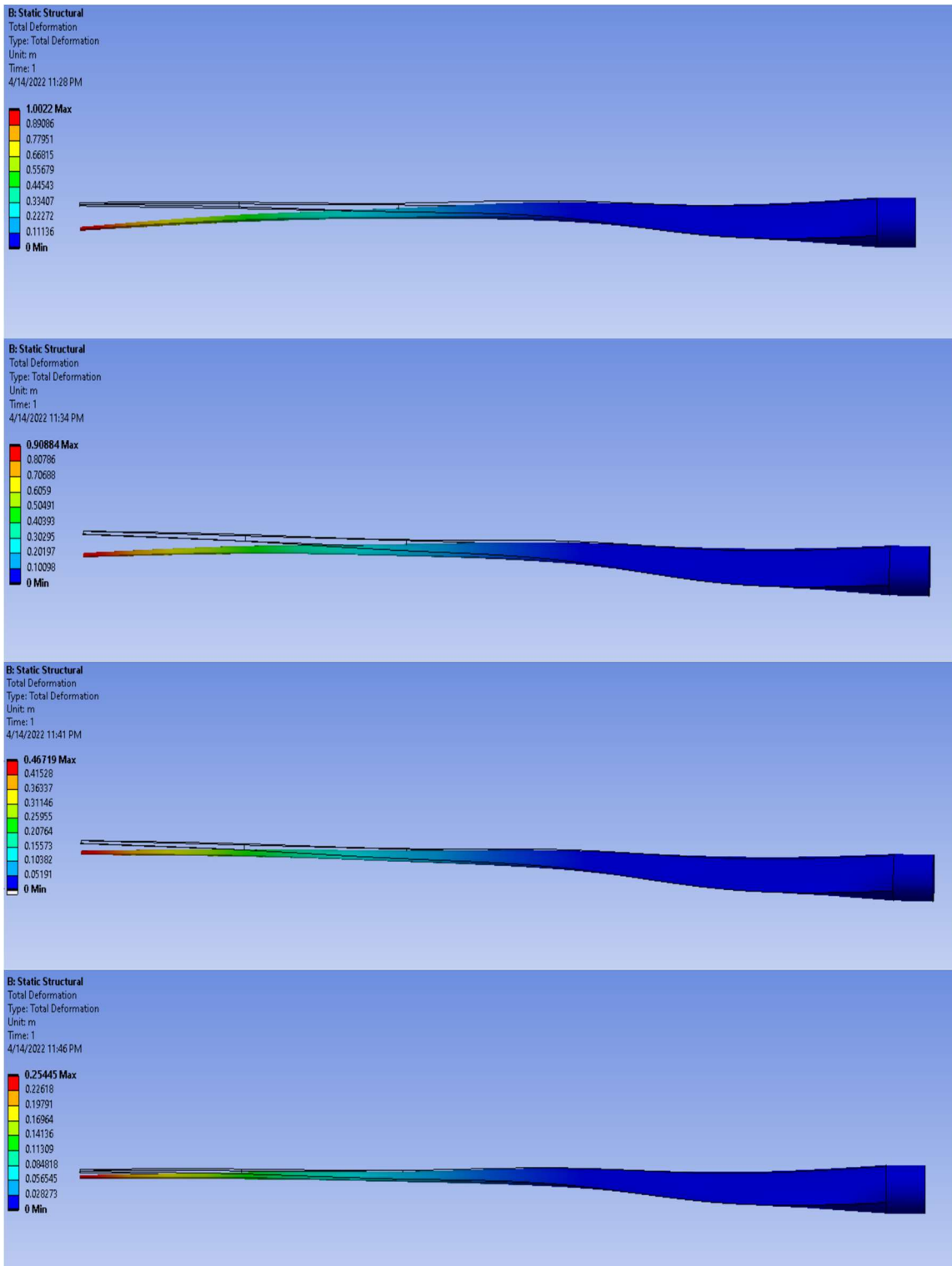


Figure 8-4: Total deformation on the blade at 15 m/s

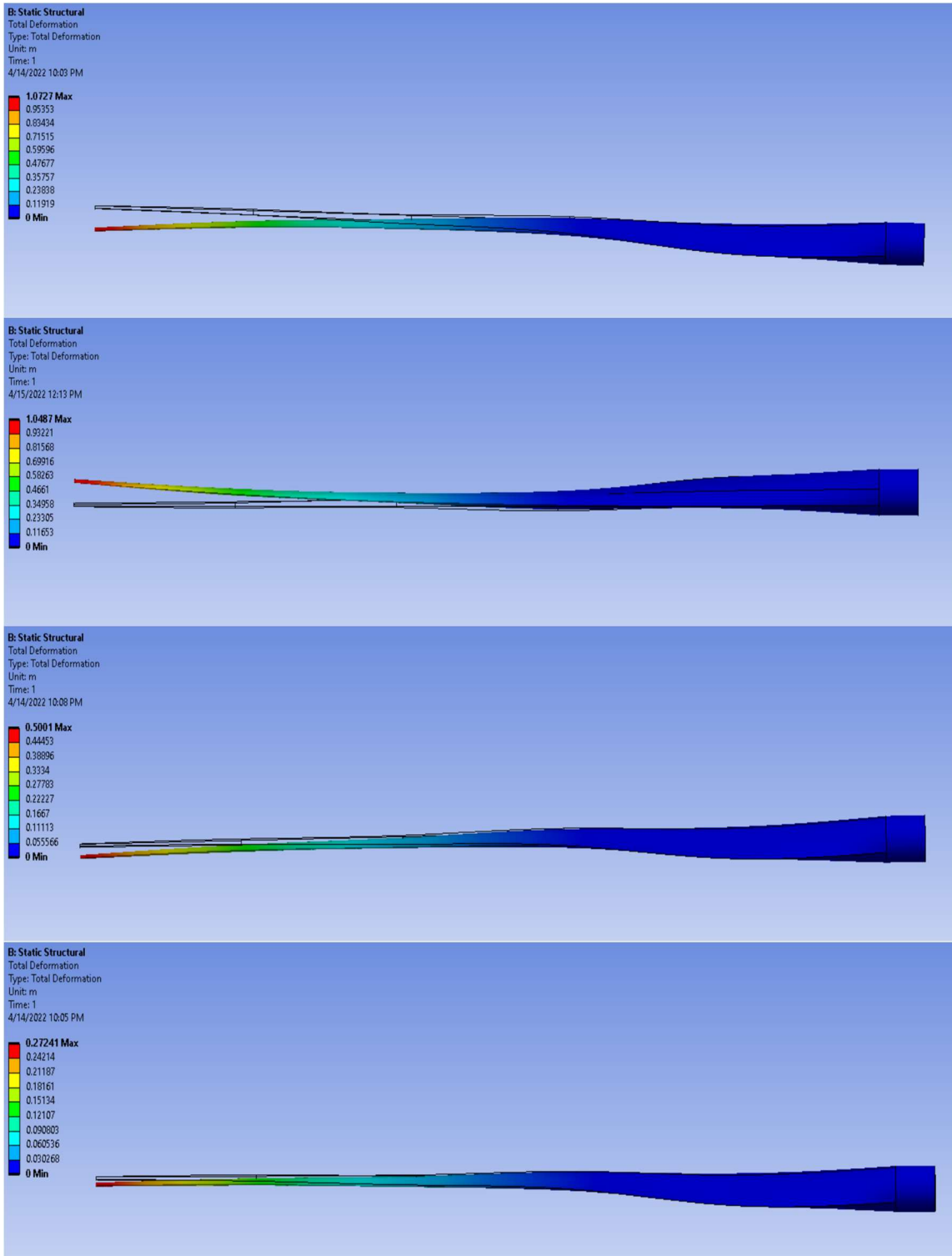


Figure 8-5: Total deformation on the blade at 18 m/s

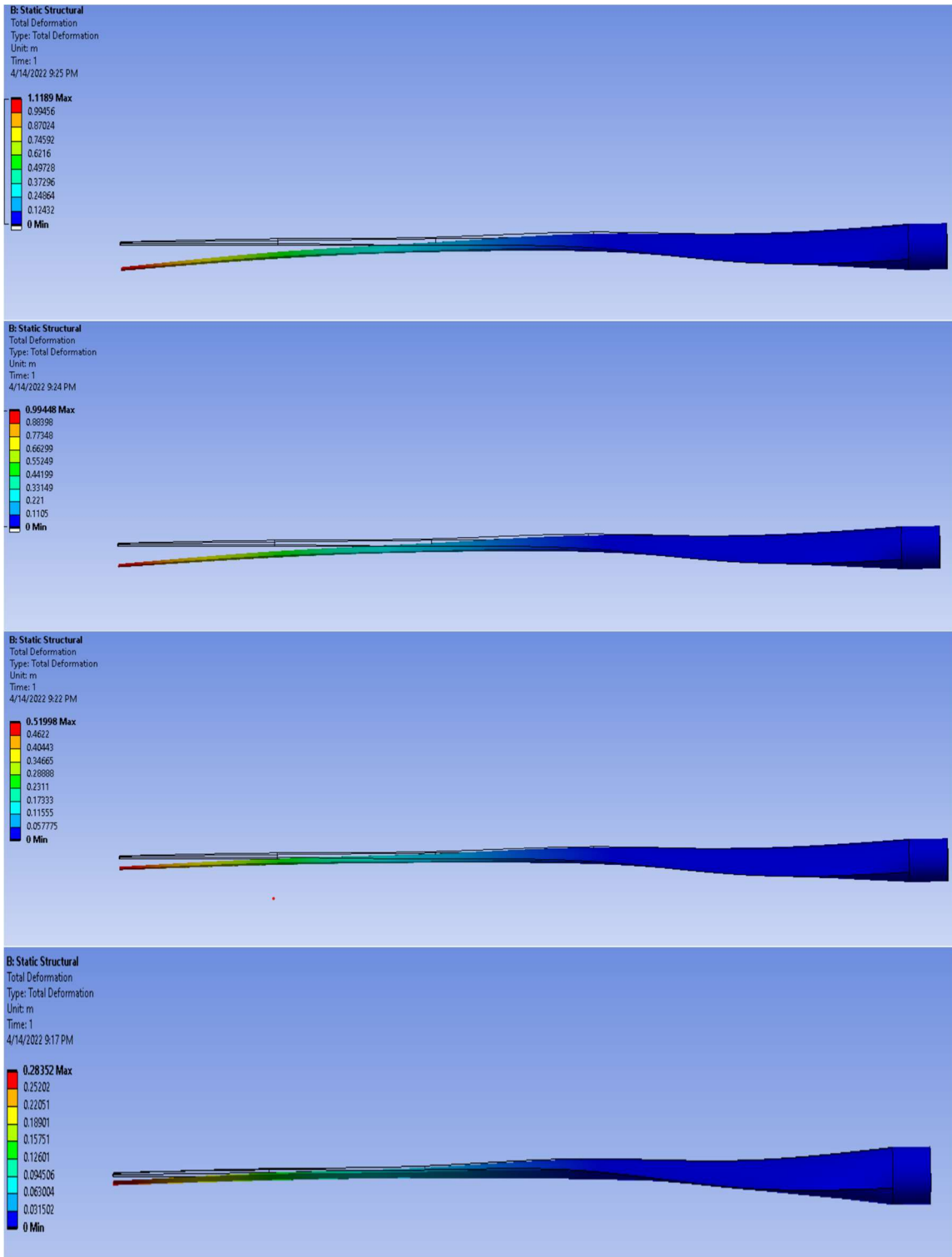


Figure 8-6: Total deformation on the blade at 20 m/s

9. APPENDIX B

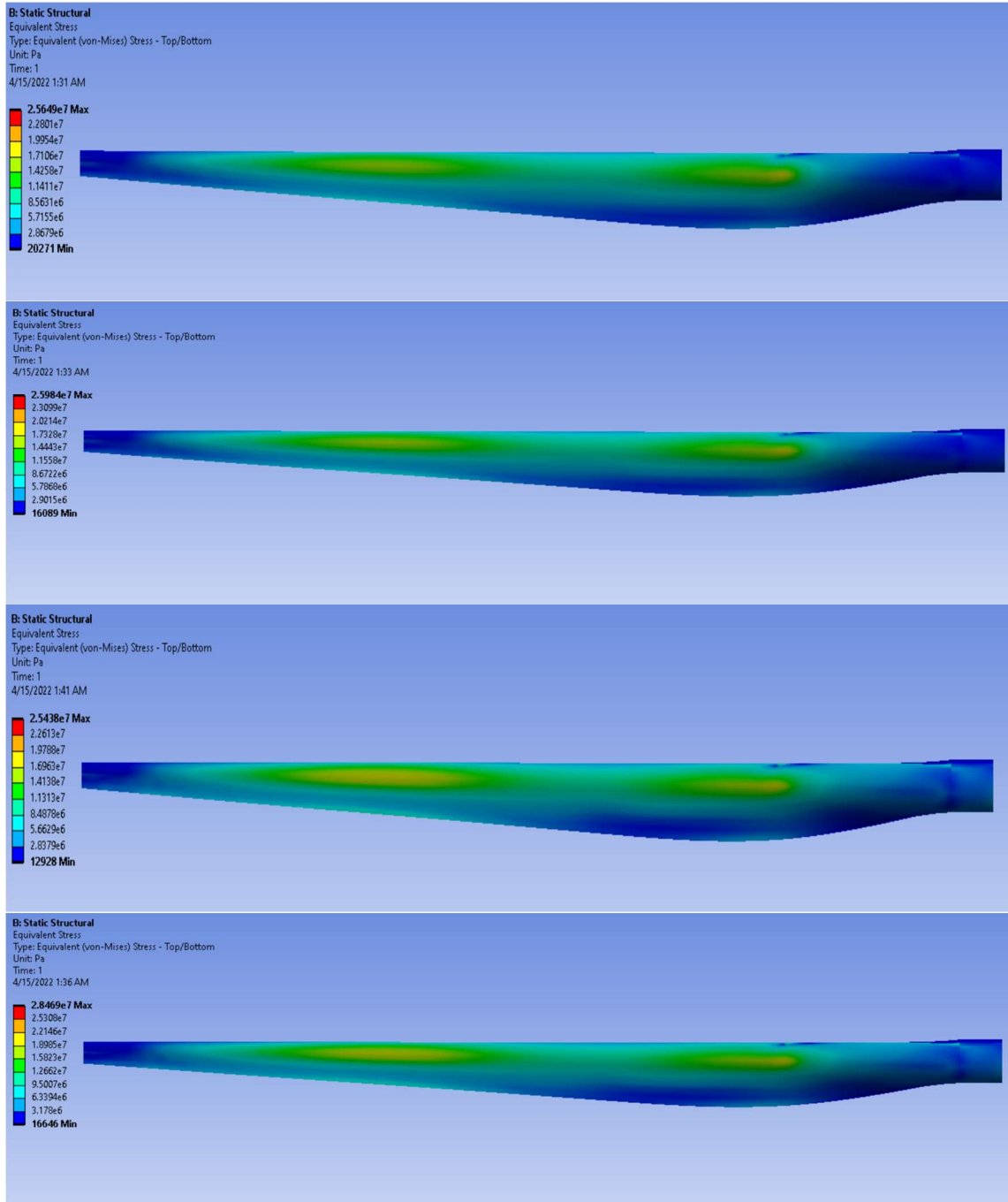


Figure 9-1: Equivalent stress on the blade at 8 m/s (from top to bottom, E-Glass, S-Glass, Carbon Epoxy, and Carbon fiber, respectively)

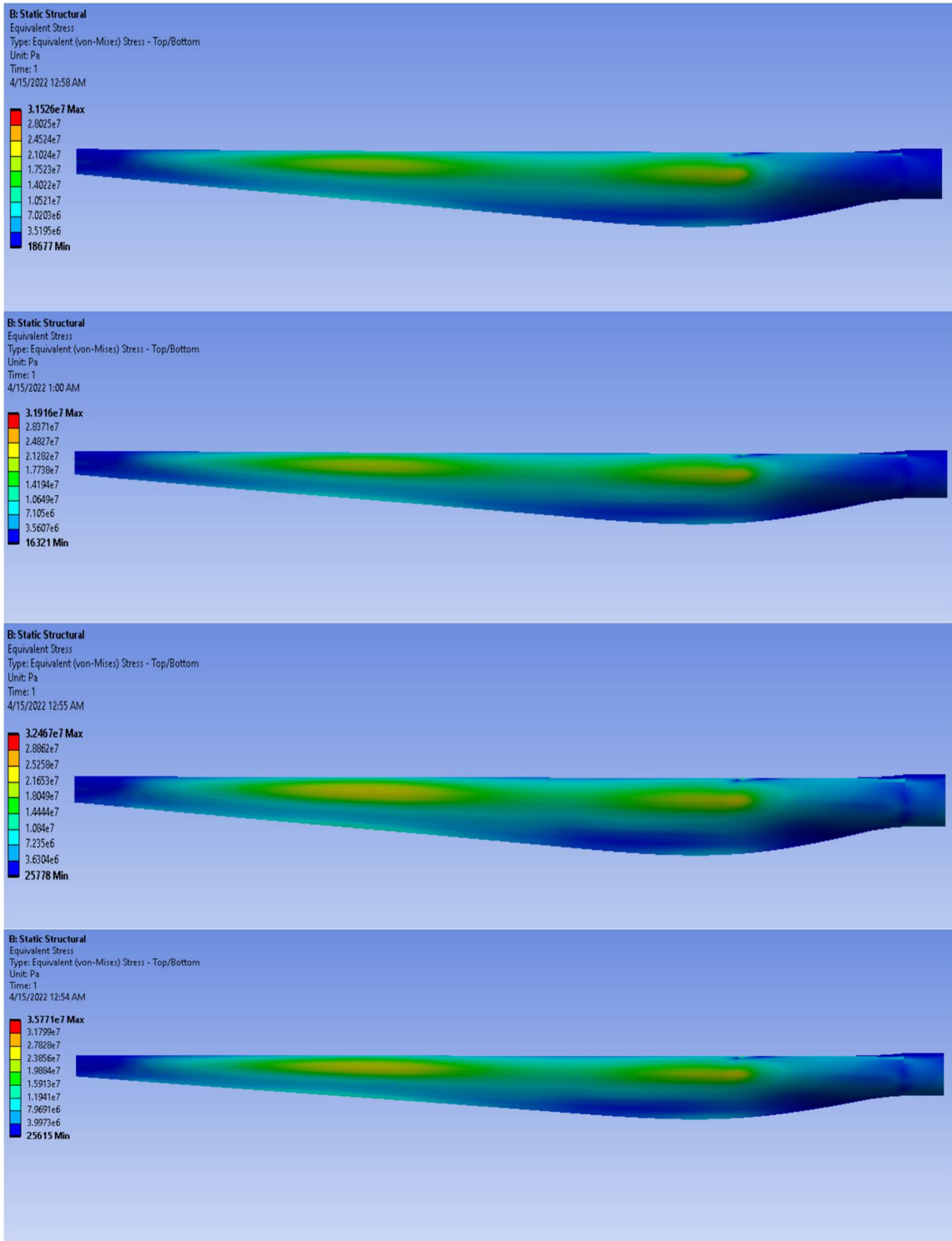


Figure 9-2: Equivalent stress on the blade at 10 m/s

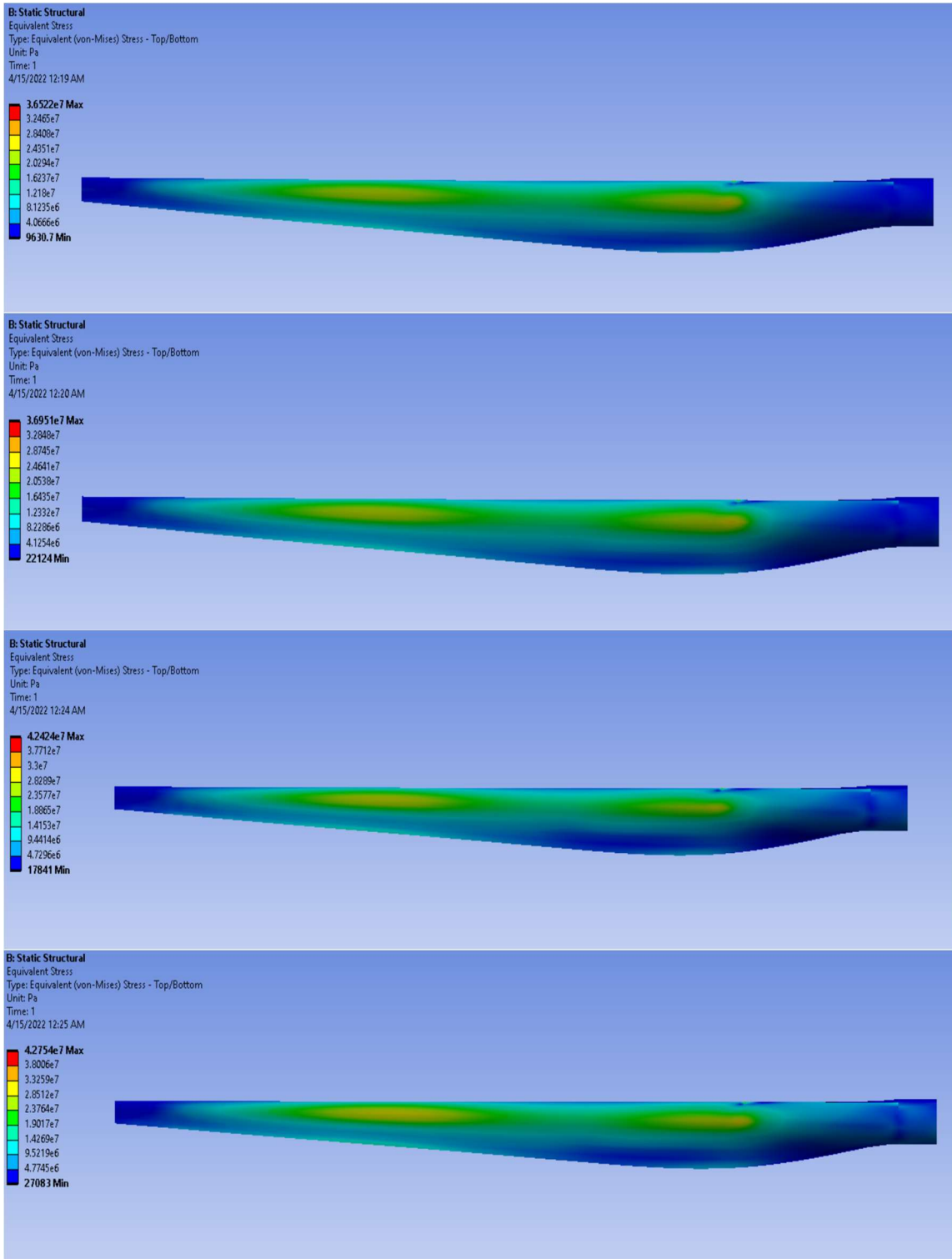


Figure 9-3: Equivalent stress on the blade at 12 m/s

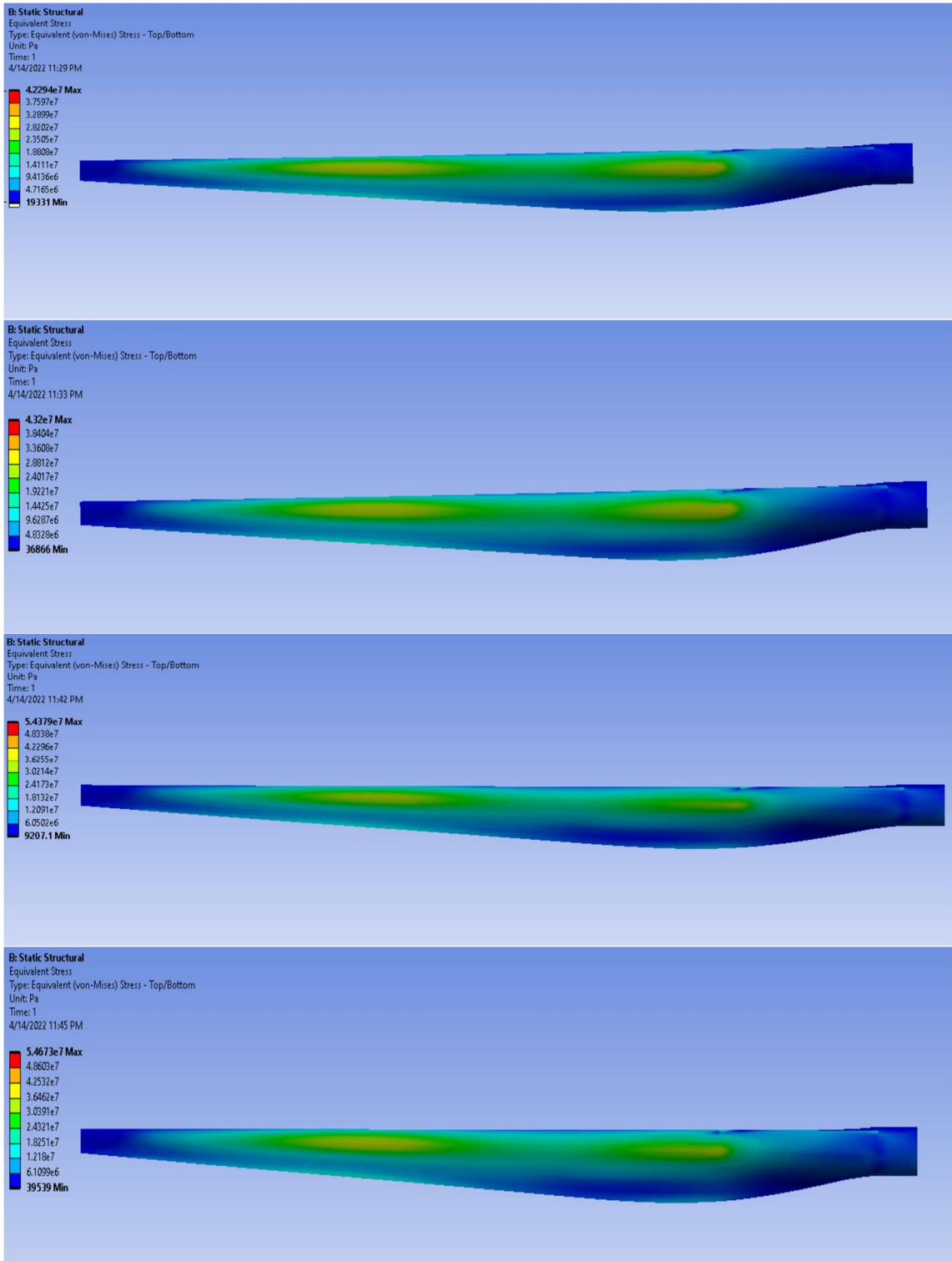


Figure 9-4: Equivalent stress on the blade at 15 m/s

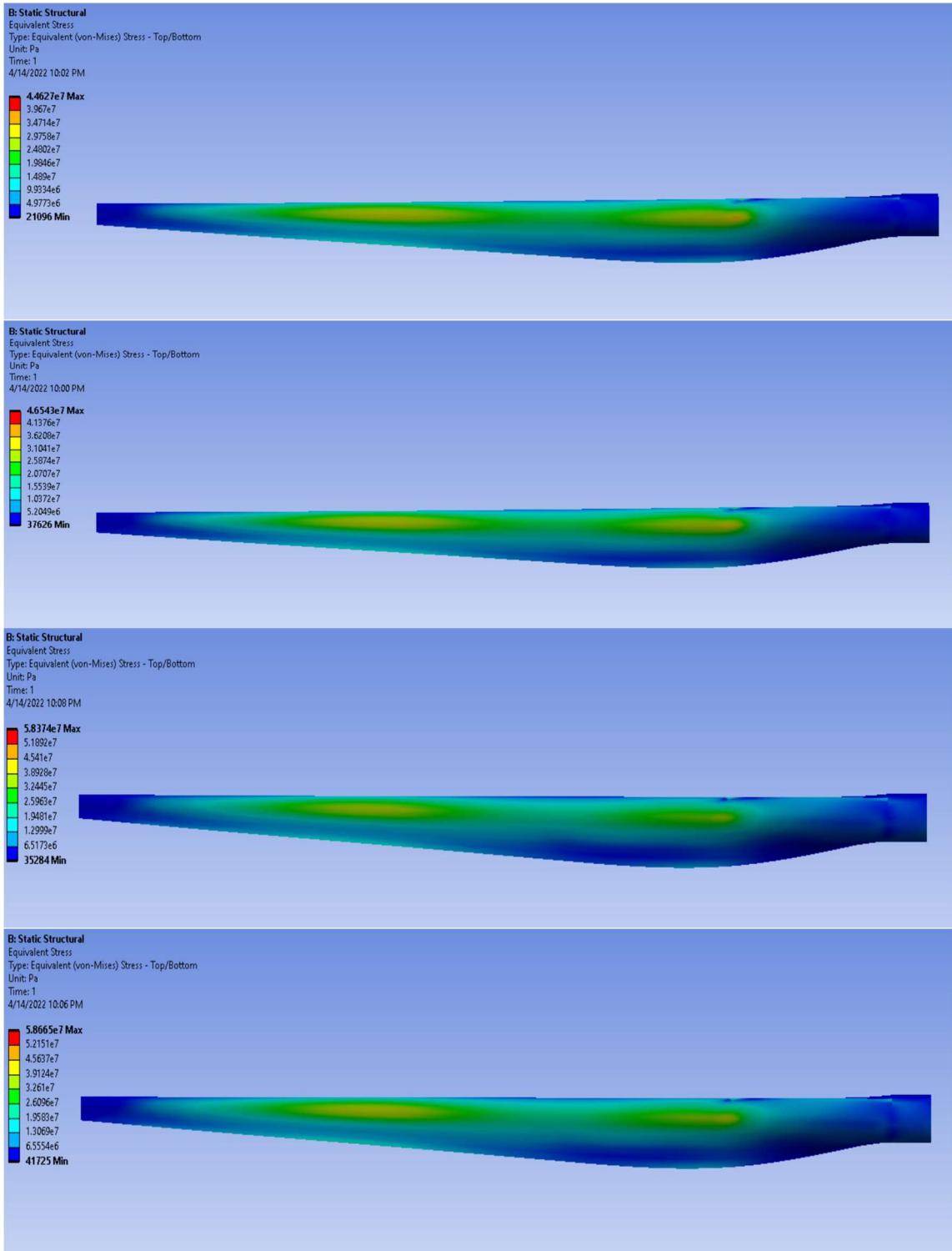


Figure 9-5: Equivalent stress on the blade at 18 m/s

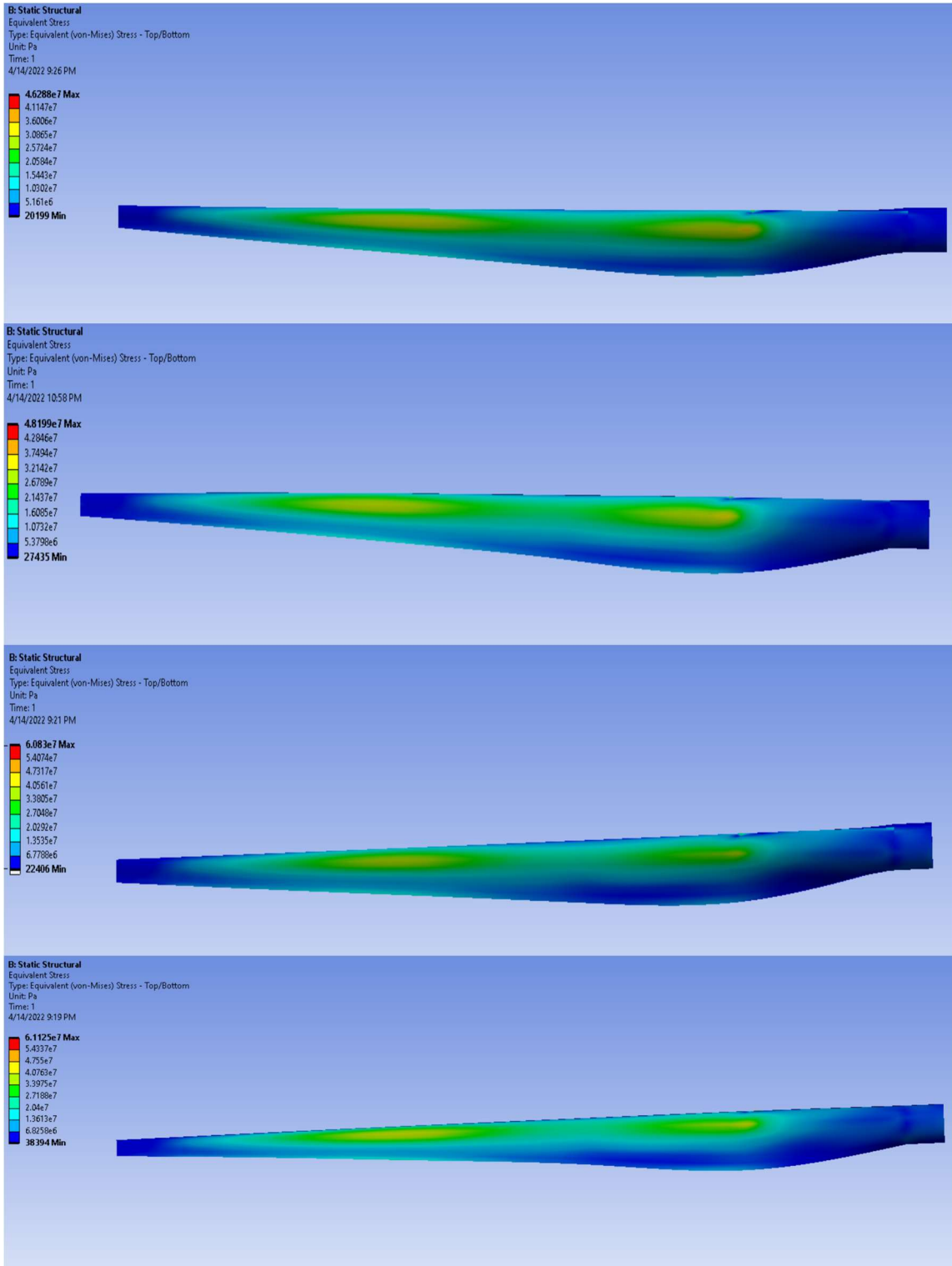


Figure 9-6: Equivalent stress on the blade at 20 m/s